iscte

**INSTITUTO
UNIVERSITÁRIO
DE LISBOA**

Impact of physical layer impairments on SDM networks based on ROADM nodes

Marco Quiteres da Silva

Master Degree in Telecommunications and Computer Engineering,

Supervisor:
PhD Luís Gonçalo Lecoq Vences e Costa Cancela, Assistant Professor,
ISCTE-IUL

Co-Supervisor:
PhD João Lopes Rebola, Associate Professor,
ISCTE-IUL

November, 2021

Department of Information Science and Technology

Impact of physical layer impairments on SDM networks based on ROADM nodes

Marco Quiteres da Silva

Master Degree in Telecommunications and Computer Engineering,

Supervisor:
PhD Luís Gonçalo Lecoq Vences e Costa Cancela, Assistant Professor,
ISCTE-IUL

Co-Supervisor:
PhD João Lopes Rebola, Associate Professor,
ISCTE-IUL

November, 2021

Agradecimentos

Quero agradecer ao ISCTE-IUL por estes cinco anos e a todos os docentes que fizeram parte do meu percurso, e em especial, aos meus orientadores, Prof. Luís Cancela e Prof. João Rebola por todo o apoio e trabalho a analisar as diferentes versões que lhes apresentei. Um agradecimento também ao Instituto de Telecomunicações, pelo acesso dado às suas instalações e material.

Quero também agradecer à minha família, mais precisamente à minha mãe que me apoiou durante estes cinco anos, e à minha namorada que teve paciência para estar comigo e apoiar-me quando as coisas não corriam bem.

Um obrigado também aos meus colegas Pedro Fonseca e Sandro Isqueiro pelo seu companheirismo e apoio.

Por último gostava de agradecer ao meu pai, que certamente estaria contente e orgulhoso por me ver alcançar esta meta.

Resumo

As redes óticas de transporte atuais estão a aproximar-se do seu limite de capacidade devido às novas aplicações e serviços que requerem uma maior quantidade de recursos de rede. Uma possível solução de curto a médio prazo para a falta de recursos é o uso de múltiplas bandas da fibra, para além da banda C. Uma solução a longo prazo será o uso de multiplexagem com divisão no espaço (SDM) no domínio óptico.

Neste trabalho são estudados, o custo por bit, consumo de energia e flexibilidade, das diferentes arquiteturas SDM (no espaço, no espaço e comprimento de onda, no comprimento de onda, fracionada no espaço e completa no comprimento de onda). Para as arquiteturas com granularidades no espaço e no espaço e comprimento de onda estuda-se analiticamente os efeitos das principais limitações do nível físico (PLIs) (ruído dos amplificadores, interferência não-linear, penalidade de filtragem e diafonia homódina), para cascatas de multiplexadores óticos de inserção/extração reconfiguráveis (ROADMs). Usa-se uma simulação Monte Carlo para calcular mais rigorosamente os efeitos das PLIs na arquitetura com granularidade no espaço e comprimento de onda.

A principal diferença, em termos de PLIs, entre uma rede SDM e uma rede com um único canal espacial é o efeito da diafonia homódina. Para uma rede com 16 direções, 19 canais espaciais e isolamento dos filtros de -25 dB, a diafonia homódina causa uma penalidade na relação sinal-ruído óptica de 2 dB e o sinal atravessa menos 9 ROADMs que numa rede com apenas um canal espacial.

Palavras-chave: diafonia homódina, filtragem ótica, multiplexadores óticos de inserção/extração reconfiguráveis, multiplexagem com divisão no espaço, ruído dos amplificadores, interferência não-linear.

Abstract

Current transport optical networks are approaching its capacity limits, mainly due to new applications and services that require a huge amount of resources. To increase the network capacity, multiband solutions, that exploit the unused capacity of actual fibers, in particular the L-band, are being currently commercially explored. However, this strategy is assumed as a short to medium term solution. A long-term solution is to use spatial-division multiplexing (SDM) in the optical domain, which leads to the concept of SDM-based optical networks.

In this work, different SDM switching architectures (spatial, spatial-wavelength, wavelength, fractional space-full wavelength) are studied and compared in terms of cost per bit, power consumption and flexibility. For the switching architectures with spatial and spatial-wavelength granularities (the architectures that have superior performance), the most relevant physical impairments (PLIs) (amplifiers noise, non-linear interference, narrowing penalty due to filtering and in-band crosstalk) are analytically studied, for a SDM reconfigurable optical add-drop multiplexer (ROADM) cascade. Furthermore, a Monte Carlo simulation is used to assess more rigorously the PLIs effects on the performance of SDM ROADMs, with spatial-wavelength switching architecture, in cascade.

The main difference, regarding PLIs, between the single spatial channel ROADM architecture and the SDM ROADM architectures is the enhanced effect of in-band crosstalk. For cascaded ROADMs with 16 directions, 19 spatial channels and filtering isolation of -25 dB, the in-band crosstalk can lead to a 2 dB optical signal-to-noise ratio penalty. Due to this penalty, the signal crosses less 9 ROADMs than in a single spatial channel ROADM architecture.

Keywords: Amplified spontaneous emission noise, in-band crosstalk, non-linear interference, passband narrowing filtering, ROADM, spatial division multiplexing.

Contents

List of Figures

List of Tables

List of Acronyms

A/D	Add and Drop
ASE	Amplified Spontaneous Emission
B&S	Broadcast and Select
B2B	Back-to-Back
BER	Bit Error Rate
CDC	Colorless, Directionless and Contentionless
CW	Continuous Wave
DEC	Direct Error Counting
EDFA	Erbium Doped Fiber Amplifier
FEC	Forward Error Correction
HD-FEC	Hard-Decision Forward Error Correction
I/Q	In phase component and Quadrature component
MC	Monte Carlo
MCF	Multicore Fiber
MCS	Multicast Switch
MEMS	Micro Electro Mechanical Systems
MF	Multiple Fibers
MIMO	Multiple Input Multiple Output
MMF	Multimode Fiber
NLI	Non-Linear Interference
OA	Optical Amplifier
OXC	Optical Cross Connect
PDM	Polarization Division Multiplexing
PLI	Physical Layer Impairment
PSD	Power Spectral Density
PSK	Phase Shift Keying
QAM	Quadrature Amplitude Modulation
R&S	Route and Select
RC	Raised Cosine
ROADM	Reconfigurable Optical Add-Drop Multiplexer
RRC	Root Raised Cosine
Rx	Receiver

SD-FEC	Soft-Decision Forward Error Correction
SDM	Spatial Division Multiplexing
Tx	Transmitter
VOA	Variable Optical Attenuator
WDM	Wavelength Division Multiplexing
WSS	Wavelength Selective Switch

List of Symbols

A	WSS isolation
$B_{m,dB}$	$-m$ dB bandwidth of the super-Gaussian filter
B_o	Optical bandwidth
B_{rc}	Raised cosine filter bandwidth
B_{ref}	Reference bandwidth
D	Number of directions
D_λ	Dispersion parameter
F_n	Noise figure
G	Number of groups of spatial channels
G_m	Signal PSD of the central channel
$H_b(f)$	Optical stop-band filter transfer function
$H_p(f)$	Optical pass-band filter transfer function
$H_{rc}(f)$	Raised cosine filter transfer function
$I_{cr,add}$	In-band crosstalk interfering terms added at the add structure
$I_{cr,drop}$	In-band crosstalk interfering terms added at the drop structure
$I_{cr,exp}$	In-band crosstalk interfering terms added at the express structure
$I_{l,WSS}$	Insertion losses of the WSS
L_{sec}	Section length
M	Number of spatial channels
N	Number of wavelength channels
N_{span}	Number of spans
N_{MC}	Number of MC simulation iterations
N_{errors}	Total number of symbols errors counted
N_{output}	Number of WSS outputs
N_r	Number of ROADMs
N_s	Number of symbols in a N_s-Quadrature amplitude modulation
$N_{symbols}$	Number of transmitted symbols in each iteration of the MC simulator
N_u	Number of inputs and outputs of the OXC
$OSNR_{network}$	OSNR measured in any point of the network
$P_{b,l}$	Line bit error probability
$R_{s,l}$	Symbol rate
S_{add}	QPSK generated signal

$S_{exp,j}$	Signal that has crossed j ROADMs
S_{margin}	System margin
T_s	Symbol period
X_T	Crosstalk level
c	Light velocity in a vacuum
f_m	Nominal frequency of channel m
g_{NLI}	NLI power spectral density
g_{SCI}	Self-channel interference noise power spectral density
g_{XCI}	Cross-channel interference noise power spectral density
g_n	amplifier gain
h	Planck constant
k	Number of outputs of the input WSS and inputs of the output WSS of the central OXC
n	Filter order
n_i	Number of interfering terms
n_{order}	Order of the interfering terms
n_u	Number of outputs of the input WSS and inputs of the output WSS of the OXC
η_{NLI}	NLI parameter of the link
$osnr_{NLI}$	Optical signal-to-noise ratio with ASE noise and NLI
$osnr_{req,B_o}$	Optical signal-to-noise ratio required at the optical signal bandwidth
$osnr_{req,B_{ref}}$	Optical signal-to-noise ratio required at the reference bandwidth
$osnr$	Optical signal-to-noise ratio with ASE noise
$osnr_{XT}$	Optical signal-to-noise ratio with ASE noise, NLI and in-band crosstalk
p	Number of polarizations
p_{NLI}	NLI power
p_{ase}	ASE noise power
$p_{ch,opt}$	Optimal channel power
p_n	Noise power at one amplifier output
p_{post}	ASE noise power originated at the post amplifier
p_{pre}	ASE noise power originated at the pre amplifier
p_s	Signal power
snr	Signal-to-noise ratio
λ_n	Wavelength channel n
λ_o	Wavelength of the central channel

ν_o	Central channel frequency
σ_m	Spatial channel m
β_2	Group velocity dispersion parameter
ΔP_T	Transmission penalty
$\Delta \nu_{ch}$	Channel spacing
$\Delta OSNR$	Optical signal to noise ratio penalty
α	Fiber attenuation coefficient
γ	Fiber non-linearity coefficient
ρ	Roll-off factor

Chapter 1: Introduction

1.1 Motivation and context

Current transport optical networks are approaching its capacity limits, mainly due to new applications and services that require a huge amount of resources (i.e., bandwidth), like video services and cloud services . To increase the network capacity transmission, as well as switching efficiency, advanced modulation formats, that allow to transport more bits in a symbol and reconfigurable optical add/drop multiplexer (ROADM) with added features, like colorless, directionless and contentionless that bring more dynamism to the network, are being used. Nevertheless, the referred strategies are nowadays almost fully exploited.

Another solution to surpass the possible capacity crunch consists in using other fiber bands, than the common C-band, the so-called multiband solution [1]. This is usually considered a short to medium term solution. A long-term solution is to use spatial-division multiplexing (SDM) in the optical domain, which leads to the concept of SDM-based optical networks [2,3]. Multicore fibers (MCF), multimode fibers (MMF) or multiple fibers (MF) in parallel are examples of SDM solutions for optical networks [2,3]. These solutions essentially create multiple parallel light paths between the selected source and destination, which corresponds to the concept of SDM brought to the optical domain. In this scenario, the network capacity increases proportionally to the number of cores used in the MCF, on the number of modes in the MMF and on the number of MF fibers in parallel.

In order to analyze and study the signal transmission in these networks, new ROADM node models need to be developed. In [2,3] several SDM ROADM node architectures are proposed. Since in SDM-ROADM nodes, switching can be done in two dimensions, space and wavelength, four switching strategies are possible: space granularity, wavelength-space granularity, wavelength granularity and fractional space-full wavelength granularity [2,4]. In this dissertation, each one of these strategies is analyzed and discussed considering the MF scenario. In particular, their cost, flexibility and physical layer impairments (PLIs) are analyzed.

1.2 Goals

1. Study of the different reconfigurable optical add-drop multiplexer (ROADMs) architectures, in terms of flexibility, cost per bit and power consumption, for SDM networks and considering the MF scenario.

2. Analytical study of the PLIs inside the SDM ROADM nodes, and also along the fiber, in particular insertion losses, amplified spontaneous emission (ASE) noise, filtering effects (as suggested in [5]), non-linear interference (NLI) and crosstalk.

3. Evaluate, through a Monte Carlo simulation, the impact of the PLIs, both from transmission and nodes, in a cascade of ROADMs in terms of optical signal-to-noise ratio (OSNR) penalty in a SDM network scenario.

1.3 Dissertation organization

This dissertation is composed by four more chapters. Chapter 2 is focused on the study of the SDM ROADM architectures and their characteristics. The four possible switching strategies in a SDM ROADM architecture are explained and the hardware used to build these architectures and its functionalities are presented. Then, the cost per bit, power consumption and flexibility of the four SDM ROADMs architectures are compared, having the ROADM architecture with a single spatial channel as a reference.

Chapter 3 is focused on the study of the network performance. In this chapter, the PLIs, ASE noise, passband narrowing due to filtering effects, non-linearity effects and in-band crosstalk, are studied analytically. The PLIs analysis is performed for the SDM ROADMs architectures with spatial and spatial-wavelength granularity, and for the reference ROADM architecture.

Chapter 4 is dedicated to the study of the PLIs in a network composed by a cascade of SDM ROADMs with spatial-wavelength architecture using Monte Carlo (MC) simulation. The PLIs analyzed in the simulation are the ASE noise accumulation, the optical filtering effects, fiber non-linear interference and in-band crosstalk. Each PLI effect is added one at a time to the network model implemented in the MC simulator, its implementation validated with results from the literature and the results obtained compared with the analytical results obtained in chapter 3. A discussion of the simulation results is also performed.

Chapter 5 summarizes the main conclusions of this work and provides some suggestions for future work.

1.4 Dissertation main contributions

The main contributions of this dissertation are:

- We present a possible implementation for each switching strategy. We also compare the throughput, cost per bit, power consumption and flexibility between the four SDM ROADMs architectures and the single spatial channel ROADM architecture.

- We assess and compare the network performance between the spatial, spatial-wavelength (these two architectures are the most adequate architectures for MF solutions in terms of cost, power consumption and flexibility) and single spatial channel ROADM architectures, considering several PLIs.

- We present equations to compute the number of interfering terms in a route and select (R&S) SDM ROADM architecture with spatial and spatial-wavelength granularity.

- A MC simulator that allows studying the PLIs on the SDM ROADM architecture with spatial-wavelength granularity more rigorously, has been developed.

Chapter 2: Literature review

2.1 Introduction

In this chapter the concept of SDM multiplexing, the ROADMs architectures (*route and select* and *broadcast and select*), Add and Drop (A/D) structures and the different switching strategies (space granularity, wavelength-space granularity, wavelength granularity and fractional space-full wavelength granularity) and their functionalities, are explained. For each one of the possible switching strategies, it is presented a possible SDM ROADM architecture, and the hardware used in each architecture. It is also compared in terms of cost per bit, power consumption and flexibility the different SDM ROADM architectures and the architecture with one spatial channel.

2.2 Spatial-division multiplexing on optical networks

Spatial-division multiplexing (SDM) in optical networks consists in using different spatial channels (i.e. multiple fibers, multiple cores or multiple modes) to transport information [2,3]. Each spatial channel can be used to transport a wavelength-division multiplexing (WDM) signal (a signal with multiple wavelength channels) [2,3].

A multi-core fiber (MCF), shown in Figure 2.1 a), has multiple cores, where each core may work as a single independent spatial channel. In the case of manufacturing imperfections, as well of environment effects, coupling between the cores can occur. However, the MCF can be designed to avoid this coupling effect [3].

A multi-mode fiber as shown in Figure 2.1 b) has multiple propagation modes, each mode working as a spatial channel. In this type of fibers, coupling between modes cannot be avoided. Due to the coupling, these signals need to remain together along the optical path and routing, until they reach the receiver (the group of wavelength channels switched together is called spatial superchannel) [2,3]. This receiver, known as SDM receiver has multiple inputs and multiple outputs (MIMO) in order to allow digital processing and separate the spatial superchannels in individual wavelengths.

In the multiple fibers approach shown in Figure 2.1 c), each optical fiber is spatially isolated from the other fibers, and the signal coupling effect is inexistent [2,3]. This is the SDM approach that is going to be considered in this work. This approach has been chosen, since it is a feasible short-term implementation solution, as the MCF and MMF solutions have still some issues to be solved [6], that postpone their massive practical implementation in the near future.

Furthermore, the multiple fibers approach simplifies the simulator implementation, since it avoids the modelling of the coupling effects.
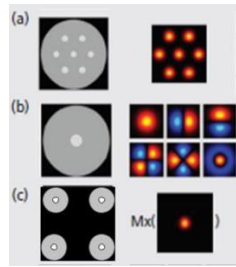
Figure 2.1: Spatial-division multiplexing approaches in optical networks (figure taken from [3]).

2.3 ROADM-based SDM optical networks

In SDM-based optical networks, characterized by M spatial channels, where each spatial channel is denoted by σ_m, with $m=1,...,M$, and N wavelength channels per spatial channel, where each wavelength channel is denoted by λ_n, with $n=1,...,N$, switching can be done in two dimensions, space and wavelength. Hence, four switching strategies are usually proposed for SDM networks: space granularity, space-wavelength granularity, wavelength granularity and fractional space-full wavelength granularity [2,3].

In the space-wavelength granularity strategy, represented in Figure 2.2 a), the switching is done between wavelength channels in any spatial channel. This strategy must use independent spatial and wavelength channels, hence, requiring uncoupled SDM fibers, such as the multiple fibers solution or the weakly-coupled MCF solution. Furthermore, this strategy can also be implemented with or without lane changes. Spatial-wavelength switching without lane changes means that a wavelength channel in one direction can be switched to another direction, but always to the same spatial channel, e.g, a wavelength channel λ_1 in spatial channel σ_1 in one direction is switched to spatial channel σ_1 of another direction. Spatial-wavelength switching with lane changes means that a wavelength channel in one direction can be switched to another direction of the node, and can be switched to a different spatial channel, e.g, a wavelength channel λ_1 in spatial channel σ_1 in one direction is switched to spatial channel σ_2 of another direction. This strategy is the one that leads to a most flexible switching architecture, since the switching is performed at the wavelength level granularity, but at the cost of more complexity [2,3].

In the space granularity strategy, represented in Figure 2.2 b), the switching is performed between spatial channels, by switching the entire spectrum corresponding to a WDM signal [2,3], e.g., spatial channel σ_1 in one direction, is switched to spatial channel 2, σ_2, on another direction [2,3]. This operation can also be further classified, as spatial switching with or without

lane changes inside the network node. The space granularity switching also demands uncoupled SDM fibers.

In the wavelength granularity strategy, represented in Figure 2.2 c), the switching is done between groups of channels with the same wavelength, which form a spatial superchannel, i.e., all wavelength channels λ_1 , forming a spatial superchannel, in one direction, are switched together to another direction. A joint switch WSS must be used to perform this operation [2,3].

In the fractional space-full wavelength strategy, represented in Figure 2.2 d), the switching is done between subgroups of channels (subgroup 1 composed by the spatial channels $\sigma_1, \sigma_2, \sigma_3$ and subgroup 2 composed by $\sigma_4, \sigma_5, \sigma_6$) with the same wavelength. As an example, all wavelength channels λ_1 of subgroup 1 in one node direction, are switched together to subgroup 1 in another direction, and wavelength channels λ_1 of subgroup 2 in one direction, are all switched together to subgroup 2 of another direction [2,3]. This solution is very similar to solution c), still supported by spatial superchannels, but with this solution, the degree of spatial granularity is increased. In this strategy, the groups are previously defined (this groups are defined in the transmission). This operation can also be further classified, as fractional space-full wavelength switching with or without lane changes inside the network node.
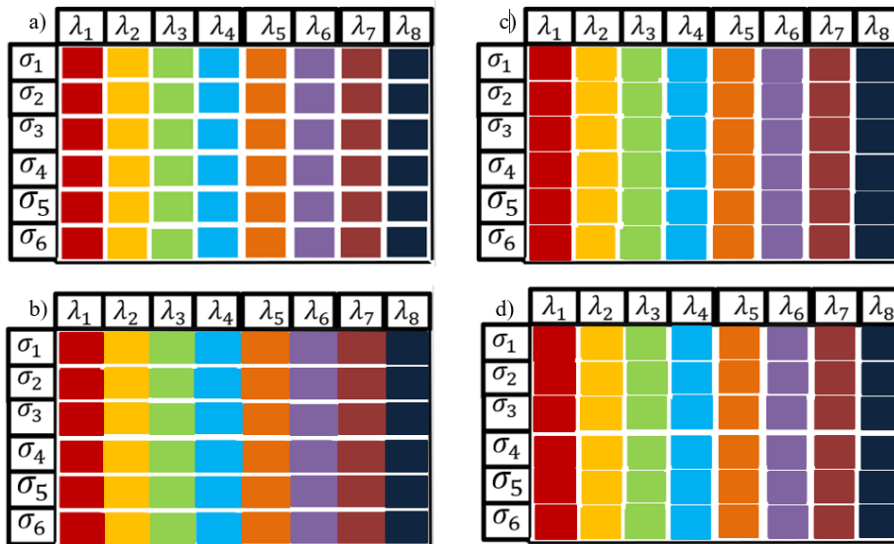
Figure 2.2: SDM switching strategies taken from [3]. The thick "white" lines define the switching granularity of the different strategies. Figure a) shows the switching strategy with spatial-wavelength granularity, b) shows the strategy with spatial granularity, c) shows the strategy with wavelength granularity and d) shows the strategy with fractional space-full wavelength granularity.

2.4 Classification of ROADM architectures and A/D structures according with their hardware and functionalities

The two most used ROADM architectures are the Route and Select (R&S) and Broadcast and Select (B&S) [7]. In Figure 2.3 a), it is shown a B&S architecture. In a B&S architecture the wavelength channels are always sent to all directions and to the A/D structure. The selection of the wavelength channels in these architectures, is performed in the output of the ROADM or in the A/D structures. Usually in these architectures are used splitters in the ROADM input and WSSs in the ROADM output [7]. In Figure 2.3 b), it is shown a R&S architecture. In these architectures the wavelength channels are selected and sent to the proper destination by the hardware in the ROADM input. Usually in these architectures are used WSSs in the ROADM input and output [7].

The A/D structures are classified according with their functionalities. In Figure 2.3 b), it is shown a ROADM with a colorless, directionless and contentionless (CDC ROADM) A/D structure. In a ROADM with this A/D structure it is possible to extract any wavelength channel (colorless) from any direction (directionless) without contention from channels with the same wavelength in different directions that are extracted at the same time (contentionless). Usually, to execute this structure are used MCSs (Multicast Switch) or WSSs with multiple entry's and multiple exits [7] (in this work we use WSSs). An A/D structure with contention is shown in Figure 2.3 a). In this A/D structure it is not possible to drop wavelength channels λ_x from different directions at the same time, because exists contention in the link between the two WSSs of the drop structure. An A/D structure without the functionality directionless is for example a drop structure that is only linked to one direction (each direction has its own drop structure). An A/D structure without the capacity colorless is a A/D structure where the wavelength channels to extract need to be pre-defined before the construction of the ROADM.
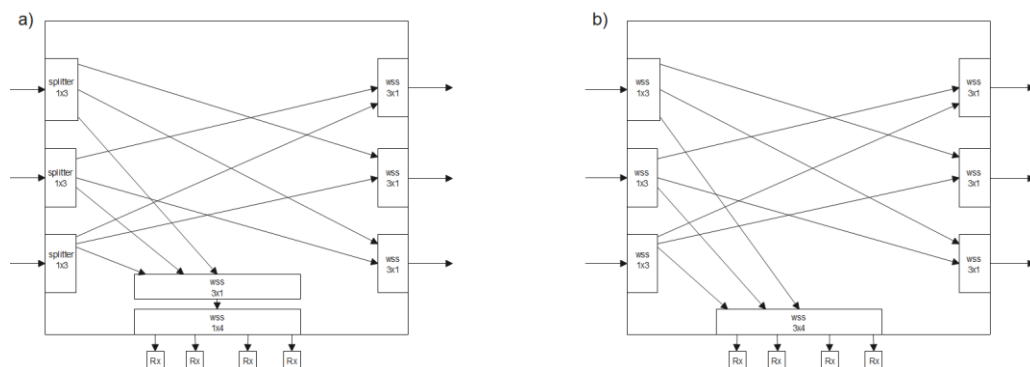
Figure 2.3: a) Broadcast and select ROADM architecture with a CD A/D structure. b) Route and select ROADM architecture with a CDC A/D structure.

2.5 Spatial granularity architecture

A SDM ROADM-based architecture with spatial granularity can be implemented with or without lane changes [2]. A SDM ROADM-based architecture with spatial granularity without lane changes, considering 2 directions (D=2) and 4 spatial channels (M=4) is represented in Figure 2.4. Each spatial channel is represented with a different color: blue, red, black and yellow. To build this architecture four, 3×3 optical cross-connects (OXCs) must be used. Each OXC is responsible for routing a particular spatial channel, σ_1 (for example, with the blue color), to a different direction and also has an input/output dedicated to the ROADM add/drop (A/D) structure [2,3].

An A/D structure, of a SDM ROADM-based architecture with spatial granularity without lane changes, is also represented in Figure 2.4, considering 80 wavelength channels (N=80) for each spatial channel, and an A/D ratio of 20%, which means that 16 channels can be added/dropped at the same structure. This drop structure has four 1×17 wavelength selective switches (WSSs), each one dedicated to a spatial channel. In this A/D structure, it is not possible to drop at the same time, wavelength channels from different directions that have the same spatial channels, this mean that in this A/D structure exists contention, hence the A/D structure is only CD (colorless and directionless). To allow this, each OXC should have an extra connection towards an extra WSS in the drop structure. Each WSS is linked to 16 receivers, and has an output link to the add structure so that the channels that are not going to be dropped can return to the ROADM. As in the drop structure, the add structure has four,17×1 WSSs. This WSSs are linked to 16 transmitters and to the drop structure.

In Figure 2.5, it is represented a route and select SDM ROADM-based architecture with spatial granularity with lane changes, considering D=2 and M=4. The spatial channels are represented in different colors: red, blue, black and yellow. This architecture has a single 12×12 OXC to perform the switching of the spatial channels between all directions and all spatial channels. This increases the spatial granularity in comparison to the case without lane changes, however, a single OXC to perform the switching represents a single point of failure. This OXC has also four inputs/outputs connected to each ROADM A/D structure dedicated to a specific spatial channel. This A/D structure is equal to the case without lane changes, it exhibits contention between WDM channels with the same spatial channel coming from different directions, but the A/D WSSs are linked to a single OXC.

8
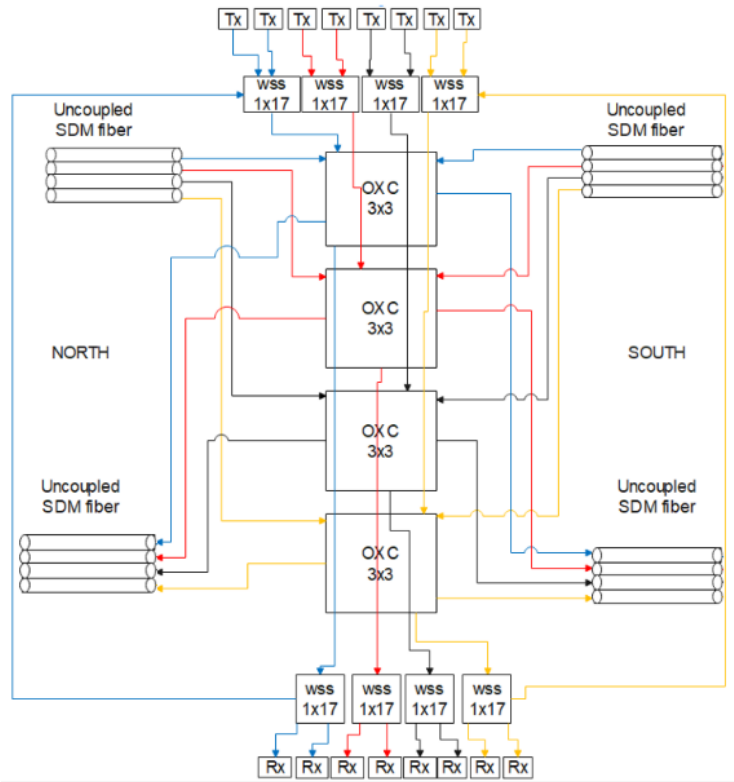
Figure 2.4: Spatial granularity architecture without lane changes (Rx- receivers, Tx-transmitters).
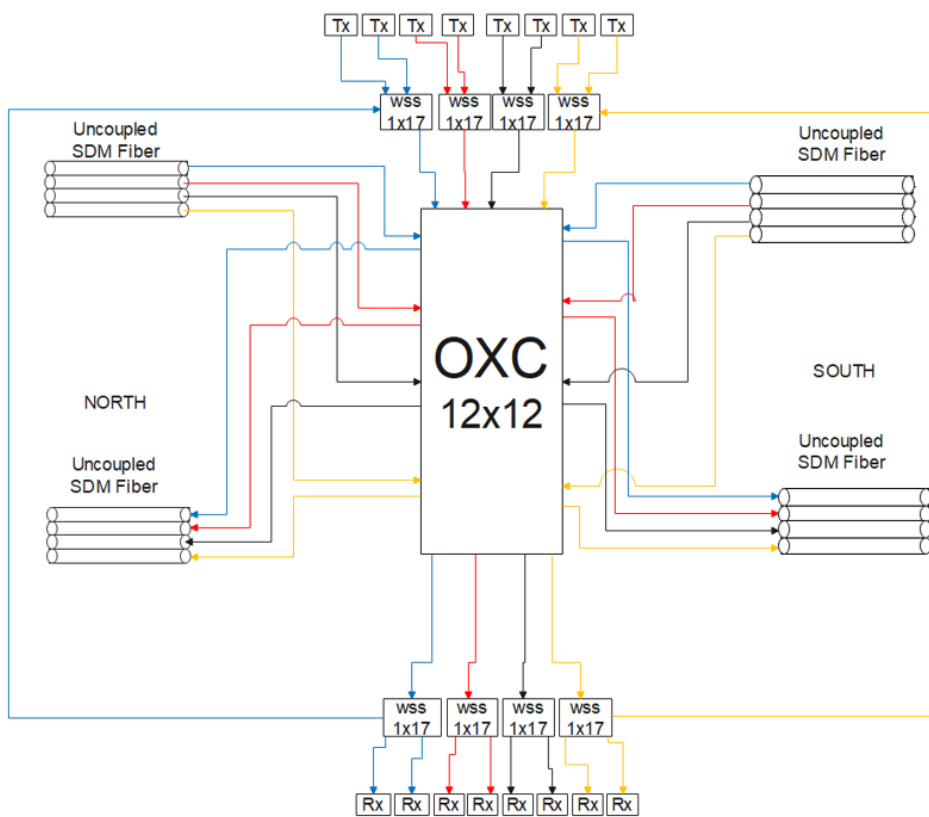
Figure 2.5: Space granularity switch architecture with lane changes.

2.6 Spatial-wavelength granularity architecture

A SDM ROADM-based architecture with spatial-wavelength granularity can be also implemented with or without lane changes. A SDM ROADM-based architecture with spatial-wavelength granularity without lane changes, considering $D=2$ and $M=4$, with the spatial channels differentiated by colors: blue, red, yellow, black, is represented in Figure 2.6. This architecture has eight, 1×5 input WSSs and eight, 5×1 output WSSs. The input WSS is responsible for routing wavelength channels from a particular spatial channel to the output WSS responsible for that spatial channel and to the drop structures. The output WSS is responsible for receiving wavelength channels from the input WSS of the other directions, and from the add structures.

In Figure 2.7, it is shown a route and select SDM ROADM-based architecture with spatial-wavelength granularity with lane changes, considering $D=2$ and $M=4$. Each spatial channel is characterized by a different color: blue, red, yellow and black. This architecture has eight 1×8 input WSSs and eight 8×1 output WSSs. Each WSS is responsible for routing/receiving wavelength channels to/from any spatial channel of any direction (in this case, four spatial channels for one output direction, which leads to four connections), and they must also have 4 inputs/outputs for assessing the ROADM A/D structure. The spatial-wavelength granularity architecture can be also built with an OXC-based solution, but the size of the OXC can make this solution prohibitively expensive and unfeasible.

The A/D structure corresponding to the ROADM architectures presented in Figures 2.6 and 2.7 can be implemented in two different ways. A 20% A/D ratio and 80 wavelength channels ($N=80$) has been considered. The first way of doing this A/D structure is doing a 8×16 WSS, using a cascade of WSSs has represented in Figure 2.8. The other way of doing this A/D structure is by replacing the 1×16 WSS by a 1×16 splitter/coupler. Each 1×8 WSS is responsible for selecting the wavelengths of each direction that are to be added/dropped. This A/D structure is CDC (colorless, directionless and contentionless) and has the same functionalities than the A/D structure presented in Figure 1 a) of [8], but in our architecture the A/D structure is divided in M A/D structures. An architecture with only one A/D structure (as in 1 a) of [8]) will need WSSs with higher dimensions, and WSSs with that level of dimension do not exist in the current market.
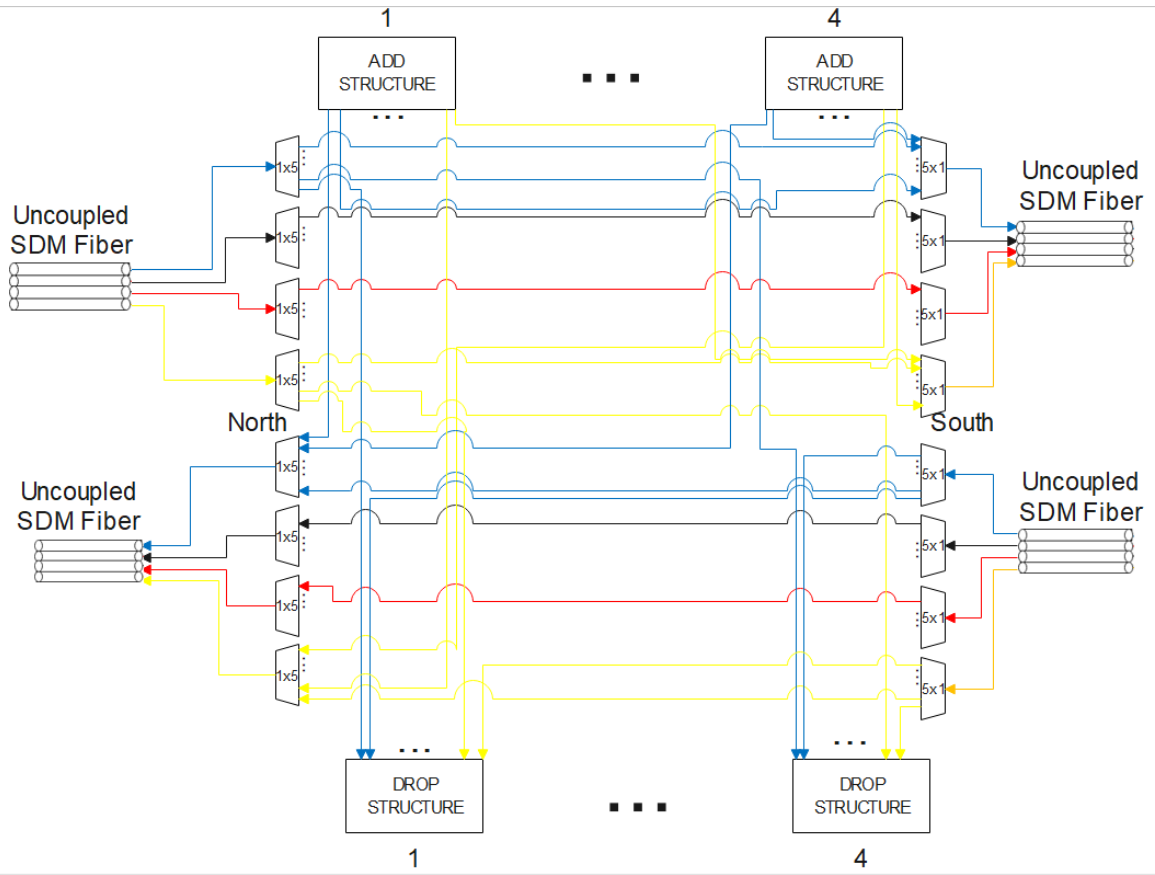
Figure 2.6: Spatial wavelength granularity architecture without lane changes.
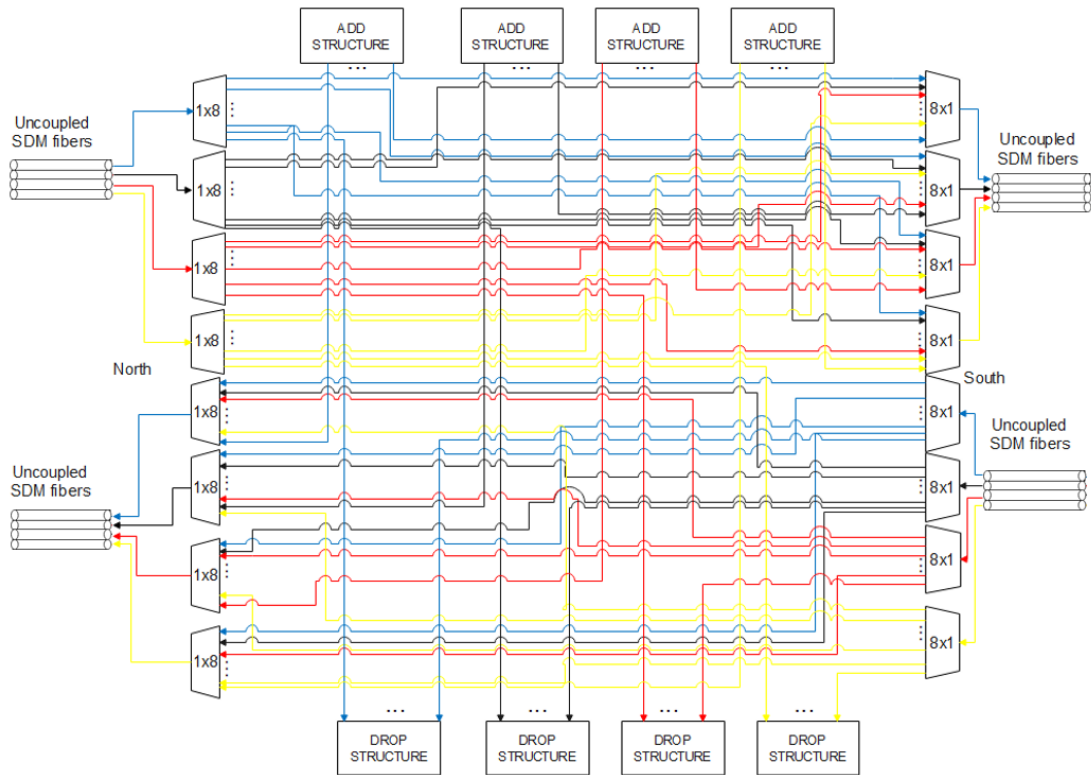
Figure 2.7: Spatial wavelength granularity architecture with lane changes.
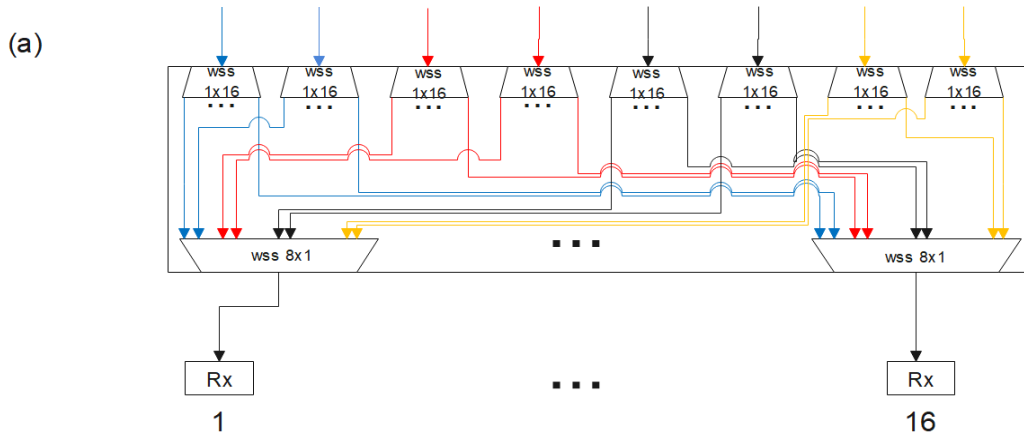
Figure 2.8: Add-drop structure for the spatial- wavelength granularity architecture with WSS.

2.7 Wavelength granularity architecture

A route and select SDM ROADM-based architecture with wavelength granularity is represented in Figure 2.9, considering 2 directions (D=2), 4 spatial channels (M=4), 80 wavelength channels (N=80), A/D ratio of 20% and with each spatial channel represented by a different color. This architecture has two, $4\times(1\times2)$ input joint switch WSSs, and two, $4\times(2\times1)$ output joint switch WSSs. The input joint switch WSSs is responsible for routing a spatial superchannel with a specific wavelength to one output direction or to the drop structure. The output joint switch WSS is responsible for receiving the spatial superchannels that come from others directions or from the add structure. Notice that, in this strategy, the traffic coming from the North direction to the South direction is independently routed from the traffic coming in the opposite direction, from the South direction to the North direction.

In Figure 2.10, it is represented an CDC (colorless, directionless, contentionless) A/D structure for an SDM ROADM-based architecture with wavelength granularity. This A/D structure is responsible to extract/add a spatial superchannel, and must use joint switch WSSs. This drop structure has a single $4\times(1\times16)$ joint switch WSS with 64 output links toward receivers and 4 input links, from an input joint switch WSS. The add structure has a single $4\times(16\times1)$ joint switch WSS with 64 inputs links that come from transmitters and 4 output links toward an output joint switch WSS. Although Figures 2.9 and 2.10 represent a wavelength granularity solution for uncoupled fibers, this solution can also be applied to coupled SDM fibers. In the coupled SDM fibers scenario, the A/D structure must use SDM receivers that uncouple the spatial superchannel into separate channels, as shown in Figure 4 b) of [3]. Concerning Figure 2.10, each group of 4 standard Rx dedicated to a spatial supperchannel must

be substituted by a SDM receiver that uncouples the 4 spatial channels composing the spatial superchannel.

A joint switch WSS has spatial channels at its input and several spatial superchannels at its outputs. In Figure 2.11, a joint switch WSS is represented, considering 3 spatial channels and 2 wavelength channels per spatial channel. The spatial channels are represented in black and the wavelength channels in blue and red. Each spatial channel hits a different section of the steering mirror [2,9]. Each section of the steering mirror will introduce a different steering angle that makes the wavelength channel with the same index of all spatial channels to go to the same direction (forming a spatial superchannel in that direction) [2,9].
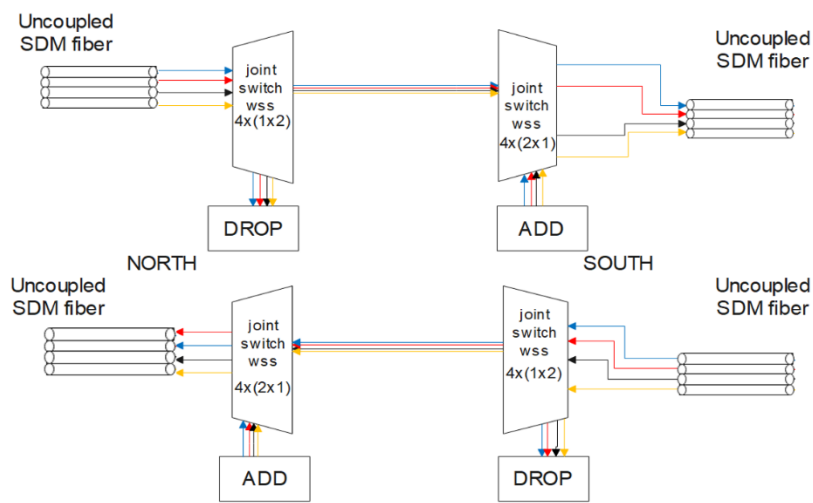
Figure 2.9: Wavelength granularity architecture.
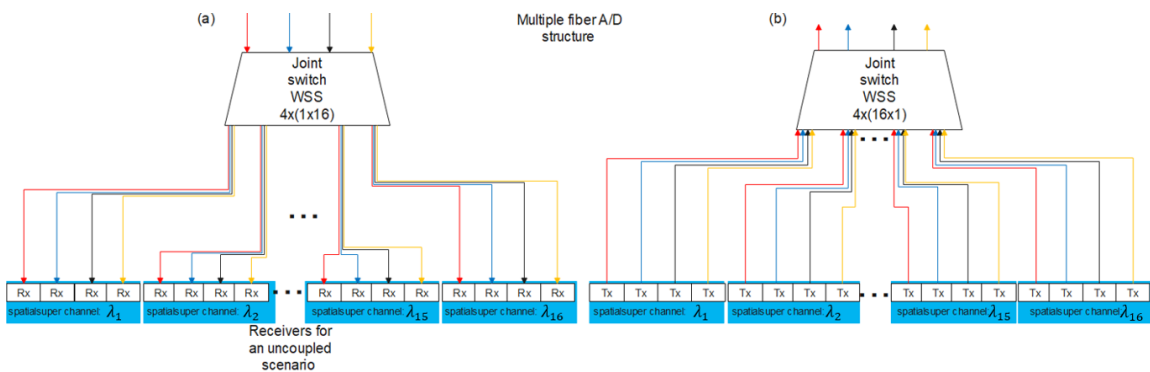
Figure 2.10: Wavelength granularity architecture add and drop.
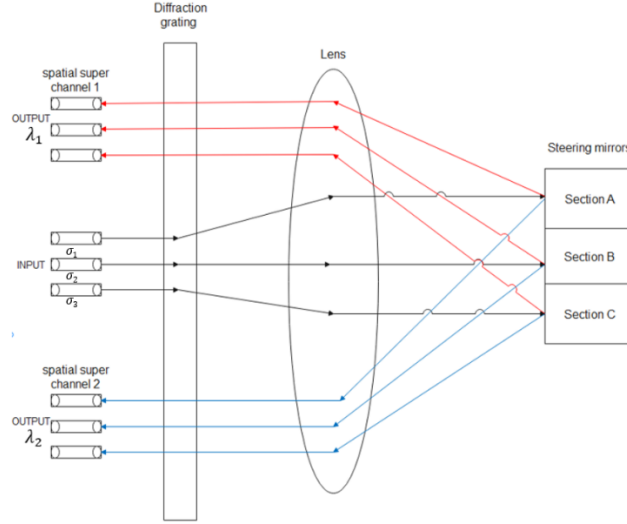
Figure 2.11: Schematic of a joint switch WSS 1x2 (based on [2]).

2.8 Fractional space-full wavelength granularity architecture

Figure 2.12 represents a route and select SDM ROADM-based architecture with fractional space-full wavelength granularity without lane changes, considering 2 directions (D=2), 4 spatial channels (M=4), and 2 spatial groups (G=2). The spatial channels are differentiated by color: blue, red, yellow and black, the first spatial group is composed by the spatial channels represented by the red and blue colors and the second spatial group is composed by the spatial channels represented by the yellow and black colors. This architecture has two, $2\times(1\times2)$ input joint switch WSSs, and two, $2\times(2\times1)$ output joint switch WSSs.

The input WSS, is responsible for routing at the same time all the wavelength channels λ_n belonging to the same spatial group to an output WSS in other direction that belong to the same spatial group. The input WSS must also have 2 output links connected to the drop structure. The output WSS is responsible for receiving and group wavelength channels, that come from the input WSS that belong to the same spatial group or from the add structure.

In Figure 2.13, it is shown a SDM ROADM-based architecture with fractional space-full wavelength granularity with lane changes, considering D=2, M=4 and G=2. This architecture has two, $2\times(1\times3)$ input joint switch WSSs and two, $2\times(3\times1)$ output joint switches WSSs.

An CDC (colorless, directionless, contentionless) A/D structure for the architecture with fractional space-full wavelength granularity must be able to extract/add each group of spatial superchannels individually. In this example, as there are two groups, two joint switches WSSs are required per A/D structure. The drop structure has two $2\times(1\times16)$ joint switches WSSs with 32 output links towards standard optical receivers and 2 input links that come from an input joint switch WSS. The add structure has two $2\times(16\times1)$ joint switches WSSs with 32 input links

14

from transmitters and 2 output links towards an output joint switch WSS. This A/D structure is shown in Figure 2.14.
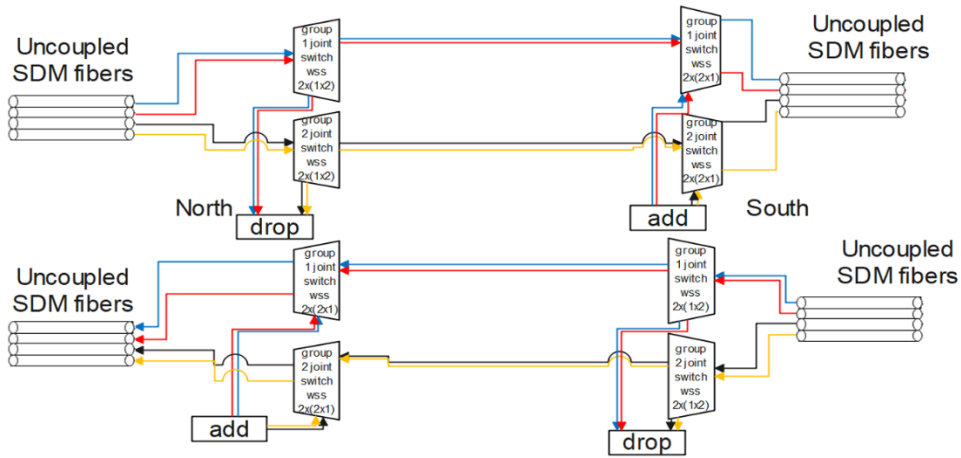
Figure 2.12: Fraction space-full wavelength granularity without lane changes architecture.
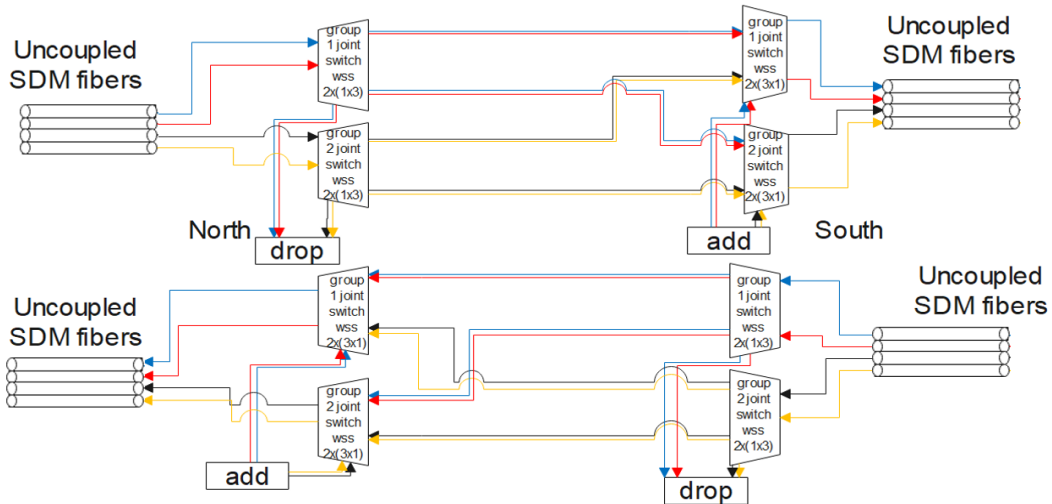
Figure 2.13: Fraction space-full wavelength granularity with lane changes architecture.
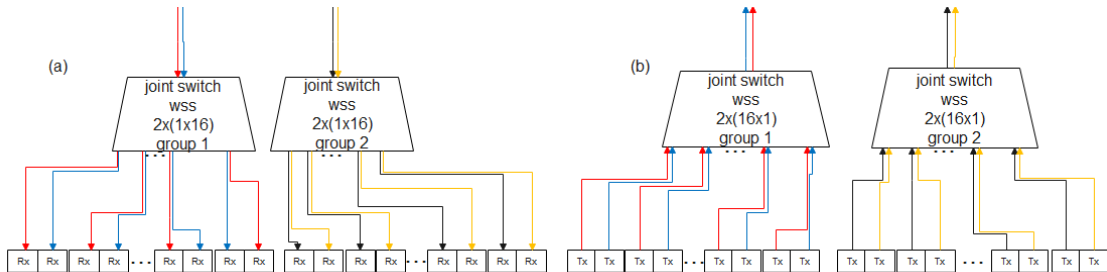
Figure 2.14: Fraction space-full wavelength granularity architecture add and drop.

2.9 Hardware cost analysis for different SDM switching architectures

In this section, we present a hardware cost analysis for the four SDM ROADM-based architectures discussed in the previous sections and having for reference a baseline scenario defined by a single fiber per direction ROADM-based architecture. First, in Tables 2.1 and 2.2, we present expressions to count the number of components (WSSs, joint switch WSSs and OXCs) and their respective dimensions (number of inputs and outputs) for the referred architectures, respectively, for the express and A/D structures. As an example, we use these expressions for a scenario with $D = 4$, $M = 12$ and $G = 4$, obtaining the results shown in Table 2.3. These results are identical to the ones presented in Table 1 of [3] and contribute to confirm the expressions presented in Table 2.1, for the express structure.

Table 2.1: Expressions used to calculate the number of components and their size in the express structure for each of the SDM architectures.

Granularity	With or without lane changes	Number of components	inputs	outputs
Spatial	Without lane changes	$N_{OXC} = M$	$D + 1$	$D + 1$
	With lane changes	$N_{OXC} = 1$	$M \times (D + 1)$	$M \times (D + 1)$
Spatial wavelength	Without lane changes	$N_{WSS} = 2 \times M \times D$	1	$D - 1 + M$
	With lane changes	$N_{WSS} = 2 \times M \times D$	1	$D \times M$
Wavelength		$N_{jointWSS} = 2 \times D$	M	$D \times M$
Fractional space-full wavelength	Without lane changes	$N_{jointWSS} = 2 \times D \times G$	$\dfrac{M}{G}$	$D \times \dfrac{M}{G}$
	With lane changes	$N_{jointWSS} = 2 \times D \times G$	$\dfrac{M}{G}$	$\dfrac{M}{G} \times [(D - 1) \times G + 1]$

Table 2.2: Expressions used to calculate the number of components and their size in the A/D structure for each of the SDM architectures.

Granularity	Number of A/D structures per architecture ($N_{A/D}$)	Number of WSSs or joint switches WSSs per A/D structure		Number of inputs of the drop structure (it is equivalent to the add structure output)		Number of outputs of the drop structure (it is equivalent to the add structure output)		Number of transponders
		Input WSS drop/ output WSS add	Output WSS drop/ input WSS add	Input WSS	Output WSS	Input WSS	Output WSS	
Spatial	2	M		1		$A/D_{ratio} \times N + 1$		$N_{A/D} \times A/D_{ratio} \times N$
Spatial-wavelength	$2 \times M$	$D \times M$	$A/D_{ratio} \times N$	1	$D \times M$	$A/D_{ratio} \times N$	1	
Wavelength	$2 \times D$	1		M		$M \times A/D_{ratio} \times N$		$M \times A/D_{ratio} \times N \times N_{A/D}$
Fractional space-full wavelength	$2 \times D$	G		$\dfrac{M}{G}$		$A/D_{ratio} \times N \times \dfrac{M}{G}$		$A/D_{ratio} \times N \times \dfrac{M}{G} \times N_{A/D} \times G$

For the architectures with spatial granularity in Table 1 of [2], the links for the A/D structures are not considered, but in Table 2.3, these connections are considered, causing a difference of M links between the results in Table 2.3 and in [2]. For the architectures with spatial-wavelength granularity, in Table 1 of [2], only one A/D link towards the A/D structure is considered, but in Table 2.3, M links towards the A/D structure are considered, which leads to a difference of $M - 1$ links between Table 2.3 and Table 1 of [2].

Table 2.3: Number of components of the express structure of a network node with degree 4, 12 spatial channels, and 4 groups.

Architectures	Number of components
Spatial granularity without lane changes	12 OXC 5×5 (in [1], the ports to the A/D structure are not considered)
Spatial granularity with lane changes	1 OXC 60×60 (in [1], the ports to the A/D structure it is not considered)
Spatial-wavelength granularity without lane changes	96 WSS 1×15 (in [1], only 1 port towards the A/D structure)
Spatial-wavelength granularity with lane changes	96 WSS 1×48 (in [1], only 1 port towards the A/D structure)
Wavelength granularity	8 joint switch WSS $12 \times (1 \times 4)$
Fractional space-full wavelength granularity without lane changes	32 joint switch WSS $3 \times (1 \times 4)$
Fractional space-full wavelength granularity with lane changes	32 joint switch WSS $3 \times (1 \times 13)$
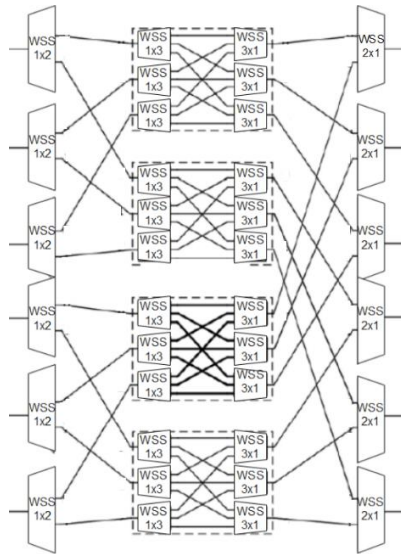
Figure 2.15: 6×6 OXC based on WSSs (taken from [10]).

For the following cost analysis, we have considered that the OXC used in the architecture with spatial granularity, is based on WSSs [10]. This OXC is more complex and have more functions that the OXC needed. The OXC needed is a OXC made with MEMS that use free space switch (an OXC with free space switch have the capacity to switch entire spatial channels but don't have the capacity to switch wavelength channels). For the cost analyses were used the OXC built with WSSs because hasn't found any cost or cost comparation for the OXC built

with MEMS. In Figure 2.15, the scheme for building an OXC 6×6 using WSSs is depicted. As can be observed, this OXC is composed only by WSSs, 12 WSSs 1×2 and 24 WSSs 1×3. In Table 2.4, the expressions used to calculate, for this type of OXC, the number of WSSs needed and the corresponding dimensions are shown. To use these expressions, the following conditions must be accomplished: $N_u = n_u \times k$ and $n_u < k$ where, *Nu* represents the number of inputs and outputs of the OXC, n_u represents the number of outputs of the input WSSs or the number of inputs of the output WSSs and *k* represents the number of outputs of the input WSSs of the central OXC or the number of inputs of the output WSS of the central OXC.

Table 2.4: Expressions used to calculate the number of elements and their size for the Expressions for the number of WSSs and their dimensions for the OXC based on WSSs.

Number of input/output WSSs of the OXC	OXC input/output
Number of outputs of the input WSSs/Number of inputs of the output WSSs	n_u
Number of central OXCs	n_u^2
Number of WSSs per central OXC	$2 \times k$
Number of outputs of input WSSs of central OXC/Number of inputs of output WSSs of central OXC	k

Next, two scenarios with 3 and 7 fibers in parallel are analyzed and compared with a reference baseline scenario with just a single fiber per direction, similarly as performed in [2]. The baseline reference scenario assumes a route and select (R&S) CDC ROADM architecture with 4 directions, 80 wavelengths per fiber and an A/D structure based on cascaded WSSs with an A/D ratio of 40% as in [2], but in [2] the A/D structure is built using multicast switches (MCSs). The cost for this scenario is normalized to one.

The scenario with 3 spatial channels considers the same features as the baseline reference scenario for all the SDM switching architectures but assumes 3 single-core single mode fibers (*M*=3) as in [2]. The scenario with 7 spatial channels considers 7 parallel single-core single-mode optical fibers (*M*=7).

The number of WSSs and their corresponding dimensions are presented in Tables 2.5 and 2.6, respectively, for the express and A/D structures, considering the baseline reference scenario, the scenario with 3 fibers and the scenario with 7 fibers.

Table 2.5: Number of components (i.e. WSSs) in the express structure for the baseline scenario, scenario with 3 spatial channels and scenario with 7 spatial channels. In the joint WSSs Table entries, the number of total ports of the WSS is also presented.

Scenarios	Architectures	Hardware required per express structure	Hardware used per express structure
Baseline reference scenario	Single spatial channel architecture	8 WSS 1 × 4	8 WSS 1 × 4
Scenario with 3 spatial channels	Spatial granularity with no lane changes	3 OXC 5 × 5	3×(6 WSS 1 × 2 + 6 WSS 2 × 1 + 12 WSS 1 × 4 + 12 WSS 4 × 1)
	Spatial granularity with lane changes	1 OXC 15 × 15	15 WSS 1 × 4 + 15 WSS 4 × 1 + 45 WSS 1 × 10 + 45 WSS 1 × 10
	Spatial wavelength granularity with no lane changes	24 WSS 1 × 6	24 WSS 1 × 10
	Spatial wavelength granularity with lane changes	24 WSS 1 × 12	24 WSS 1 × 20
	Wavelength granularity	8 joint switches WSS 3 × (1 × 4)	8 joint switches WSS 4× (1 × 4) (20 ports)
	Fraction space-full wavelength granularity without lane changes	16 joint switches WSS 2× (1 × 4)	16 joint switches WSS 2× (1 × 4) (10 ports)
	Fraction space-full wavelength granularity with lane changes	16 joint switches WSS 2× (1 × 7)	16 joint switches WSS 2× (1 × 9) (20 ports)
Scenario with 7 spatial channels	Spatial granularity with no lane changes	7 OXC 5 × 5	7×(6 WSS 1 × 2 + 6 WSS 2 × 1 + 12 WSS 1 × 4 + 12 WSS 4 × 1)
	Spatial granularity with lane changes	1 OXC 35 × 35	35 WSS 1 × 10 + 35 WSS 10 × 1 + 175 WSS 1 × 10 + 175 WSS 1 × 10
	Spatial wavelength granularity with no lane changes	56 WSS 1 × 10	56 WSS 1 × 10
	Spatial wavelength granularity with lane changes	56 WSS 1 × 28	56 WSS 1 × 40
	Wavelength granularity	8 joint switches WSS 7× (1 × 4)	8 joint switches WSS 8× (1 × 4) (40 ports)
	Fraction space-full wavelength granularity without lane changes	16 joint switches WSS 4× (1 × 4)	16 joint switches WSS 4× (1 × 4) (20 ports)
	Fraction space-full wavelength granularity with lane changes	16 joint switches WSS 4× (1 × 7)	16 joint switches WSS 4× (1 × 9) (40 ports)

In Tables 2.5 and 2.6, in the column named "hardware required", the minimum hardware number and corresponding dimensions required to build each of the SDM architectures are shown (Table 2.5 express structure, Table 2.6 A/D structure). In the column named "hardware used", the number of WSSs considered in each one of the scenarios and architectures is shown, assuming that the existing WSSs have only as possible dimensions, the dimensions considered in [2] and shown in Table 2.7.

From Table 2.5, it can be concluded that the spatial granularity architecture with lane changes is the architecture that requires more WSSs, to build the express structure. This architecture needs a total of 120 WSSs for the scenario with 3 spatial channels and 420 WSSs for the scenario with 7 spatial channels. The other SDM switching architectures are less stringent in terms of the number of WSSs in the express structure. In particular, considering the scenario with $M=3$, for the architecture with spatial-wavelength granularity, 24 WSSs 1×20

are needed, for the wavelength granularity architecture, 8 $4 \times (1 \times 4)$ joint switch WSSs are needed and for the fractional spatial-full wavelength granularity architecture, 16 $2 \times (1 \times 9)$ joint switch WSSs are needed, being the hardware count of the express structure in these three architectures very similar. Similar conclusions can be taken from Table 2.5, for the SDM architectures without lane changes.

For the scenario with M=7, in comparison with the scenario with 3 spatial channels, a significant difference exists between the hardware count of the express structure of the architecture with spatial-wavelength granularity and the hardware count of the express structure of the architectures with wavelength and fractional space-full wavelength granularity. The architecture with space-wavelength granularity has 56 WSSs, while the architectures with wavelength and fractional space-full wavelength granularity have only 8 and 16 joint switches WSSs, respectively.

With the analyses of Table 2.5, it can be concluded that, for both scenarios, the most complex express structure leads to the higher hardware count and corresponds to the express structure in the architecture with space granularity. It can be also concluded that with the increase of the number of spatial channels, the difference between the hardware count of the architecture with spatial-wavelength granularity, wavelength granularity and fractional space-full wavelength granularity becomes higher.

Table 2.6: Number of components (i.e. WSSs) in the A/D structure for the baseline scenario, scenario with 3 spatial channels and scenario with 7 spatial channels.

Case	Architecture granularity	Number of Add/Drop structures per architecture	Hardware required per Add/Drop structure	Hardware used per Add/Drop structure	Number of 100 Gbit transponders used
Baseline case	Single spatial channel architecture	2	WSS 12×32 Is done using a cascade of WSS 12 WSS 1×32 + 32 WSS 12×1	4 WSS 1×40 + 32 WSS 4×1	64
scenario with 3 spatial channels	Spatial	2	3 WSS 1×33	$3 \times$ WSS 1×40	192
	Spatial-wavelength	6	WSS 12×32	12 WSS 1×40 + 32 WSS 20×1	192
	Wavelength	8	Joint switch WSS $3 \times (1 \times 32)$	Joint switch WSS $4 \times (1 \times 39)$ (160 ports)	768
	Fraction space-full wavelength	8	2 Joint switch WSS $2 \times (1 \times 32)$	2 Joint switch WSS $2 \times (1 \times 39)$ (80 ports)	1024
scenario with 7 spatial channels	Spatial	2	7 WSS 1×33	7 WSS 1×40	448
	Spatial-wavelength	14	WSS 28×32	28 WSS 1×40 + 32 WSS 40×1)	448
	Wavelength	8	Joint switch WSS $7 \times (1 \times 32)$	Joint switch WSS $8 \times (1 \times 39)$ (320 ports)	1792
	Fraction space-full wavelength	8	2 Joint switch WSS $4 \times (1 \times 32)$	2 Joint switch WSS $4 \times (1 \times 39)$ (160 ports)	2048

From Table 2.6, it can be concluded that the architecture that requires a higher number of WSSs in the A/D structure is the architecture with spatial-wavelength granularity. For

20

the scenario with 3 spatial channels, this architecture needs 6 A/D structures, each one with 44 WSSs, whereas for the scenario with 7 spatial channels, 14 A/D structures each one with 60 WSSs are required.

The architectures that need less WSSs to build the A/D structures are the architectures with fractional space-full wavelength granularity and wavelength granularity. In these architectures, the number of joint switch WSSs is the same for the scenarios with 3 spatial channels and 7 spatial channels, but for the scenario with 7 spatial channels, the WSSs have higher dimensions. The architecture with fractional space-full wavelength granularity needs 8 A/D structures with 2 joint switch WSSs each, and the architecture with wavelength granularity needs 8 A/D structures with a single joint switches WSSs each. To build the A/D structure for the architecture with space granularity, 2 structures with 3 and 7 WSSs are needed, respectively, for the scenario with 3 and 7 spatial channels.

Furthermore, it can be concluded that the WSSs needed to build the A/D structures for architectures with fractional space-full wavelength granularity and wavelength granularity have a larger dimension and complexity in comparison with the WSSs needed to build the A/D structure for the architecture with space granularity.

The ROADM A/D structure, besides the WSSs presented in Table 2.6, have another hardware component that has influence in the cost of a ROADM node, the transponder. In Table 2.6, it is shown the number of transponders that each architecture needs. This work is portraying future networks and in future networks will be used coherent detection, hence the transponder chosen in this work, in a first analysis, is the 100 Gbit/s coherent detection transponder present in [11]. The architectures that need a higher number of transponders are the architectures with wavelength granularity and fractional space-full wavelength granularity. For the scenario with 3 spatial channels, 792 and 1024 transponders are needed, respectively, and for the scenario with 7 spatial channels, 1792 and 2048 are needed, respectively.

As a final step in this analysis, we are going to use the WSSs and transponder costs presented in Table 2.7 to obtain the total cost for each scenario. The cost of each scenario is then presented in Table 2.8. The WSSs dimensions considered in each scenario are limited to the ones presented in Table 2.7, and in agreement with [2].

The costs for the WSSs and joint switches WSSs presented in Table 2.7 were obtained following the method explained in [2](in this method it is stated that a WSS with two times the complexity is 50% more expensive e.g., A WSS 1×20 has 2 times the complexity of a WSS 1×10, hence this WSS will cost 50% more than the WSS 1×10) and normalized to the

cost of the 1×10 twin WSS (A twin WSS works as an entry WSS and exit WSS at the same time [2]). The transponder is a hardware component that is not considered in [2], for the cost calculation, and therefore, the transponder cost has been taken from [11], where it was shown that this hardware has a cost 4.54 times higher than a 1×4 WSS. Using this information, it is possible to normalize the transponder cost to the cost of the 1×10 twin WSS, e.g., if the transponder is 4.54 times more expensive than a 1×4 WSS, is 2.27 times more expensive than a twin 1×4 WSS. Hence, if a twin 1×4 WSS has a normalized cost of 0.5, the transponder will have a normalized cost of 1.14.

Table 2.7: Cost of WSSs, joint switch WSS and transponder, normalized at the cost of the 1×10 WSS [3], and power consumption of each WSS, joint switch WSS and transponder.

Twin WSS	Cost	Power (W)
1 × 2	0.25	50
1 × 4	0.5	100
1 × 10	1	150
1 × 20	1.5	200
1 × 40	2.25	240
Joint switch WSS		
20 ports	1	100
40 ports	1.5	120
80 ports	2.25	140
160 ports	3.375	160
320 ports	5.0625	180
100 Gbit/s transponder	1.14	120
400 Gbit/s transponder	2.73	200

The power consumption for each WSS has been taken from [11]. For the joint switch WSSs, it was considered that WSSs with the same complexity (number of ports) lead to the same power consumption, e.g., a joint switch WSS with 10 ports has the power consumption as a 1×10 WSS.

In Table 2.8, the total cost of the SDM architectures with and without the transponders cost is shown. When analyzing Table 2.8, it is visible that, there exists a huge difference in the architectures cost, when the transponder is considered and when it is not considered. When the transponder is considered, the architectures cost is 47% to 96% higher than when the transponder it is not considered. Hence, it can be concluded that the transponder is the hardware component that most contributes to the overall cost of the SDM architectures.

Table 2.8: Cost analysis for baseline scenario, scenario with 3 spatial channels and scenario with 7 spatial channels.

CASES	Architecture granularity	Total cost of express structure	Total cost of Add/Drop structures	Total cost without transponders	Transponder cost per architecture	Total cost with transponders
Baseline case	Single spatial channel architecture	2	25	27	72.96	99.96
Scenario with 3 spatial channels	Spatial without lane changes	22.5	6.75	29.25	218.88	248.13
	Spatial with lane changes	52.5	6.75	59.25	218.88	278.13
	Spatial wavelength without lane changes	12	225	237	218.88	455.88
	Spatial wavelength with lane changes	18	225	243	218.88	461.88
	Wavelength	8	27	35	875,52	910.52
	Fractional spatial-full wavelength without lane changes	8	36	44	1167.36	1211.36
	Fractional spatial-full wavelength with lane changes	16	36	52	1167.36	1219.36
Scenario with 7 spatial channels	Spatial without lane changes	52.5	15.75	68.25	510.72	578.97
	Spatial with lane changes	210	15.75	225.75	510.72	736.47
	Spatial wavelength without lane changes	28	945	973	510.72	1483.72
	Spatial wavelength with lane changes	63	945	1008	510.72	1518.72
	Wavelength	12	40.5	52.5	2042.88	2095.38
	Fractional spatial-full wavelength without lane changes	16	54	70	2334.72	2404.72
	Fractional spatial-full wavelength with lane changes	24	54	78	2334.72	2412.72

In Figure 2.16, a cost comparison between the different SDM architectures normalized to the cost of the baseline scenario is shown, considering the cost of the transponders. When the transponders are considered, the most expensive architectures are the architectures with wavelength granularity (with 3 and 7 spatial channels, it costs, respectively, about 9 and 20 times more than the baseline architecture) and fractional space-full wavelength granularity (with 3 and 7 spatial channels, it costs, respectively, about 12.2 and 24.1 times more than the baseline). The less expensive architecture is the architecture with space granularity (for the scenarios with 3 and 7 spatial channels, this architecture costs only, respectively, 2.78 and 7.37 times more than the baseline). The spatial-wavelength granularity costs 4.6 (*M*=3) and 15.2 (*M*=7) times more than the baseline.
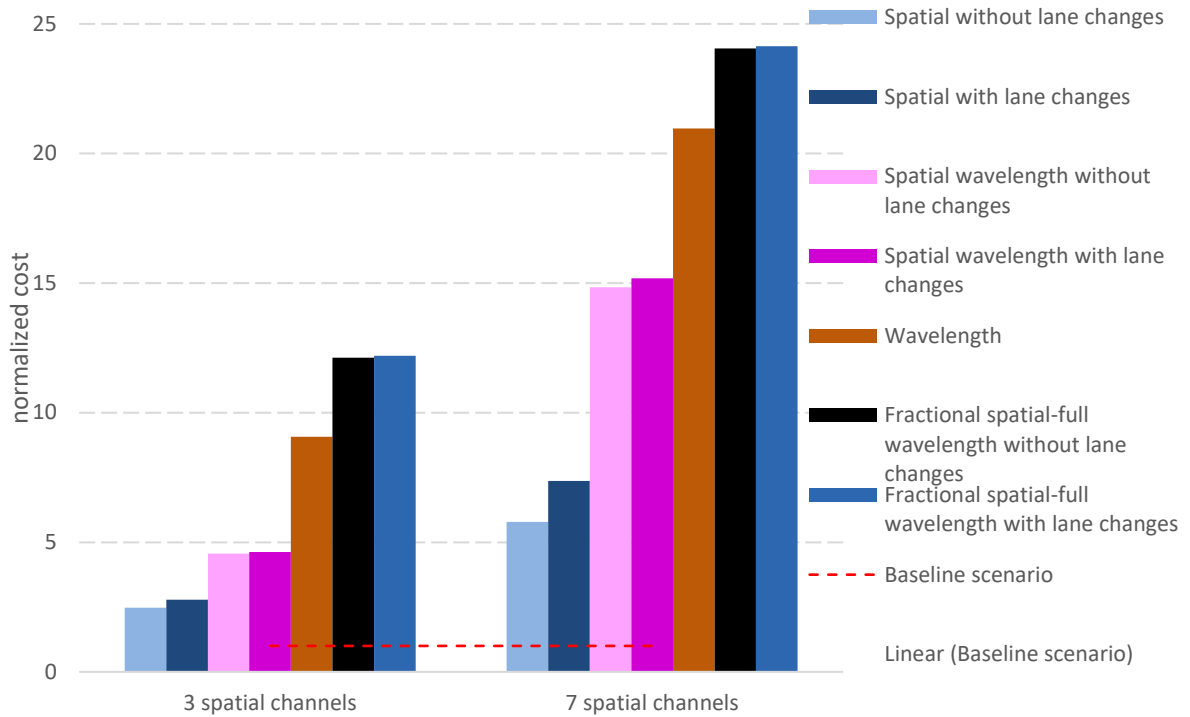
Figure 2.16: Cost normalized to the baseline scenario cost of all SDM architectures considering the transponder cost, in baseline, 3 spatial channels and 7 spatial channels scenarios.
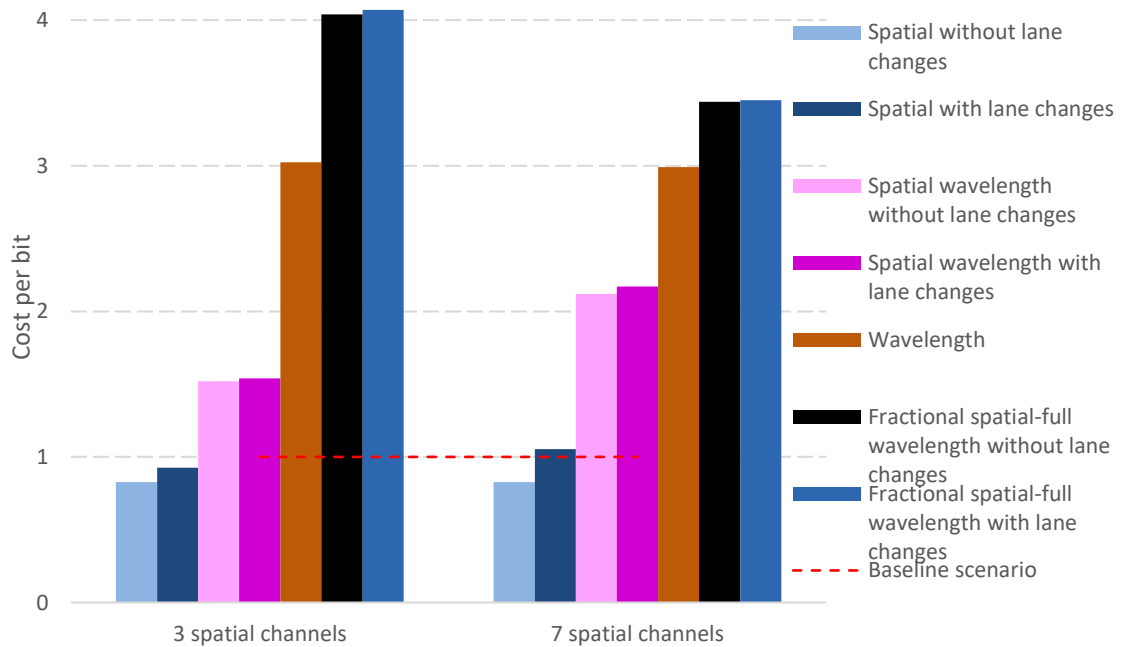
Figure 2.17: Cost per bit, normalized to the cost of the baseline scenario, of each one of the architectures considering SDM architectures, with M=3, M=7 and considering in both scenarios the transponder cost.

In Figure 2.17, it is shown the cost per bit of each SDM architecture. This cost is obtained dividing the total cost of the architecture by the transport capacity gain achieved by the use of that architecture (for example, when *M*=3, the transport capacity is 3). The cost is normalized

to the cost per bit of the baseline scenario. The comparison presented in Figure 2.17 is a more fair comparison than the one shown in Figure 2.16, because in Figure 2.17, the cost comparison is done considering the transport capacity increase brought by SDM networks. The fractional space-full wavelength granularity is the architecture with the higher cost per bit (for 3 and 7 spatial channels, it costs 4 and 3.5 times more, respectively, than the baseline). The architecture with wavelength granularity has a cost per bit 3 times higher for both scenarios, $M=3$ and $M=7$, indicating that its cost does not depend much on the number of spatial channels. The architecture with spatial granularity has a cost per bit similar to the cost per bit of the architecture considered in the baseline scenario. The architecture with space-wavelength granularity has a cost per bit of 1.5 (case with 3 spatial channels) and 2 (case with 7 spatial channels) times higher than the cost per bit of the baseline architecture.

From the analysis of Table 2.8, Figures 2.16 and 2.17, it can be concluded that the architectures with wavelength granularity and with fractional space-full wavelength granularity, do not have advantages when used in an uncoupled scenario, due to the high number of transponders required. Hence, their implementation is only advisable in scenarios with MMFs or MCFs, where the WDM signals are coupled, and the coupled channels need to be routed spatially together making mandatory the use of one of these architectures. Hence, for a scenario with uncoupled fibers (as considered in this work), the architectures that show more benefits are the architecture with space granularity (the less expensive architecture), and the architecture with space-wavelength granularity, which is the most flexible in terms of routing, and not so much costly architecture.

In Figure 2.18, the cost per bit, for the different SDM architectures, without considering the transponder is shown. In [2], where the cost of the transponders has not been also taken into account, the A/D structure is built using MCSs, while in this work, the A/D structures is built using WSSs (in a cascade). This means that, in this work, the baseline architecture and the architecture with space-wavelength granularity have a total cost, respectively, 4 and 5.66 times higher, for $M=3$, than the corresponding architectures in [2]. With the increase of the number of spatial channels to 7, the architecture with spatial-wavelength granularity have more 8 A/D structures, causing a higher difference between the cost per bit presented in Figure 2.18 and the one shown in [2].

The architecture with wavelength granularity has the same hardware in this work and in [2], but the baseline scenario in this work is more expensive. This means that, in this work, the cost per bit normalized to the cost of the baseline scenario, of the architecture with wavelength

granularity is lower than in [2]. But the cost behavior with the increase of the number of spatial channels, obtained in both works is very similar.
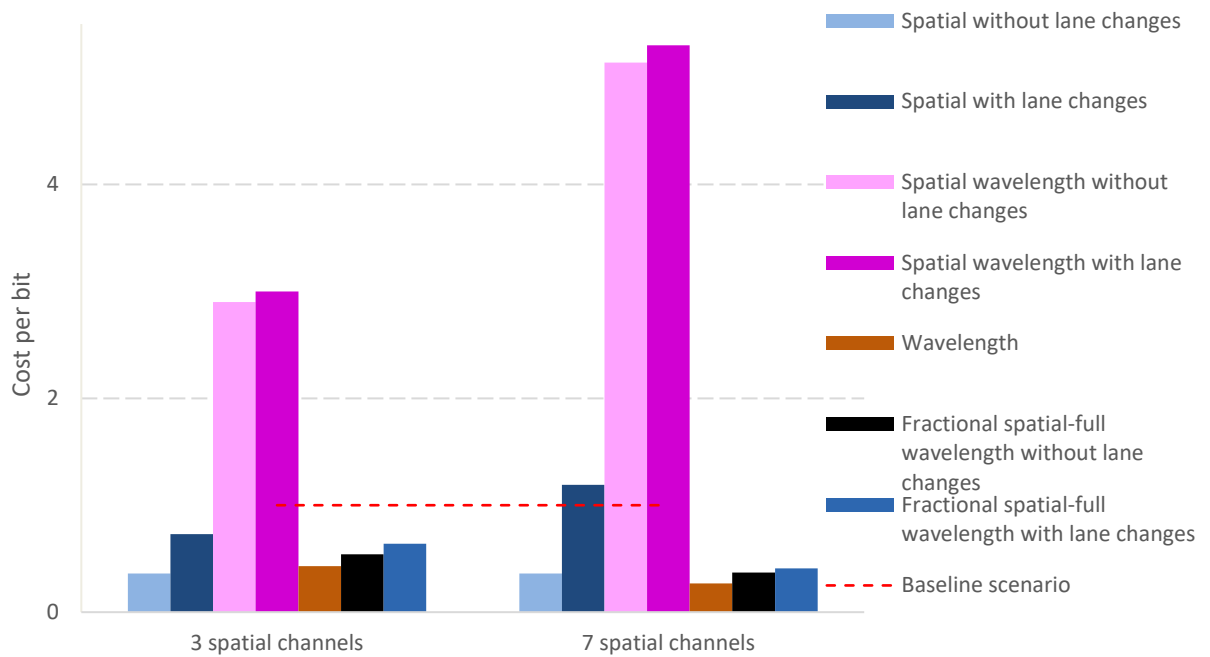
Figure 2.18: Cost per bit of each one of the architectures considering SDM architectures with M=3, M=7 and excluding the transponder cost.
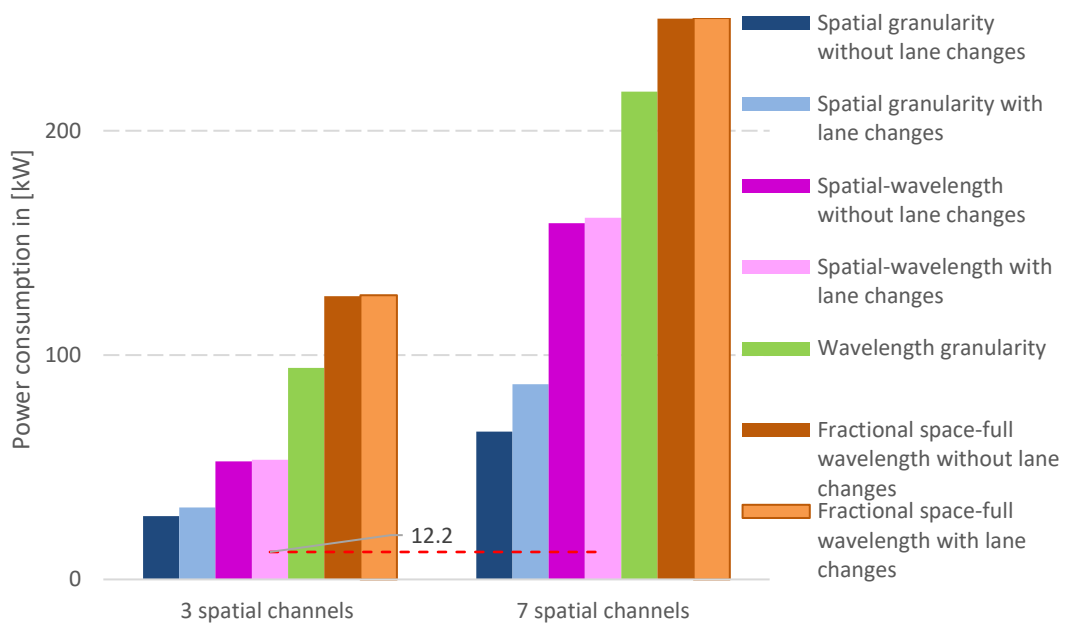
Figure 2.19: Power consumption for each one of the SDM architectures, for 3 and 7 spatial channels.

In Figure 2.19 the power consumption of each one of the SDM ROADM-based architectures with and without lane changes is shown. In Figure 2.19, the baseline scenario is presented to allow a comparison between the power consumption of SDM ROADM-based

architectures and ROADM based architecture used in the present (year 2021). The baseline scenario architecture has a power consumption of 12.2 kW. The architectures with lane changes and without lane changes have a very similar power consumption, except for the architecture with space granularity. This architecture without lane changes costs 28.3 kW and 32 kW, and with lane changes costs 65.9 kW and 86.9 kW, respectively, for the scenario with M=3 and M=7.

The architecture with the highest power consumption is the architecture with fractional space-full wavelength granularity. This architecture presents a power consumption of 126.7 kW and 250 kW, respectively, for the scenario with 3 and 7 spatial channels (with the increase of spatial channels, the power consumption practically doubles). The second most power demanding architecture is the architecture with wavelength granularity. This architecture exhibits a power consumption of 94.2 kW and 217.4 kW for M=3 and M=7, respectively. The third most power demanding architecture is the architecture with spatial-wavelength granularity, with powers demands of 53.3 kW and 161.3 kW, respectively, for M=3 and M=7. The architecture that requires less power is the architecture with space granularity.

With the analysis of Figure 2.19, as a final conclusion and in agreement with the conclusions taken from the hardware cost analysis, the architectures with wavelength and fractional space-full wavelength granularity do not bring advantages when used in an uncoupled scenario, due to their higher power consumption and lower flexibility when compared with the architecture with spatial wavelength granularity.

2.10 Cost dependence of the SDM architectures on the transponder type, number of directions, spatial channels and groups of spatial channels

In this section, we present a cost behavior analyzes, when the parameters number of spatial channels(M), number of directions (D), number of groups (G) and transponder type are changed. The cost per bit is almost the same regardless of the G, and therefore the study of the cost per bit in function of the number of groups, G, is placed in appendix A.

In Figure 2.20, the cost per bit of all SDM ROADM-based architectures and baseline scenario is presented, when 100Gbit/s and 400Gbit/s transponders are used.
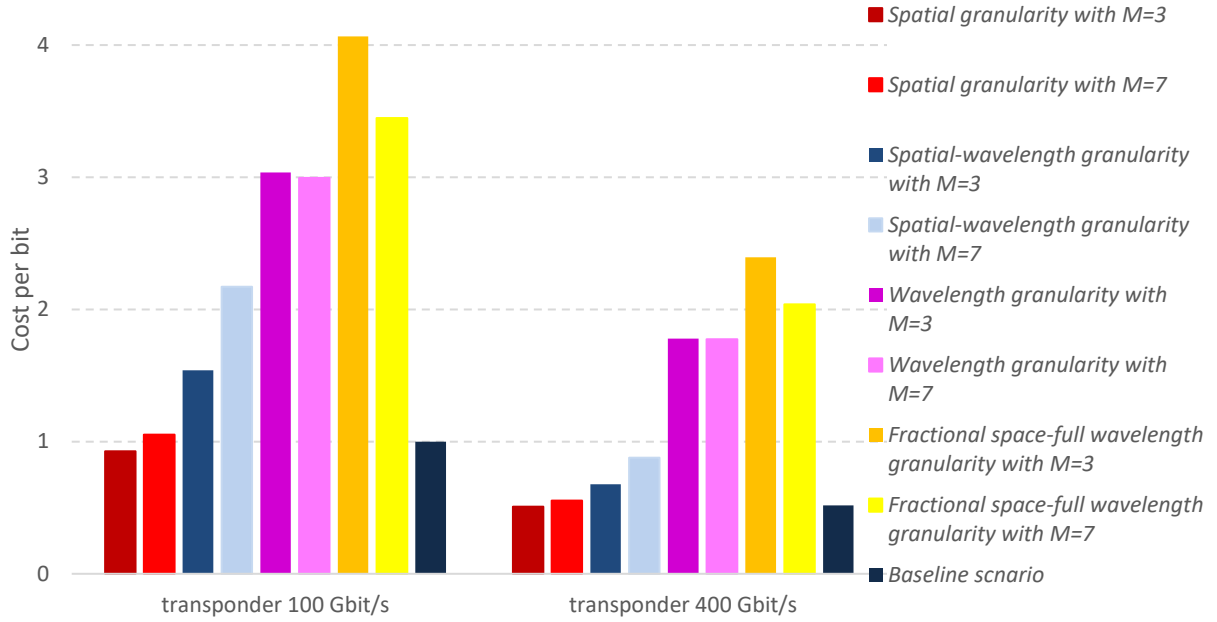
Figure 2.20: Cost per bit for SDM architectures with lane changes for 100 Gbit/s and 400 Gbit/s transponder. The cost per bit is normalized to the cost of the baseline scenario with 100G transponders.

The bandwidth usually used in an optical fiber is 4.8 THz (from 1530nm to 1565nm). For the scenario with 100 Gbit/s transponders, the following parameters are considered: 80 wavelength channels, 50 GHz of channel spacing, and the transmitted signals use a QPSK modulation format [12]. With these parameters, the bandwidth occupied per fiber is 4 THz and the transported capacity per fiber is 8 Tbit/s. In order to perform a fair comparison between scenarios with different transponders, we decided to keep the same bandwidth in both scenarios (4THz). For the scenario with 400 Gbit/s transponders, 53 wavelength channels with a 75 GHz of channel spacing and 16-QAM signals have been considered [12]. With these parameters, the bandwidth occupied in this scenario is nearly the same as the one occupied in the 100 Gbit/s transponders (4 THz), but the transport capacity is higher (21.2 Tbit/s).

It can be concluded from Figure 2.20 that scenario with 400 Gbit/s transponders, when compared with the scenario that uses 100 Gbit/s transponders has 2.65 times more capacity using 1.45 times less transponders, but the transponders are 2.4 times more expensive. Hence, the cost per bit in the 400 Gbit/s SDM architectures is always lower than the 100 Gbit/s scenario cost per bit, because the capacity increase and number of transponders decrease contribute more to the cost per bit than the transponder cost increase.
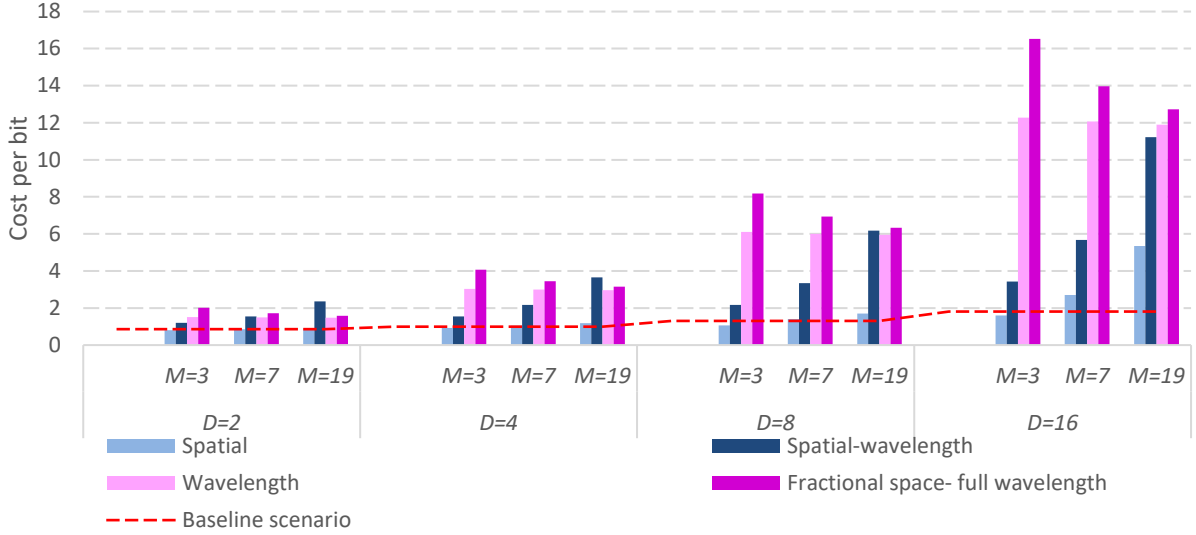
Figure 2.21: Cost per bit of the SDM ROADM-based architectures with lane changes, normalized to the cost per bit of the baseline scenario with 4 directions, as a function of the number of ROADM directions, D, and number of spatial channels, M.

In Figure 2.21, the cost per bit, as a function of the number of ROADM directions and number of spatial channels, for all SDM ROADM-based architectures and for the baseline scenario is shown. This cost is normalized to the cost of the baseline scenario with $D = 4$. For all directions, it can be concluded that an increase of the number of spatial channels causes: 1) an increase of the cost per bit of the architectures with spatial and spatial-wavelength granularity, 2) a decrease of the cost per bit of the architecture with fractional space-full wavelength granularity and 3) practically does not affect the cost per bit of the wavelength granularity architecture. When the number of directions is increased, a substantial increase in the cost per bit of all architectures is observed, except for the architecture with space granularity, where the cost increase is not so pronounced.

From Figure 2.21, it can be also concluded that the architectures with wavelength and fractional space-full wavelength granularity can lead to some cost advantages, in uncoupled scenarios, when $D < 8$ and $M = 19$ because, in these conditions, they are less expensive than the architecture with space-wavelength granularity. The architectures with wavelength and fractional space-full wavelength granularity in this conditions are less expensive than the architecture with space-wavelength granularity, because with the increase of the number of spatial channels the number of WSSs for the architecture with spatial-wavelength increase (causing a high increase in the cost), but for the architectures with wavelength and fractional space-full wavelength granularity this increase in the number of WSSs does not exist, for this architectures the number of WSSs increase when the number of directions increase. Therefore, when the number of spatial channels is high, and the number of directions is low the

architectures with wavelength and fractional space- full wavelength are less expensive than the architecture with space-wavelength granularity and have some cost advantages in being use.

Figure 2.22: Power consumption of all SDM ROADM-based architectures with lane changes, as a function of the number of ROADM directions, D, and number of spatial channels, M.

In Figure 2.22, the power consumption in [KW], as a function of D and M, for all SDM ROADM-based architectures, is shown. The power consumption for the baseline scenario is not shown in Figure 2.22, because it is too low. The power consumption for the baseline scenario varies from 9.9 kW (scenario with 2 directions), to 21.1 kW (scenario with 16 directions). For all architectures, a higher number of directions or number of spatial channels causes a higher power consumption. The increase of spatial channels leads to a more significant power consumption growth, for the architecture with spatial-wavelength granularity. For example, with D=8 the increase of spatial channels from 7 to 19 leads to a power consumption, 2.91, 4.78, 2.69 and 2.47 times higher, respectively, for the architectures with space, spatial-wavelength, wavelength and fractional space-full wavelength granularities. The increase of the number of directions causes a higher power consumption for the architectures with wavelength, spatial-wavelength and fractional space-full wavelength granularity. This appends because for the architecture with space granularity the increase of the number of directions does not increase, the number of WSSs or number of A/D structures, as much as in the others architectures. For example, with 19 spatial channels and increasing the number of directions from 4 to 8, the architectures with wavelength and fractional space-full wavelength granularity have an increase of 2 times and the architectures with space and spatial-wavelength granularity have an increase of 1.2 and 1.6 times, respectively).

30

From Figure 2.22, it can be concluded that the architectures with wavelength and fractional space-full wavelength granularity can lead to some advantages regarding the power consumption when $D < 8$ and $M = 19$, in comparison with the architecture with space-wavelength granularity. The reason for this has explained when Figure 2.21 has analyzed.

Table 2.9: Evaluation of the SDM ROADM-based architectures in terms of cost, power consumption and flexibility. The architectures are ranked in a scale, where (4) denotes the best and (1) denotes the worst architecture.

Architectures	Cost	Power consumption	Flexibility
Spatial granularity	(4)	(4)	(1)
Spatial-wavelength granularity	When $M \neq 19$ or $D > 4$, (3) Otherwise (1)	When $M \neq 19$ or $D > 4$, (3) Otherwise (1)	(4)
Wavelength granularity	When $M = 19$ or $D < 4$, (3) Otherwise (2)	When $M = 19$ or $D < 4$, (3) Otherwise (2)	(2)
Fractional space-full wavelength granularity	When $M = 19$ or $D < 4$, (2) Otherwise (1)	When $M = 19$ or $D < 4$, (2) Otherwise (1)	(3)

In Table 2.9, a ranking based evaluation for the SDM ROADM-based architectures, is presented. The architectures are ranked by numbers (4-best to 1-worst) in three categories: cost, power consumption and flexibility. The architectures with wavelength and fractional space-full wavelength granularity do not have benefits in being used, in the majority of the cases. These architectures are more expensive, more power demanding and less flexible than the architecture with spatial-wavelength granularity. The architecture with space granularity is the less expensive, less power demanding and the least flexible. The architecture with space-wavelength granularity is the most flexible but is more expensive and more power demanding than the architecture with space granularity. Hence, for uncoupled networks, when the choice is based just on cost per bit, power consumption and flexibility, the most promising architectures are the architectures with space-wavelength granularity and space granularity. The choice of the ideal architecture will depend on the flexibility required. For example, if we want to transport signals from city to city is not needed an architecture with high flexibility. Therefore, in this case we can choose the architecture with space granularity but if we want to transport signals inside a city, a certain level of flexibility that can't be delivered by the architecture with space granularity is needed. Hence, in this case we need to use the architecture with space-wavelength granularity.

2.11 Conclusion

In this chapter, the different SDM architectures were analyzed in terms of cost, power consumption and flexibility, for an uncoupled scenario. The architectures with wavelength granularity and fractional space-full wavelength granularity were developed to be used in coupled scenarios, because in a coupled scenario the coupled wavelength channels need to be routed together until the receiver. However, these architectures can also be use in uncoupled scenarios. The architecture with spatial granularity can be constructed with WSSs-based OXCs or with MEMS-based OXCs. The cost and power consumption analyzes were only done for the architecture with WSSs-based OXCs, because we didn't found any relation between the MEMS cost and the others hardware cost. The cost of the architecture with spatial granularity done with MEMS-based OXCs was considered close to the cost of the architecture with spatial granularity done with WSSs-based OXCs.

The architecture with spatial-wavelength granularity is the more flexible architecture and in the majority of the cases, has less cost and power consumption than the architectures with wavelength and fractional space-full wavelength granularities. The architecture with spatial granularity is the less expensive and has less power consumption, but it is also the architecture with less flexibility. The architectures with wavelength and fractional space-full wavelength granularities are less flexible and have higher cost and power consumption than the architecture with spatial-wavelength granularity. In this chapter was also analyzed the cost per bit when used 100 Gbit/s transponders and 400 Gbit/s transponders and was verified that the 400 Gbit/s transponder has lesser cost per bit.

With this analyses was concluded that the architectures with wavelength and fractional space-full wavelength granularities do not have advantages in being used in an uncoupled scenario, because these architectures have less flexibility, higher cost and higher power consumption than the architecture with spatial-wavelength granularity.

Chapter 3: Physical impairments in SDM ROADM-based networks

3.1 Introduction

In this chapter, the study of the physical layer impairments (PLIs) that impair the performance of the SDM ROADM-based networks considering the architectures that have spatial and spatial wavelength granularities, is performed. This study is performed only for these two architectures, because in the evaluation of cost and power consumption performed in the previous chapter, it has been concluded that the architectures with wavelength and fractional space-full wavelength granularity do not have advantages for uncoupled scenarios. The physical impairments that are going to be analyzed are the SDM ROADM architecture insertion losses, ASE noise arising from amplification in the network, crosstalk due to signal leakage inside the nodes, and passband narrowing due to the optical filtering performed by the WSSs inside the node.

3.2 Insertion losses in SDM ROADM-based networks

The insertion losses depend on the losses of the various components that a signal crosses along an optical path inside the node. In this section, we analyze the insertion losses of each node component, the insertion losses along each node path and the amplification needed to compensate all these insertion losses.
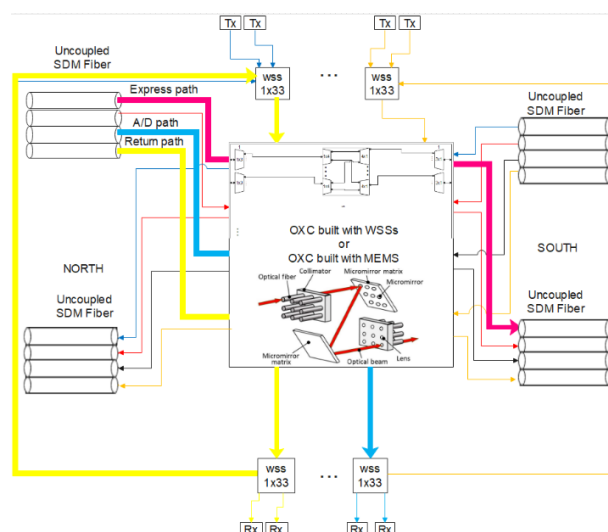
Figure 3.1: The three optical paths of the signal inside the architecture with spatial granularity with WSSs-based OXC or with 3D MEMS-based OXC: A/D path (blue bold line), express path (pink bold line) and return path (yellow bold line).

In Figure 3.1, the optical paths that a signal can travel inside a ROADM with spatial granularity with M=4, D=2, N=80 and a A/D ratio of 40% that leads to an extraction capacity of 32 wavelength channels [2] are shown, particularly, the A/D (blue bold line), express (pink bold line) and return paths (yellow bold line), considering OXCs to perform the optical switching. The OXCs can be built using WSSs or 3D-MEMSs.

For the architecture with spatial granularity built with WSS-based OXCs, a spatial channel needs to pass through the OXC no matter the path, crossing at least 4 WSSs. Hence, a spatial channel in an express path has to pass a total of 4 WSSs. In the A/D path, a spatial channel has to pass a total of 5 WSSs. In an A/D scenario, for the architecture with spatial granularity, the wavelengths channels that form a spatial channel that are not dropped, must return to the ROADM. These wavelength channels that are not dropped cross a total of 10 WSSs.

In Figure 3.1, it is also shown a scheme of a 3D MEMS-based OXC. In Table 2 of [13], several MEMS switches with different technologies and with a different number of input/output ports are shown. The most suitable MEMS-based OXC for a particular application scenario can be chosen from Table 2 of [13], depending on several parameters, e.g., the number of ports, insertions losses, switching time and crosstalk. For the scenarios with M=3 and M=7, respectively, 15×15 and 35×35 OXCs, are required. For both scenarios, due to the limitations due to the number of input/output and insertion losses, the most adequate OXCs are:

1) A 80×80 OXC that uses a MEMS switch with free-space switching [13]. This OXC has 2.6 dB of insertion losses, switching time of 1 ms and crosstalk of around -60 dB.

2) A 64×64 OXC that uses a MEMS switch with waveguide switching [13], with insertion losses of 3.7 dB, switching time of 0.91 μs and crosstalk of around -60 dB.

In networks where the switching time is of most importance, the second OXC should be chosen, but in this work, we have given more relevance to the insertion losses and since the first OXC has lower insertion losses than the second, the first OXC has been chosen to be used in the spatial node architecture.

In the architecture with spatial granularity that uses 3D MEMS-based OXCs, the express channels cross only one time the OXC. The A/D channels pass by an OXC and a WSS and the spatial channels that are returned to the ROADM cross two WSSs and two times the OXC.

34
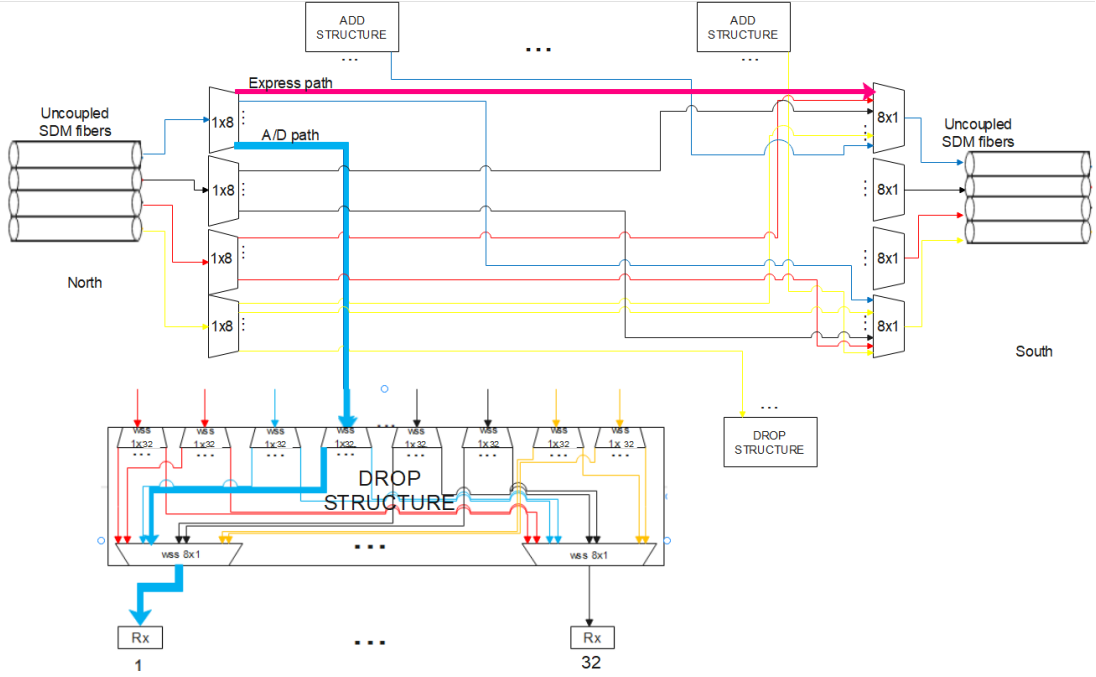
Figure 3.2: Optical paths that the signal crosses inside the architecture with spatial-wavelength granularity: A/D (blue bold line) and express paths (pink bold line).

In Figure 3.2, the optical paths that a signal travels inside the architecture with spatial-wavelength granularity with 2 directions, 4 spatial channels and an A/D of 40%, are shown. Figure 3.2 is an illustrative figure that represents part of a SDM ROADM-based architecture. The express path, is represented by the pink bold line and the A/D path, is represented by the blue bold line. The wavelength channels in the A/D path need to pass by an input WSS and by the A/D structure where, as shown in Figure 3.2, they cross two WSSs. For the A/D path, the wavelength channels pass a total of 3 WSSs. Hence, for the express path, the wavelength channels pass a total of 2 WSSs.

Table 3.1: Number of hardware components crossed by the channels along the express, A/D and return paths and corresponding insertion losses for the SDM ROADM-based architectures with spatial and spatial-wavelength granularities, considering M=3 and M=7.

Architectures	Hardware in the express path	Hardware in the A/D path	Hardware in the return path	Insertion losses in the express path (dB)	Insertion losses in the A/D path (dB)	Insertion losses in the return path (dB)
Spatial granularity with OXC built with WSSs and with M=3	4 WSSs	5 WSSs	10 WSSs	25.6	32.5	64.9
Spatial granularity with OXC built with WSSs and with M=7	4 WSSs	5 WSSs	10 WSSs	25.8	32.6	65.2
Spatial granularity with OXC built with MEMS and with M=3 and M=7	one 80×80 OXC	one 80×80 OXC + 1 WSS	two 80×80 OXC + 2 WSSs	3	9.6	19.2
Spatial wavelength granularity with M=3	2 WSSs	3 WSSs	-	13.1	19.9	-
Spatial wavelength granularity with M=7	2 WSSs	3 WSSs	-	13.5	20.4	-

In Table 3.1, the number of hardware components that a channel passes in each node path and corresponding insertion losses, are presented for the SDM ROADM-based architectures with spatial and spatial-wavelength granularities, for M=3 and M=7. The WSS insertion losses (I_{l_WSS}) in dB are calculated using [14]:

$$I_{l\_WSS} = \log_2(N_{output} + N + 1) \tag{3.1}$$

where N represents the number of wavelength channels and N_{output} represents the number of outputs of a WSS. For the typical number of WDM channels (considering a channel spacing of 50 GHz) and WSS outputs used in optical networks (from 80 to 96 wavelength channels and from 4 to 35 WSS outputs), equation (3.1) gives insertion losses between 6 and 7 dB. The architecture with spatial-wavelength granularity has around 13 dB of insertion losses for the express path and 20 dB of insertion losses for the A/D path, for both M=3 and M=7, hence, leading to the conclusion that the insertion losses do not depend much on the number of spatial channels. The architecture with space granularity when the OXC is built with WSSs has around 25, 32 and 65 dB of insertion losses, respectively, for the express, A/D and return paths, for both M=3 and M=7. The architecture with spatial granularity when the OXC is built with MEMS has around 3, 10 and 19 dB of insertion losses, respectively, for the express, A/D and return paths, for both M=3 and M=7, which means that the insertion losses are practically independent on the number of spatial channels, and depend only on the number of hardware components traversed. The architecture with spatial granularity that uses WSSs-based OXCs is excluded from the subsequent analysis because of its high insertion losses.
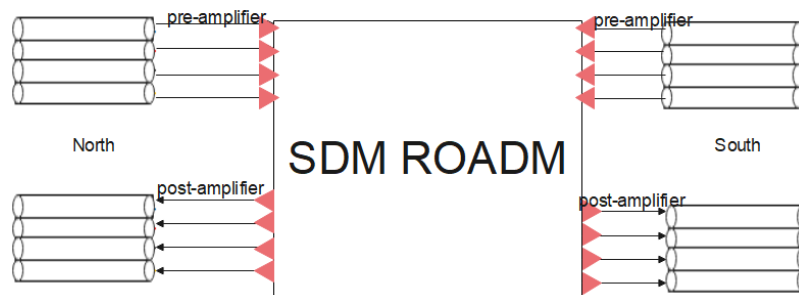
Figure 3.3: Post and pre-amplifiers that are required to compensate the losses of the SDM ROADM-based architectures.

In Figure 3.3, the optical amplifiers (OAs) used to compensate the fiber span and ROADMs losses for the architectures with spatial and spatial-wavelength granularities, are shown. The OAs considered are erbium-doped fiber amplifiers (EDFAs). To compensate the losses of a ROADM that uses the architecture with spatial granularity with MEMS-based OXCs or the architecture with spatial-wavelength granularity, only post amplification is required. The pre-

amplifier compensates the losses that are caused by the fiber span. The gain of this amplifier depends on the span length and fiber attenuation coefficient, e.g., for a section with L_{sec} =80 km (section length) and with α=0.2 dB/km (fiber attenuation coefficient), the gain of the pre-amplifier must be 16 dB. The gain of the post-amplifier is set to compensate the insertion losses of the ROADM, add, express or return optical path, with the highest insertion losses. Therefore, the gain of the pos-amplifier depends on the SDM ROADM-based architecture used. In the optical paths with lower insertion losses, variable optical attenuators (VOA) are used to level the signal power of all channels that leave the node.

The SDM ROADM-based architecture with spatial granularity that uses 3D MEMS-based OXCs has a post-amplifier with 19.2 dB of gain, set by the return path losses, and two groups of VOAs. The first group VOAs is placed in the expressed path at the OXC output and adds 16.2 dB of losses. The second group of VOAs is placed in the A/D path between the OXC and 1×33 WSS, and adds 9.6 dB of losses. The SDM ROADM-based architecture with spatial-wavelength granularity has a post-amplifier with 20.4 dB of gain to compensate the losses of the add path and VOAs, in the express path located between the input and output WSSs that adds 6.9 dB of losses.

3.3 ASE noise accumulation in SDM ROADM based networks

In this section, we are going to analyze the ASE noise accumulation in networks with ROADM architectures with spatial and spatial-wavelength granularities. This analysis is done by assessing the ASE noise in an optical path along a cascade of ROADMs, as shown in Figure 3.4.

Figure 3.4: Optical path along an optical network, represented as a cascade of SDM ROADM nodes. The pink triangles represents the pre-amplifiers, the green triangles represents the post-amplifiers and N_r represents the number of ROADMs.

The ASE noise is caused by the OAs and accumulates along the optical path. The ASE noise power at the end of the cascade is given by:

$$p_{ase} = p_{post} + p_{pre} \tag{3.2}$$

$$p_{pre} = \sum_{i=1}^{N_r-1} p_{n,pre,i} \tag{3.3}$$

$$p_{post} = \sum_{i=1}^{N_r-1} p_{n,post,i} \tag{3.4}$$

where $p_{n,pre,i}$ represents the ASE noise power originated in the ith optical pre-amplifier, $p_{n,post,i}$ is the ASE noise power originated in the ith post-amplifier, p_{pre} represents the accumulated ASE noise power that is originated from pre-amplification and p_{post} represents the accumulated ASE noise power arising from post-amplification. Equations (3.2)-(3.4) are only suitable if the network gain is 0 dB (exact loss compensation). In a network with exact loss compensation, the post-amplifier compensates exactly the ROADM losses and the pre-amplifier compensates the fiber span losses.

The noise power originated in each amplifier for two polarizations can be calculated with:

$$p_n = f_n \times (g_n - 1) \times B_o \times h \times \nu_o \tag{3.5}$$

where f_n and g_n are, respectively, the noise figure and gain of each optical amplifier. The gain is typically set to exactly compensate the losses, i.e., $g_n = g_{pre}$, if it refers to the gain of a pre-amplifier, and $g_n = g_{post}$, if it corresponds to a post-amplifier. The parameter ν_o is the center channel frequency, h is the Planck constant (6.62607×10^{-34} m^2 kg/s) and B_o is the optical bandwidth. To use equation (3.5), it is considered that all spans are similar.

The optical bandwidth B_o in a coherent detection scenario can be calculated using [15], [16], [17]:

$$B_o = R_{s,l} \tag{3.6}$$

where $R_{s,l}$ is the symbol rate in one polarization. In a coherent system the optical bandwidth corresponds to the symbol rate, because it is used a pulse with a square-root raised-cosine spectrum with zero roll-off factor (ρ) [15],[16],[17]. This bandwidth allows the best spectral efficiency. The symbol rate $R_{s,l}$ for one polarization is calculated using:

$$R_{s,l} = \frac{R_{b,l}}{2 \times \log_2(N_s)} \tag{3.7}$$

where $R_{b,l}$ is the line rate and N_s is the number of symbols used in a N_s-Quadrature amplitude modulation (QAM) scheme.

Table 3.2: Network parameters used to analyze the ASE noise accumulation in the architectures with spatial and spatial-wavelength granularities, with M=7.

Architectures	R_b (Gbit/s)	FEC overhead (%)	$R_{b,l}$ (Gbit/s)	N_s	B_o (GHz)	F_n (dB)	ν_o (THz)	L_{sec} (km)	α (dB/km)	G_{pre_amp} (dB)	G_{post_amp} (dB)
Spatial granularity	100	20	120	4	30	6.9	193.8	80	0.2	16	19.2
Spatial-wavelength granularity											20.4

In Table 3.2, the network parameters considered to calculate the ASE noise accumulation, are shown. The typical values for F_n, ν_o, α and overhead due to Forward error correction (FEC) are, respectively, between 4 and 7 dB (we have considered a F_n of 6.9 dB [18]), 193.1 THz, 0.2 dB/km [19] and soft decision (SD)-FEC with an overhead of 20% [20]. The ASE noise power originated per polarization in each post-amplifier of the architecture with spatial granularity is 0.77 µW, in each post-amplifier of the architecture with spatial-wavelength granularity is 1.02 µW and in each pre-amplifier, in both architectures, is 0.365 µW.

Considering a cascade with $N_r = 10$, the accumulated ASE noise power in two polarization at the optical receiver input obtained with (3.2) is 20.47 µW for a network with a ROADM-based architecture with spatial granularity and 24.95 µW for a network with a ROADM-based architecture with spatial-wavelength granularity.

The system performance can be quantified by the optical signal-to-noise ratio (OSNR) that for a fiber with linear transmission can be defined by [21]:

$$osnr = \frac{p_s}{p_{ase}} \tag{3.8}$$

where p_s represents the signal power measured in any point of the optical communication system, and p_{ase} represents the ASE noise power measured at that same point. Typically, the OSNR is measured at the receiver input and must be higher than the OSNR required to ensure a specific bit error ratio (BER) [21]. The higher the measured OSNR, the higher the system margin.

In this case, with exact loss compensation, for a p_s of 0 dBm, the network that uses the ROADM architecture with spatial granularity has an OSNR of 16.9 dB at the optical receiver input and the network that uses the ROADM architecture with spatial-wavelength granularity

has a OSNR of 16 dB. So, for a purely linear fiber transmission the architecture with spatial granularity is slightly better in terms of OSNR, 0.85 dB, for the example considered.

3.4 Nonlinear interference in SDM ROADM-based networks

In this section, we are going to analyze the system performance for the same scenario analyzed in section 3.3 but considering the NLI. The NLI power at the WDM center channel is given by [22]:

$$p_{NLI} = B_o \times g_{NLI}(v_o) \tag{3.9}$$

where $g_{NLI}(v_o)$ is the NLI power spectral density (PSD), that can be obtained using [23]:

$$g_{NLI}(v_o) = N_{span} \times [g_{XCI}(v_o) + g_{SCI}(v_o)] \tag{3.10}$$

where N_{span} represents the number of fiber spans, $g_{SCI}(v_o)$ is the self-channel interference noise power spectral density and $g_{XCI}(v_o)$ is the cross-channel interference noise power spectral density. The NLI power and PSD are calculated for the central wavelength channel because, the central wavelength channel is the most affected by the NLI effects, this is shown in Figures 5 and 6 of [24] and in Figure 3 of [23]. The self-channel interference noise power spectral density can be calculated using [23]:

$$g_{SCI}(f_m) = G_m^3 \times \frac{3\gamma^2}{2\pi\alpha|\beta_2|} \times \text{arcsinh}\left(\frac{\pi^2|\beta_2|}{2\alpha} \times \Delta f_m^2\right) \tag{3.11}$$

where f_m represents the nominal frequency of channel m, γ represents the fiber non-linearity coefficient, Δf_m represents the bandwidth of the WDM channel, which for the Nyquist spectrum shaping, $\Delta f_m = R_{s,l}$, $|\beta_2|$ represents the group velocity dispersion parameter, G_m represents the signal PSD of the central channel. The signal PSD and group velocity are calculated, respectively, by using [23], [24]:

$$G_m = \frac{p_s}{\Delta f_m} \tag{3.12}$$

$$|\beta_2| = \frac{D_\lambda \times \lambda_0^2}{2\pi \times c} \tag{3.13}$$

where D_λ is the fiber dispersion coefficient, c is the light velocity and λ_0 is the wavelength of the central channel. The cross-channel interference noise PSD is calculated using [23]:

$$g_{XCI}(f_m) = G_m \times \frac{3\gamma^2}{2\pi\alpha|\beta_2|} \times \sum_{\substack{m'=1 \\ m \neq m'}}^{N} \left[G_{m'}^2 \times \ln\left(\frac{|f_m - f_{m'}| + \frac{\Delta f_m}{2}}{|f_m - f_{m'}| - \frac{\Delta f_m}{2}} \right) \right] \tag{3.14}$$

where $f_{m'}$, represents the frequency of the channel m' and $G_{m'}$ is the signal PSD of the cross channel m'.

To assess the NLI effect on the link performance, the NLI parameter η_{NLI} of the link must be calculated using [22]:

$$\eta_{NLI} = \frac{p_{NLI}}{p_s^3} \tag{3.15}$$

where the NLI power is obtained using equation (3.9) for a specific signal power p_s. With the NLI parameter, it is possible to characterize the NLI induced degradation in the optical link and calculate the optimum channel power that must be launched to maximize the OSNR in presence of ASE noise and NLI, using [24]:

$$p_{ch,opt} = \sqrt[3]{\frac{p_{ase}}{2 \times \eta_{NLI}}} \tag{3.16}$$

The OSNR in presence of ASE noise and NLI noise can be obtained using [22],[21]:

$$osnr_{NLI} = \frac{p_s}{p_{ase} + p_{NLI}} \tag{3.17}$$

The OSNR obtained for the optimum channel power in presence of NLI and ASE noise, as given by equation (3.17), have an OSNR penalty of 1.76 dB in relation to the OSNR obtained for the same channel power with only ASE noise, as given by equation (3.8).

Table 3.3: Network parameters considered to calculate the NLI noise power

$R_{s,l}$ (GBaud)	N	D_λ (ps/nm/km)	γ (W^{-1}km^{-1})	Signal power P_s in two polarizations (dBm)	Δv_{ch} (GHz)
30	80	18	1.1	0	50

Table 3.4: OSNR with the NLI and ASE noise effects.

Architectures	P_s (dBm)	$G_{SCI}(v_o)$ (dBm/GHz)	$G_{XCI}(v_o)$ (dBm/GHz)	$G_{NLI}(v_o)$ (dBm/GHz)	p_{NLI} (μW)	η_{NLI}	OSNR (dB)
Spatial-wavelength granularity	0	-54.11	-48.82	-38.15	9.17	36695	14.67
Spatial granularity	0						15.28
Spatial-wavelength granularity	0.43, optimum signal power	-52.77	-47.49	-36.82	12.5		14.70
Spatial granularity	0.15, optimum signal power	-53.6	-48.4	-37.68	10.2		15.29

In Table 3.3, the network parameters considered to calculate the NLI power are presented. Also, in Table 3.4, the results of the self-channel interference PSD, cross-channel interference PSD, NLI PSD, NLI power and OSNR are presented. These results are calculated, for a channel power of 0 dBm and for the optimum channel power, after a cascade of 10 ROADMs considering ROADM-based architectures with spatial and spatial-wavelength granularities. It was verified that our results lead to an OSNR penalty of 1.76 dB in relation to the absence of NLI noise. For example, for a network with ROADMs architectures with spatial-wavelength granularity, the OSNR using (3.8) is 16.46 dB and using (3.17) is 14.7 dB, hence the OSNR penalty is 1.76 dB.

The achieved OSNR, when the optimum channel power is considered, is only slightly better than for the 0 dBm channel power, because the estimated optimum channel power is nearly 0 dBm, when considering a QPSK modulation. For an optical link considering the NLI effects, the network with the ROADM architecture with spatial granularity leads to a 0.6 dB better OSNR in comparison with the one obtained for the architecture with spatial-wavelength granularity.

3.5 In-band crosstalk in SDM ROADM-based networks

In this section, the in-band crosstalk that is generated inside SDM ROADM architectures with spatial and spatial-wavelength granularities is analyzed. The crosstalk is a physical layer impairment, that is caused mainly by the finite isolation of optical components [25], [26]. The imperfect isolation of these components causes power leakages that lead to signal degradation

at the receiver. These power leakages are the interfering terms that will impair the selected signal.

The crosstalk can be classified in two types [25]:

1) In-band crosstalk or homodyne crosstalk: this crosstalk occurs when the interfering signals have the same nominal wavelength of the selected signal [27],[25], [26]. This crosstalk can be originated from the same optical source or from different sources. The in-band crosstalk that is originated from the same source can be coherent or incoherent [27],[25]. The in-band crosstalk that is originated from different sources is always incoherent [25]. In this work, we are going to study the in-band incoherent crosstalk originated from different optical sources, since it is usually the one that leads to a higher performance degradation [28].

2) Out-of-band crosstalk or heterodyne crosstalk: this crosstalk is originated when the interfering signals have a different nominal wavelength than the selected signal [25]. This type of crosstalk is not very harmful, if the channel spacing is sufficiently large, because, in this case, it can be effectively removed by filtering at the optical receiver. In this work, it is considered a bit rate of 100 Gbit/s, 50 GHz of WDM channel spacing, and sharp optical filtering. Hence, the out-of-band crosstalk can be considered insignificant, as shown in [29].

Furthermore, the order of the interfering signal (or term) corresponds to the number of times that an interfering signal beats the components isolation. Typically, only first and second order interfering terms are meaningful to the performance degradation caused by crosstalk and are the ones that are usually analyzed as can be observed in [7].
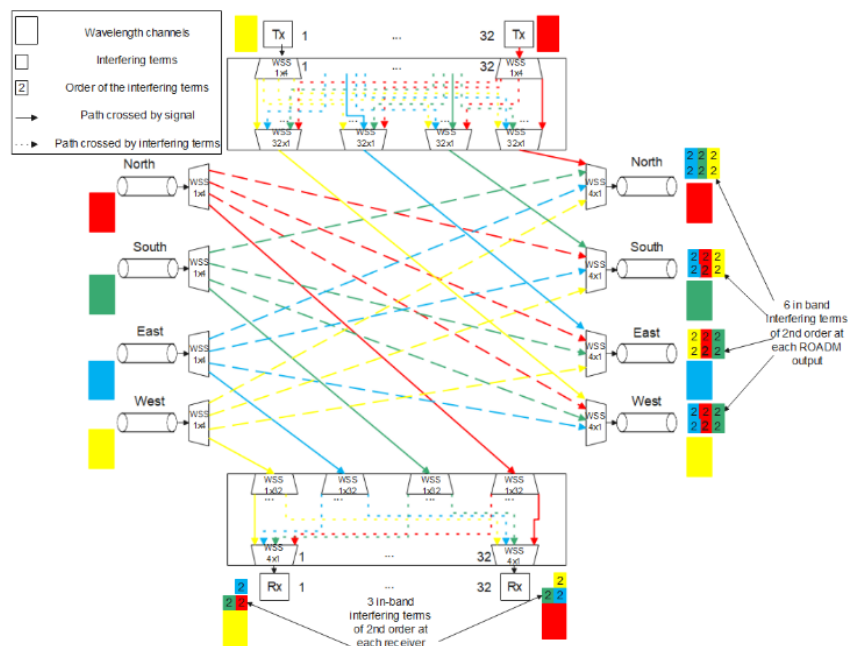
Figure 3.5: In-band crosstalk interfering terms for the baseline architecture for D=4, M=1, N=80 and a A/D ratio of 40%. The different colors are just used to clarify the different paths that the wavelengths λ_1 travel along the node.

In Figure 3.5, the interfering terms in the baseline architecture with D=4 and with an A/D ratio of 40%, caused by in-band crosstalk at the nominal wavelength λ_1, are shown for the worst-case scenario. This worst-case scenario occurs when all input wavelength channels λ_1 are dropped and new wavelength signals are added at the same nominal wavelength and directed to the ROADM outputs. As the baseline architecture has 4 directions, the worst-case scenario occurs when four wavelength channels λ_1 are dropped and four wavelength channels λ_1 are added. In Figure 3.5, the rectangles represent wavelength channels at λ_1, the squares represent the in-band crosstalk interfering terms appearing at the ROADM outputs, the number inside of the squares represents the order of the interfering term, the solid lines represents the selected path used by the wavelength signal inside the node, the dashed lines represents the path used by an in-band interfering term and the different colors represent the different sources, e.g., the red lines represent optical paths traveled by signals or interfering terms that come from or go to the north direction.

The selected signal at the optical receiver input of the drop structure is interfered by three in-band interfering terms of 2nd order. These three interfering terms are originated by leakage in three WSSs 1×32 of the drop structure, that are sent to WSSs 4×1 of the drop structure. These three in-band interfering terms also beat the isolation of these WSSs 4×1 of the drop structure becoming interfering terms of 2nd order, whose paths are represented by the three dashed lines linked to WSS 4×1 input.

In the ROADM output of each direction, the added signal is interfered by six interfering terms of 2nd order. In Figure 3.5, it is shown that, three of these terms come from the ROADM inputs concerned to other directions, and travel the optical paths represented by the three dashed lines, that come from the input WSSs 1×4. The other three interfering terms come from the add structure. In the add structure, due to leakage on the WSS 1×4, at each WSS 32×1 input, 3 in-band interfering terms of 1st order can arrive. Due to leakage at these WSSs, the interfering terms reach the output of the ROADM as in-band interfering terms of 2nd order.
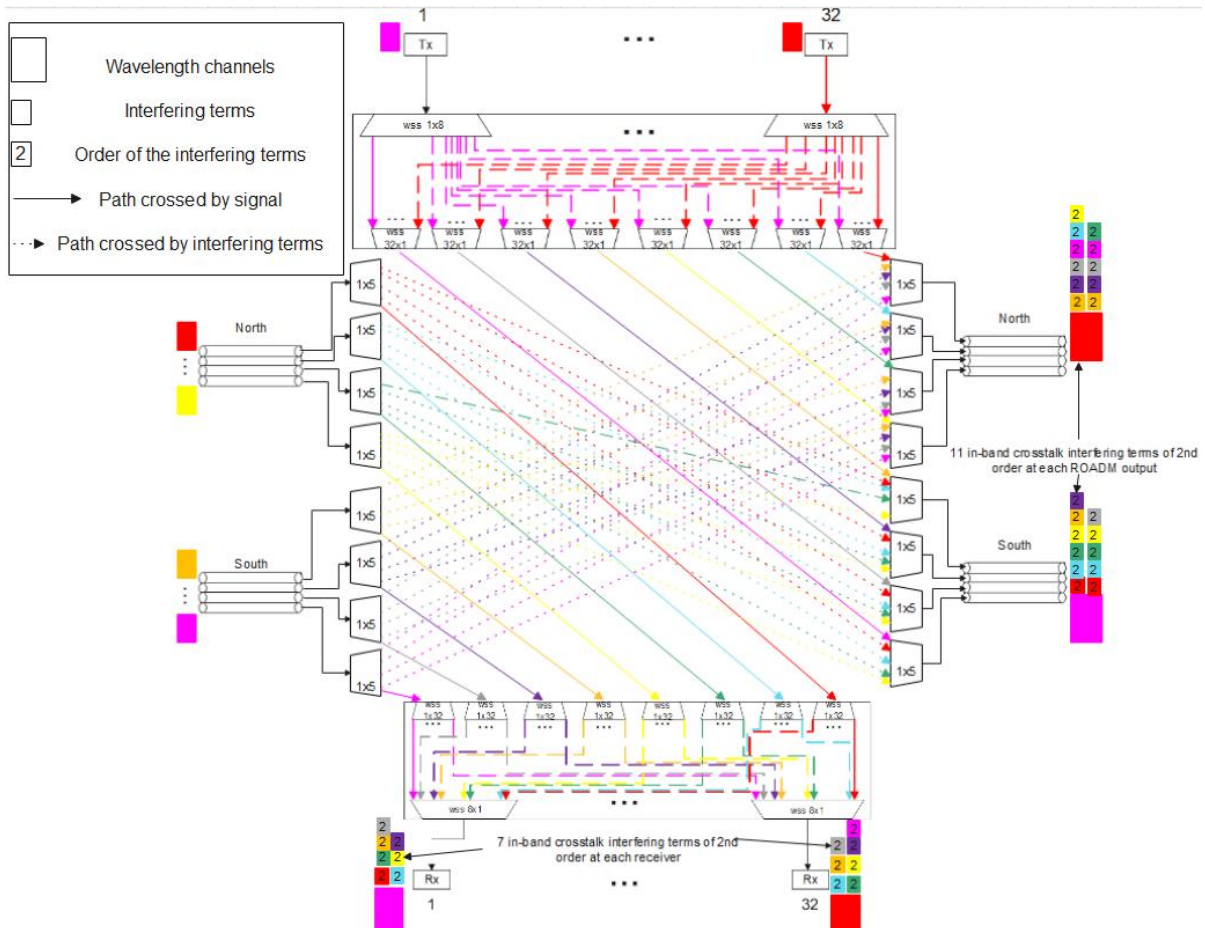
Figure 3.6: In-band crosstalk interfering terms for the architecture with spatial-wavelength granularity with D=2, M=4 and A/D ratio of 40%. The different colors are used to clarify the different paths that the wavelengths λ_1 follow along the node.

In Figure 3.6, the interfering terms that are caused by in-band crosstalk in the architecture with spatial-wavelength granularity with 2 directions, 4 spatial channels, 80 wavelength channels and an A/D of 40%, are shown. The worst-case scenario in this architecture is the same as in the baseline architecture. This architecture has four times more fibers per direction than the baseline architecture analyzed in Figure 3.5, hence, in order to simplify the analysis only two directions have been considered.

The selected signal λ_1 at the receiver input of the drop structure may be interfered by seven 2nd order in-band interfering terms, due to leakage on the WSSs 1×32 and 8×1. The path traveled by these interfering terms is represented in the drop structure by the dashed lines that come from the WSS 1x32 to WSS 8x1.

At the ROADM outputs of each direction, the added signal is interfered by eleven interfering terms of 2nd order. Four of the eleven interfering terms result from leakage on the input WSSs 5×1 and output WSSs 1×5. The four dotted lines that come from the input WSS to the output WSS represent the express paths traveled by these four in-band interfering terms. The remaining seven interfering terms are added in the add structure due to leakage on the WSSs 1×8 and 32×1, which after are sent to the ROADM output with the added wavelength signal λ_1.
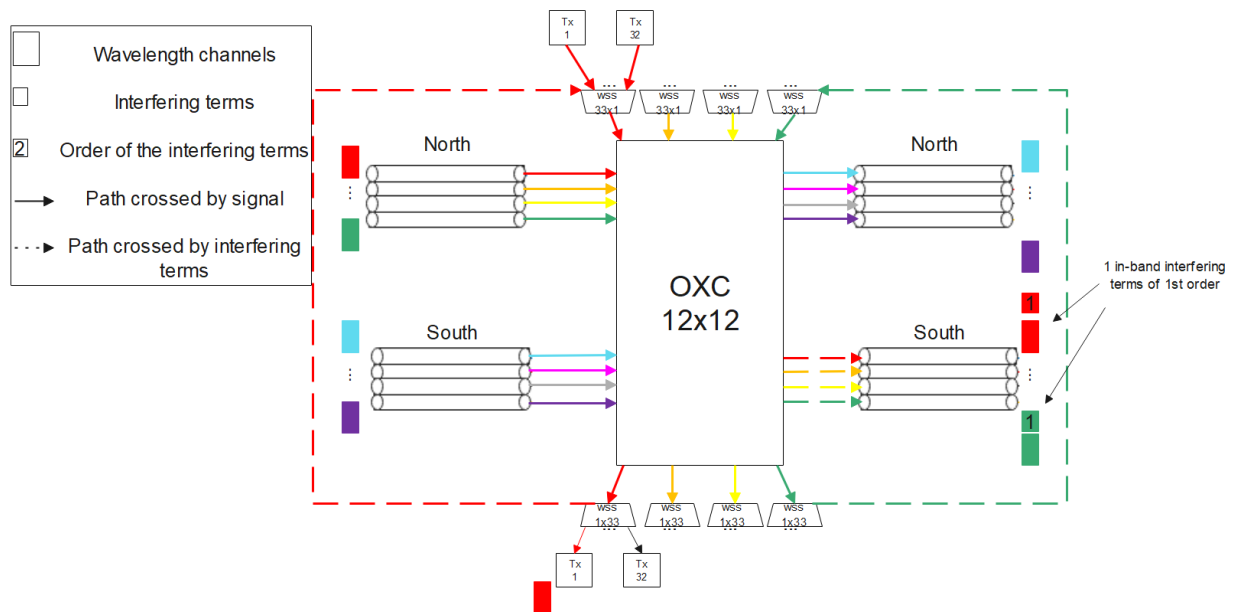
Figure 3.7: In-band crosstalk interfering terms for the architecture with spatial-granularity. The different colors are just used to clarify the different paths that the wavelengths λ_1 travel along the node.

In Figure 3.7, the interfering terms that are caused by in-band crosstalk in the architecture with spatial granularity with *D*=2, *M*=4, *N*=80 and an A/D ratio of 40%, are analyzed. The worst case scenario in this architecture occurs when: 1) four wavelength channels λ_1 from the four spatial channels of the north direction are dropped; 2) the spatial channels from the south direction are expressed to the output of the north direction; 3) four wavelength channels λ_1 are added and directed to the ROADM output of the south direction. The worst-case scenario in this architecture is different from the worst-case scenario in the baseline architecture and in the architecture with spatial-wavelength granularity, because in the spatial architecture considered in this work and in [2], it is not possible to drop wavelength channels that have the same spatial channel but are in different directions. To allow the simultaneous drop of wavelength channels that have the same spatial channels but are in different directions, the node hardware components should be re-designed and improved.

46

In this architecture, a MEMS-based OXC with -60 dB of crosstalk is considered. Therefore, the high isolation of the OXC leads to insignificant crosstalk introduction. Hence, in this architecture, a wavelength channel λ_1 may be only interfered at the ROADM output by one in-band interfering term of 1st order. The interfering term results from leakage on the WSS 1×33 at the drop structure, which is sent to the WSS 33×1 at the add structure by the return path and sent to the ROADM output with the added signal at λ_1.

Table 3.5: Number of in-band interfering terms at the ROADM output and at the input of the optical receivers of the drop structure in the baseline, spatial-wavelength granularity and spatial granularity architectures.

Architectures	2nd order interfering terms at the receivers input of the drop structure	2nd order interfering terms at the ROADM output	1st order interfering terms at the ROADM output
Baseline architecture or SDM architecture with spatial wavelength granularity	$(D \times M) - 1$	$((D - 1) \times M) + ((D \times M) - 1)$	-
SDM architecture with spatial granularity	−	−	1

In Table 3.5, the expressions that allow the calculation of the number of 1st order and 2nd order in-band interfering terms at one ROADM output for the worst-case scenario in the baseline, spatial-wavelength and spatial granularities architectures, are presented. The architecture with less in-band interfering terms is the architecture with space granularity. This architecture has always one in-band interfering term, because the switching in this architecture is performed by the OXC, which has a very high isolation. The architecture with more in-band interfering terms is the architecture with spatial-wavelength granularity. This architecture has more interfering terms because, as shown in Table 3.5, the number of interfering terms increases with the number of spatial channels. The baseline architecture is a special case of the spatial-wavelength granularity architecture, by considering *M*=1. The derived expressions of the baseline scenario have been validated and are in agreement with the expressions presented in Table 4.1 of [27].

In Figure 3.8, the number of interfering terms in the architecture with spatial-wavelength granularity as a function of the ROADM directions (*D*) and number of spatial channels (*M*), is shown. The results for the baseline architecture correspond to the ones obtained for *M*=1. With the increase of the number of directions or spatial channels, the number of signals that pass across the ROADM also increases.
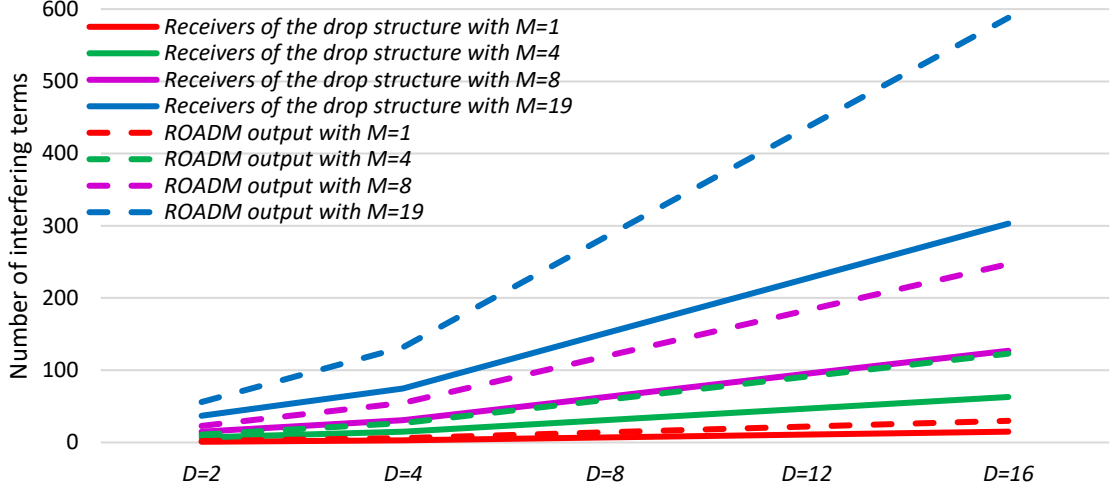
Figure 3.8: Number of interfering terms in the architecture with spatial-wavelength granularity as a function of the ROADM directions and number of spatial channels.

Therefore, in the architecture with spatial-wavelength granularity, the number of interfering terms increases with the increasing number of directions and spatial channels, has shown by expressions of Table 3.5 and in Figure 3.8. For example, the baseline scenario with 16 directions has 15 interfering terms at one receiver input of the drop structure and 30 at one ROADM output. With the increase of spatial channels to 19, for D=16, the number of interfering terms increases to 303 interfering terms (20 times more interfering terms than in the baseline architecture) in the receivers of the drop structure and 588 interfering terms (19.5 times more interfering terms than in the baseline architecture) at one ROADM output.

Table 3.6: Number of interfering terms and total crosstalk for A=- 35 dB and for the baseline architecture, architecture with spatial granularity and architecture with spatial-wavelength granularity with D=16.

Architectures with D=16	Number of interfering terms	Total crosstalk (dB)
Receiver of the drop structure (baseline architecture, M=1)	15 interfering terms of 2nd	-58.2
ROADM output (baseline architecture, M=1)	30 interfering terms of 2nd	-55.2
Receiver of the drop structure (Spatial granularity, M=19)	0	0
ROADM output (Spatial granularity, M=19)	1 interfering terms of 1st	-35
Receiver of the drop structure (Spatial-wavelength granularity, M=19)	303 interfering terms of 2nd	-45.2
ROADM output (Spatial-wavelength granularity, M=19)	588 interfering terms of 2nd	-42.3

In Table 3.6, it is shown the number of interfering terms and the total in-band crosstalk in ROADMs with the baseline architecture, architecture with spatial granularity and architecture with spatial-wavelength granularity. In this analysis, it is considered that each WSS has a typical isolation (*A*) between *A* = -30 and *A* = -40 dB [30], [31]. The total crosstalk level can be calculated using:

48

$$X_T[dB] = 10 \times \log_{10}\left(n_i \times 10^{\frac{(-A)\times n_{order}}{10}}\right) \qquad (3.18)$$

where n_i is the number of interfering terms, A is the isolation of the WSSs and n_{order} is the order of the interfering term.

From Table 3.6, it can be concluded that, for a single ROADM node, the architecture with less tolerance to in-band crosstalk is the architecture with spatial granularity. This architecture has only one interfering term of 1st order that leads to a total crosstalk of -35 dB. The architecture with spatial-wavelength granularity has more in-band interfering terms than the architecture with spatial granularity, but these terms are 2nd order and lead to less total crosstalk than the interfering term of 1st order present in the architecture with spatial granularity (-45.2 dB). These levels of crosstalk (in the worst case -35dB) are not significant, according with figure 6 of [32] and with figure 5.13 of [33].

In the following, we are going to analyze the impact of in-band crosstalk in a cascade of ROADMs. When a wavelength channel goes through a cascade of ROADMs, three scenarios occur: add, express and drop. In this analysis, we are going to consider the worst in-band crosstalk cases for the add, express and drop scenarios.

1) For the add scenario, that occurs one time when the signal is added to the network, in the worst case of crosstalk, the number of interfering terms at the ROADM output can be calculated with the expression presented in Table 3.5 and can be observed in Figure 3.6 at the ROADM output; 2) The express scenario occurs 8 times, and in the worst crosstalk case the selected wavelength channel is interfered by one less interfering term than when the signal is added. Therefore, the number of interfering terms, in this scenario, can be calculated by subtracting one to the result obtained from the expression used in the worst add scenario; 3) The drop scenario occurs 1 time, and the number of interfering terms at the receiver of the drop structure, in the worst-case, can be calculated using the expression shown in Table 3.5 and can be observed in Figure 3.6 at the receivers input.

In Table 3.7, the number of interfering terms and the total crosstalk after a cascade of 10 ROADMs for the baseline, spatial granularity and spatial-wavelength granularities is presented for A =-25, A =-30, A =-35 and A =-40 dB.

Table 3.7: Total crosstalk and number of interfering terms in a cascade of 10 ROADMs, for the baseline, spatial granularity and spatial-wavelength architectures with D=16 and M=19.

Architectures	Interfering terms in a worst add scenario	Interfering terms in a worst express scenario	Interfering terms in a worst drop scenario	Total number of interfering terms ROADM	Total crosstalk with A = -25 dB (dB)	Total crosstalk with A = -30 dB (dB)	Total crosstalk with A = -35 dB (dB)	Total crosstalk with A = -40 dB (dB)
Baseline	30	29	15	277, 2nd order	-25.58	-35.6	-45.6	-55.6
Spatial granularity	1	0	0	1, 1st order	-25	-30	-35	-40
Spatial-wavelength granularity	588	587	303	5587, 2nd order	-12.53	-22.5	-32.5	-42.5

From Table 3.7, it can be concluded, that after crossing 10 ROADMs with WSSs with $A = -25$, $A = -30$ and $A = -35$ dB, the less tolerant architecture to in-band crosstalk is the architecture with spatial-wavelength granularity. If the WSSs used has an isolation of $A = -40$ dB, the architecture that leads to a higher crosstalk level after 10 cascaded ROADMs is the architecture with spatial granularity. The architecture with spatial-wavelength granularity has 5587 interfering terms of 2nd order and the architecture with spatial granularity has only one interfering term of 1st order. When the isolation is high ($A = -40$ dB), the in-band interfering terms of 2nd order lead to an insignificant contribution to the total crosstalk, hence, the interfering term of 1st order in the spatial granularity architecture causes more total crosstalk. When the isolation is lower, the high number of in-band interfering terms of 2nd order lead to a the total crosstalk level in the spatial-wavelength granularity architecture higher than the ones obtained for the spatial granularity architecture.

According with [32], [33], if the total level of crosstalk is less than -30 dB, the OSNR penalty due to in-band crosstalk can be considered neglected. To calculate the OSNR penalty caused by in-band crosstalk, we are going to consider that the in-band crosstalk can be modelled as an additive noise with a Gaussian distribution [34]. With this assumption, the effect of the in-band crosstalk in the OSNR is calculated using:

$$osnr_{XT} = \frac{p_s}{p_{ase} + p_{NLI} + p_{XT}} \qquad (3.19)$$

where p_{XT} represents the total crosstalk power measured at the optical receiver input. This equation is equivalent to equation (2) of [34]. The crosstalk power can be obtained using:

$$p_{XT}[\text{mW}] = 10^{\frac{P_s(dBm)-X_T}{10}} \qquad (3.20)$$

where X_T is given by equation (3.18). The OSNR penalty due to crosstalk is obtained by:

$$\Delta OSNR = OSNR_{NLI} - OSNR_{XT} \qquad (3.21)$$

where $OSNR_{NLI}$ is the OSNR without crosstalk given by equation (3.17) and $OSNR_{XT}$ is the OSNR with crosstalk given by equation (3.19). From equation (3.21), the OSNR penalty due to in-band crosstalk in the architecture with spatial-wavelength granularity with $A = -30$ dB and $A = -25$ dB is, respectively, 0.66 dB and 4.23 dB. According with the simulation results presented in [33], for a total crosstalk of -30 dB, the OSNR penalty for the architecture with spatial-wavelength granularity will be 0.2 dB, which is on the same order of magnitude than the OSNR penalty obtained through equation (3.21). For the architecture with spatial granularity with $A = -30$ dB, the OSNR penalty obtained from (3.21) is only 0.14 dB. For all the other cases shown in Table 3.6, where the total crosstalk is lower than -30 dB, the OSNR penalty can be neglected.

By considering the OSNR penalties due to in-band crosstalk, for WSSs with isolation of -30 dB, the OSNR at the optical receiver input after a cascade of 10 ROADMs with $D = 16$, $M = 19$ and spatial-wavelength granularity architecture, is 14.05 dB, while for the same scenario but using the architecture with spatial granularity, the OSNR is 15.15 dB. So, by considering the in-band crosstalk penalty, our results show that the architecture with spatial granularity leads to an OSNR improvement of about 1.1 dB in relation to the spatial-wavelength architecture.

3.6 Passband narrowing due to optical filtering in SDM ROADM-based networks

In this section, we are going to describe the types of filters used to model the WSS operation, the transfer functions used to characterize these filters and analyze their performance in the architectures with spatial and spatial-wavelength granularities in terms of passband narrowing due to WSSs cascading. The WSS operation can be modelled using two types of filtering, the passband filter and the stopband filter [27], [35]. The wavelength channels that pass through the WSS are filtered by the passband filter (these wavelength channels are affected by the passband narrowing) and the wavelength channels blocked by the WSS are filtered by the stopband filter (these wavelength channels correspond to the crosstalk terms) [27], [35].

The optical passband filter is modeled by a nth order Super-Gaussian optical filter [7], [35] as:

$$H_p(f) = e^{-\left[\frac{f^2}{2\times\sigma_{sg}^2}\right]^n} \tag{3.22}$$

where n is the order of the filter, f is the frequency and σ is obtained using [7], [35]:

$$\sigma_{sg} = \frac{B_{mdB}}{2 \times \left[2 \times \left(\ln\sqrt{10^{\frac{m}{10}}}\right)^{\frac{1}{n}}\right]^{\frac{1}{2}}} \tag{3.23}$$

where B_{mdB} is the -m dB bandwidth of the filter and m is the filter bandwidth parameter. For example, if the filter bandwidth is measured at -3 dB, from the maximum point, then, $m = 3$. The stopband filter is modeled by the inversion of the transfer function of the optical passband filter and by setting a blocking amplitude [7]:

$$H_b(f) = 1 - (1-a) \times e^{-\left[\frac{f^2}{2\times\sigma_{sg}^2}\right]^n} \tag{3.24}$$

where a is the blocking amplitude A in linear units.

The signals more affected by the passband narrowing are the signals that pass through more WSSs. In Table 3.1, the number of hardware components that a signal crosses in each path, inside a SDM ROADM node is presented. A wavelength signal, that crosses a ROADM with the spatial-wavelength granularity architecture crosses, respectively, for the express and A/D scenarios 2 and 3 WSSs. Therefore, in a ROADM with this architecture, the signals that are dropped or added are more affected by the filtering effects. A signal that crosses a ROADM with the spatial granularity architecture crosses, respectively, for the express, A/D and return scenarios 0, 1 and 2 WSSs. Therefore, in a ROADM with this architecture, the signals that are returned to the ROADM are more affected by the filtering effect.

In a cascade of 10 ROADMs with the architecture with spatial-wavelength granularity, a wavelength channels needs to cross 22 WSSs, considering its insertion at the first ROADM and extraction at the last ROADM. In a cascade of 10 ROADMs with the architecture with spatial granularity, a wavelength channels crosses a total of 18 WSSs. In the in-band crosstalk analysis it is also considered the return path, but in terms of in-band crosstalk interfering terms the return path and express path are the same.

According with [29], the OSNR penalty after 20 WSSs, for a network with WSSs modulated by a Super-Gaussian optical filter of order 4.2 with a B_{-3dB} of 46.4 GHz,

polarization-division multiplexing quadrature phase-shift keying modulation (PDM-QPSK), R_b =100 Gbit/s, $\Delta v_{ch} = 50$ GHz and $R_s = 32.5$ Gbaud , is 0.3 dB. This network parameters are similar to the ones considered in this chapter. Hence, we can consider that the OSNR penalty due to the passband narrowing along the cascade of nodes corresponds approximately the values taken from [29]. Therefore, by including this penalty in the OSNR given by equation (3.19), the OSNR estimated along a cascade of 10 ROADMs with the spatial-wavelength granularity architecture is 13.75 dB, considering ASE noise, NLI, in-band crosstalk and optical filtering passband narrowing. For the cascade of 10 ROADM nodes with the architecture with spatial granularity, the OSNR obtained with the same PLIs is 14.85 dB. Hence, the use of the ROADM architecture with spatial granularity leads to a 1.1 dB higher OSNR than when the ROADM architecture with spatial-wavelength granularity is used.

3.7 Required OSNR in SDM based networks

The BER is the number of bit errors divided by the total number of transferred bits during a studied time interval, and is typically the ultimate quality performance indicator of an optical network. To ensure a pre-determined quality, the line BER (before FEC at the optical receiver) must be lower than a pre-defined limit that depends on the FEC implementation [20], [36]. For a FEC overhead of 20%, the post-FEC BER is 10^{-15} and the line required BER must be typically in the order of 2.7×10^{-2} [36]. To guarantee this line BER, the minimum OSNR required at the optical receiver input must be satisfied. For a N_s-QAM modulation, the theoretical bit error probability, which is equivalent to the line BER, can be obtained from [21]:

$$P_{b,l} = \frac{2}{\log_2(N_s)} \times \left(1 - \frac{1}{\sqrt{N_s}}\right) \times \text{erfc}\left(\sqrt{\frac{3 \times snr}{2 \times (N_s - 1)}}\right) \tag{3.25}$$

where *snr* defines the electrical signal-to-noise ratio. The *snr* for a specific line BER can be obtained by solving equation (3.25) and related with the OSNR using [21]:

$$osnr_{req,B_{ref}} = \frac{p \times R_{s,l} \times snr}{2 \times B_{ref}} \tag{3.26}$$

where *p*=2, if the signal transmission uses polarization-division multiplexing (PDM) or *p*=1, in the absence of PDM, and B_{ref} is the reference bandwidth (typically 12.5 GHz [7]). The $OSNR_{req,B_{ref}}$ calculated using equation (3.26) is for the reference bandwidth, but the OSNRs

calculated for the networks in this work are obtained for the signal bandwidth, therefore they must be converted using [21]:

$$osnr_{req,signal} = \frac{B_{ref}}{B_o} \times osnr_{ref,B_{ref}} \tag{3.27}$$

Table 3.8: System margin and OSNR required in the signal bandwidth and reference bandwidth, for a network with PDM-4-QAM and both spatial architectures, for a transmission penalty of 1.5 dB.

Architectures	A (dB)	FEC overhead (%)	Post-FEC BER	Line BER	$OSNR_{req,B_{ref}}$ (dB)	$OSNR_{req,signal}$ (dB)	$OSNR_{network}$ (dB)	System Margin (dB)
Spatial granularity	-30	20	10^{-15}	2.7×10^{-2}	9.5	5.7	14.85	7.6
Spatial-wavelength granularity							13.75	6.5

In Table 3.8, the OSNRs required to reach a certain line BER in the reference bandwidth, and in the signal bandwidth, the OSNRs that reach an optical receiver in the networks with both architectures and corresponding system margin, are shown. The system margin (in [37], called residual margin) can be obtained with [37]:

$$S_{margin} = OSNR_{network} - OSNR_{req,signal} - \Delta P_t \tag{3.28}$$

where ΔP_t represents the transmission penalty, that is usually between 1 and 1.5 dB and is used to set a safety margin and to account for additional system performance degradation [37].

From Table 3.8, it can be observed that the use of a ROADM architecture with spatial granularity leads to a 7.6 dB margin to achieve the specified target line BER and the use of the ROADM architecture with spatial-wavelength granularity leads to a 6.5dB margin. Therefore, our theoretical results indicate that, both ROADM architectures, after 10 cascaded ROADMs, can accomplish safely the BER performance criterion, by considering that in order to safely accomplish the BER performance criterion the system margin should be over 3 dB (by considering this we have a safety margin of 3 dB to count with unexpected effects).

The maximum number of ROADMs that can be crossed by a signal without compromise the network performance, can be obtained by increasing the number of cascaded ROADMs until the system margin reaches 3 dB. For a network with a ROADM architecture with spatial

54

granularity it was concluded that a signal can cross 25 ROADMs, and for a network with a ROADM architecture with spatial-wavelength granularity a signal can cross 21 ROADMs.

3.8 Conclusion

In this chapter, the insertion losses of the architectures with spatial granularity built with WSSs, spatial granularity built with MEMS and spatial-wavelength granularity have been analyzed. From the calculated insertion losses, the gain of the optical amplifiers and VOAs in the network has been defined, and it has been concluded that the ROADM architecture with spatial granularity built with WSSs is the one that leads to the highest insertion losses, therefore, requiring much more amplification gain than the other two architectures. Hence, the ROADM architecture with spatial granularity built with WSSs has been neglected in the subsequent analyses.

Then, the ASE noise accumulation in a network with 10 cascaded ROADMs with a ROADM architecture with spatial granularity built with MEMS and spatial-wavelength granularity has been analyzed. It has been concluded that the OSNR of the network with the ROADM architecture with spatial granularity is 0.85 dB higher than the OSNR of the network with the ROADM architecture with spatial-wavelength granularity. Then, we have analyzed the NLI impact for the same networks. With the NLI, and considering the optimum signal power, the architecture with spatial granularity leads to an OSNR 0.6 dB higher than the architecture with spatial-wavelength granularity. By adding the in-band crosstalk effect, we have shown that, the network with the ROADM architecture with spatial granularity has a OSNR degradation of 0.14 dB due to in-band crosstalk and that the OSNR is 1.1 dB higher than the OSNR achieved in the network with the ROADM architecture with spatial-wavelength granularity that exhibits a 0.66 dB OSNR degradation due to in-band crosstalk. This 0.66 dB of OSNR degradation seems a low value but with the increase of the number of ROADMs in cascade or a decrease of the WSS isolation this value can increase, and we need to point that the route and select architecture with CDC add/drop structures with multiple entry's multiple exits WSSs is the most resistant architecture to crosstalk [7]. From the analysis of the passband narrowing effect, a 1 dB degradation in the OSNR that reaches the optical receiver input on both architectures has been foreseen.

From the OSNRs obtained with the aforementioned effects, ASE noise, NLI, in-band crosstalk and passband narrowing, after 10 cascaded ROADMs, the system margin for a specified target BER has been estimated considering both ROADM architectures. A network

that uses a ROADM-based architecture with spatial granularity has a system margin of 7.6 dB and a network that uses a ROADM-based architecture with spatial-wavelength granularity has a system margin of 6.5 dB. These systems margins allow us to conclude that both networks can accomplish the BER performance criterion. Therefore, the network that we have chosen to study in the next chapter is the network with a ROADM architecture with spatial-wavelength granularity, because this network accomplishes the networks performance parameters with about 1 dB margin degradation in relation to the spatial granularity architecture, but provides a much higher routing flexibility than the spatial granularity architecture.

Chapter 4: Simulation of PLIs in an optical network based on SDM ROADMs with spatial-wavelength granularity

4.1 Introduction

In this chapter, the performance of a network relying on the ROADM architecture with spatial-wavelength granularity, is assessed by Monte Carlo (MC) simulation using Matlab. Initially, in Section 4.2, it is explained how the optical transmitter and coherent receiver are modelled and a back-to-back (B2B) system configuration is studied to confirm the accuracy of the performance assessment implementation in the simulator. In section 4.3, the WSSs modelling is presented and the passband narrowing effect is studied. In section 4.4, the model of a ROADM-based network, with spatial-wavelength granularity, with the PLIs optical amplification, passband narrowing and NLI effects is presented, explained and assessed. In section 4.5, the in-band crosstalk effect is added to the network simulation model. In section 4.6, the final chapter conclusions are presented.

4.2 Back-to-back simulation

In this section, we present the B2B simulation model for a 100 Gbps QPSK system and we compute the respective required OSNR to reach a target BER. We also validate this OSNR analytically with the formalism presented in section 3.8.

The two main blocks of the simulation model of a B2B communication system for a 100 Gbps QPSK signal are the transmitter and the receiver blocks. In the following subsections, these are described with more detail.

4.2.1 Optical transmitter

In this sub-section, the optical transmitter simulation model is presented, and the signal generation is explained with detail.
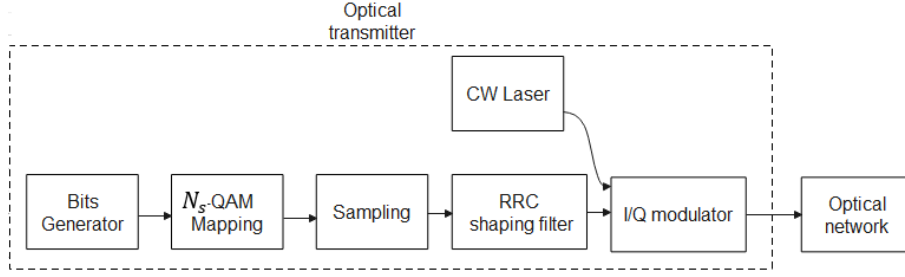
Figure 4.1: Optical transmitter model

In the block diagram shown in Figure 4.1, an ideal optical transmitter is considered, meaning that the electrical signal does not suffer any distortion due to bandwidth limitations of the transmitter components and is converted linearly to the optical domain [38]. The block functionalities represented in Figure 4.1 are the generation of the bit sequence, mapping to N_S-QAM modulation, sampling, root raised cosine (RRC) filter shaping, continuous wave (CW) laser and an I/Q modulator. In Figure 4.2, the ideal QPSK constellation with Gray coding, generated by the simulator at the transmitter after the mapping is shown.
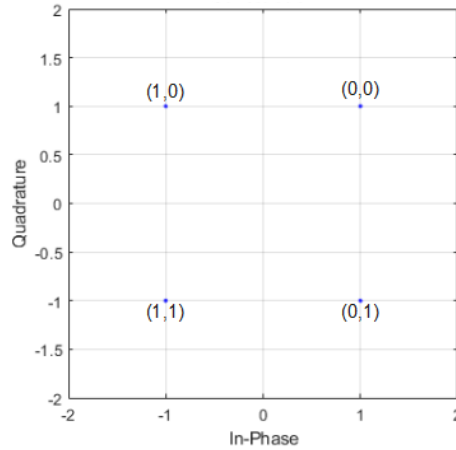
Figure 4.2: Ideal QPSK constellation at the optical transmitter output obtained by simulation. The numbers in each symbol represent the bits attributed to each QPSK symbol.

Table 4.1: Optical transmitter parameters considered

$R_{b,l}$ (Gbit/s)	$R_{s,l}$ (GBaud)	Modulation	N_{bits}	$N_{symbols}$
120	30	QPSK	8192	4096

In Table 4.1, the parameters considered for the optical transmitter description and corresponding signal generation are shown. To obtain reliable results, we have generated a pseudo-random binary Bruijn sequence with 2^{13} bits to have a high number of simulated bits.

58
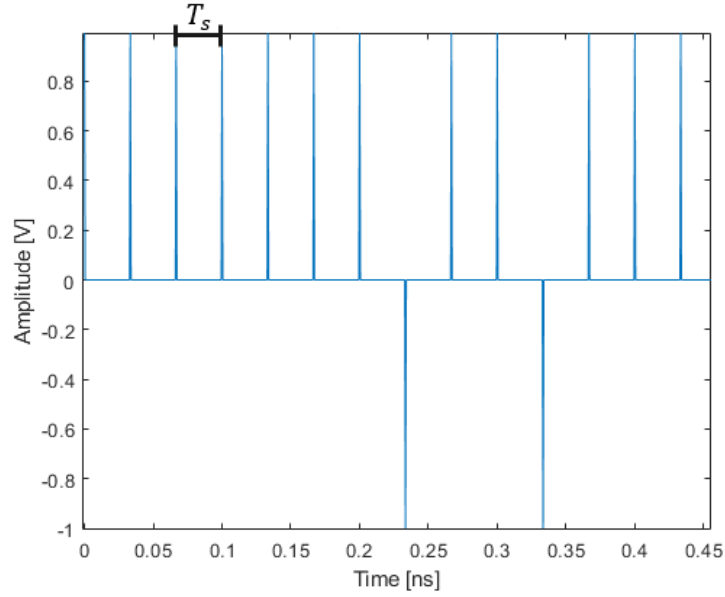
Figure 4.3: Sequence of the first 14 QPSK symbols of the in-phase component, corresponding to Dirac impulses after sampling with a 30 GBaud symbol rate.

After symbol mapping, the sequence of symbols is sampled to generate Dirac impulses at the input of the RRC filter. Figure 4.3 shows the first 14 generated QPSK symbols in the in-phase component. With Figure 4.3, it is possible to see that the amplitudes of the in-phase component vary between -1 and 1 V and that the symbol period is $T_s = 0.0333$ ns corresponding to a symbol rate $R_s = 30$ GBaud, as expected.
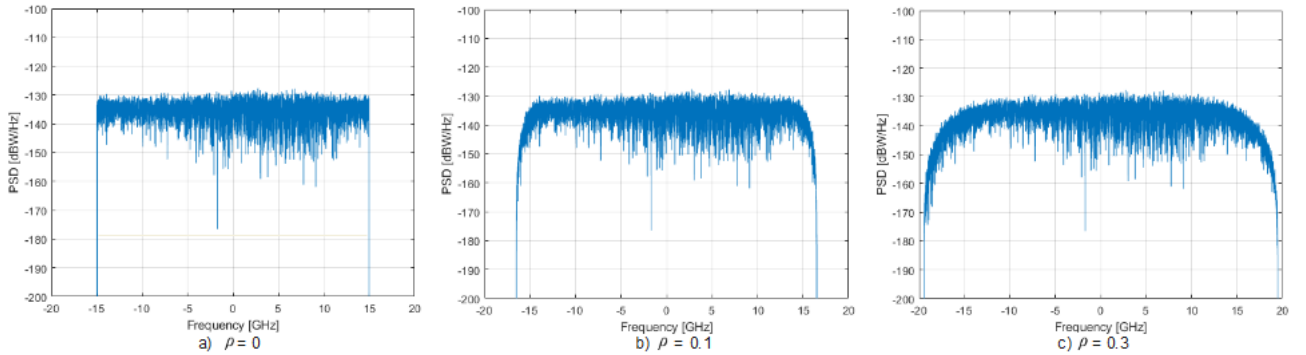
Figure 4.4:PSD of the QPSK signal, with 30 GBaud and 0.43 dBm of signal power, at the optical transmitter output (after the RRC shaping filter) for several roll-off factors.

The QPSK signal is passed by the RRC filter to acquire a RRC shape. The RRC filter transfer function is obtained by applying a square root to the raised cossine (RC) filter with transfer function given by [39], [40]:

$$H_{RC}(f) = \begin{cases} 1, & 0 \le |f| < \dfrac{1-\rho}{2T_s} \\[2mm] \cos\left[\dfrac{\pi T_s}{2\rho} \times \left(|f| - \dfrac{1-\rho}{2T_s}\right)\right]^2, & \dfrac{1-\rho}{2T_s} \le |f| < \dfrac{1+\rho}{2T_s} \\[2mm] 0, & |f| > \dfrac{1-\rho}{2T_s} \end{cases} \qquad (4.1)$$

where f is the low-pass equivalent frequency and ρ is the roll-off factor. The RC filter bandwidth is obtained with [39]:

$$B_{RC} = R_s \times (1 + \rho) \qquad (4.2)$$

and the noise equivalent bandwidth of the RRC filter is R_s, independently of the ρ value [40].

In Figure 4.4, the PSDs of a QPSK signal with $R_s = 30$ Gbaud, signal power of 0.43 dBm (ideal power obtained in section 3.4) and $\rho = 0, 0.1$ and 0.3 are depicted, respectively, in Figure a), b) and c). From Figure 4.4, it is possible to see that with $\rho = 0$ (Figure 4.5 a)), the QPSK PSD has an ideal rectangular shape and has a -3 dB bandwidth of 30 GHz, as given by equation (4.2). With $\rho = 0.1$ (Figure 4.4 b)), the QPSK signal PSD is no longer rectangular, the transition on the PSD edges has been smoothed and the signal -3 dB bandwidth has increased to 33 GHz, as predicted by equation (4.2). In Figure 4.4 c), the RRC filter has a $\rho = 0.3$, which leads to a signal PSD with a higher bandwidth (39 GHz), and an even smoother transition at the passband edges. Figure 4.4 demonstrates that our simulator imposes the RRC filter shape on the PSD of the signal at the output of the optical transmitter as intended.

4.2.2 Optical coherent receiver

The model used to simulate the coherent receiver is presented in Figure 4.5.
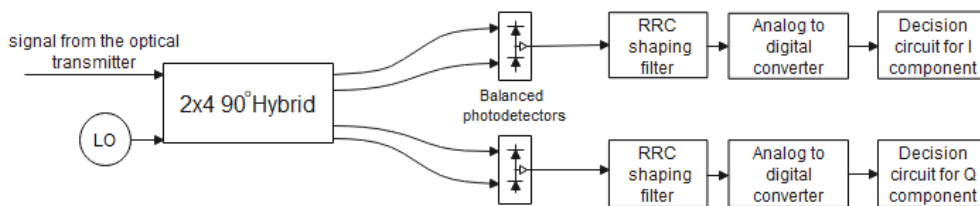
Figure 4.5: Model of the coherent receiver for one polarization. LO *represents the local oscillator.*

The coherent receiver represented considers only one signal polarization, since in this work, we assume that the transmission in the fiber is ideal in terms of signal polarization and, therefore, the performance of the coherent receiver can be evaluated for a single polarization [41]. The coherent receiver for a single signal polarization consists of a 2×4 90° hybrid,

followed by two balanced photodetectors and by a RRC shaping filter. After the 2×4 90º hybrid, the optical signal is converted to an electrical signal in the balanced photodetectors and the electrical signal in-phase component and quadrature component passes through a RRC filter that must have the same bandwidth of the RRC transmitter filter, to perform matched filtering [40]. After that, the signal goes through the analog to digital converter and finally reaches the decision circuit, where the estimated QPSK symbols are generated and the BER is assessed.
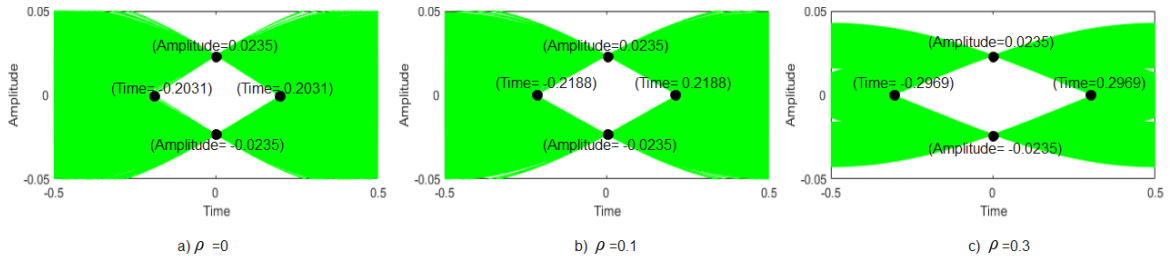
Figure 4.6: Eye diagrams at the optical receiver output for a) ρ=0, b) ρ=0.1, c) ρ=0.3.

In Figure 4.6, the eye diagrams obtained at the optical receiver output in the absence of noise for a B2B configuration, for $\rho = 0$, $\rho = 0.1$ and $\rho = 0.3$, are shown. The eye diagram of the in-phase component and quadrature component are very similar, therefore in Figure 4.6, it is only presented the eye diagram of the received quadrature component. It is possible to observe that with the increase of the roll-off factor, the eye diagrams at the best sampling instant, $t = 0$, (where the eye-opening is maximum), exhibit zero inter-symbol interference, as expected in a matched filtering case and have the same eye opening in all three examples. With the increase of the roll-off factor, the eye-diagrams exhibit less jitter, hence facilitating the synchronization of the received signal. It is possible to measure the jitter, using the eye diagram by measuring the time interval between the zero crossing points and divide it by the symbol period. This allow us to quantify the jitter as a percentage, that corresponds to 59%, 56% and 41%, respectively, for $\rho = 0$, $\rho = 0.1$ and $\rho = 0.3$.

Before the decision circuit, the signal is sampled at the optimum sampling instant obtained from the eye diagram. From that samples, the decision on the received symbol is performed and from comparison with the corresponding transmitted symbol, the BER is estimated. In the ideal B2B situation, in absence of noise, the received constellation is the same as the one shown in Figure 4.2.

4.2.3 Study of the OSNR required to achieve a target BER in B2B configuration

The model used to perform the study of the OSNR required to achieve a target BER at the decision circuit is shown in Figure 4.7. The OSNR at the coherent receiver input in a B2B configuration is set by ASE noise loading. Then the QPSK symbols are estimated at the decision circuit and finally the BER is estimated by direct error counting (DEC).
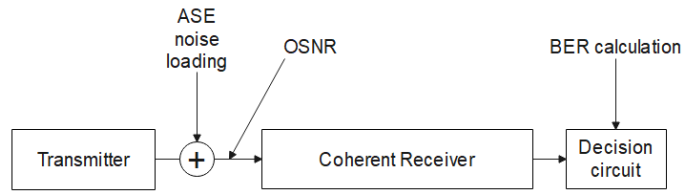
Figure 4.7: Model of the B2B system used to study the OSNR required to achieve a target BER.

The OSNR is imposed, using equation (3.8), with p_s corresponding to optimum signal power calculated in chapter 3, table 3.4. The ASE noise power needed to achieve an imposed OSNR in the simulator, is calculated on the reference bandwidth (12.5 GHz) by setting $B_o = B_{o,ref}$ in equation (3.5). After calculating the ASE noise power needed, in the simulator, sample functions of the quadrature and in-phase components of the ASE noise are generated by considering a Gaussian distribution with zero mean and variance equal to the desired ASE noise power given by equation (3.5). In order estimate the BER for a specific OSNR, in each iteration of the MC simulation, two sample functions corresponding to the I and Q components of the ASE noise are generated.
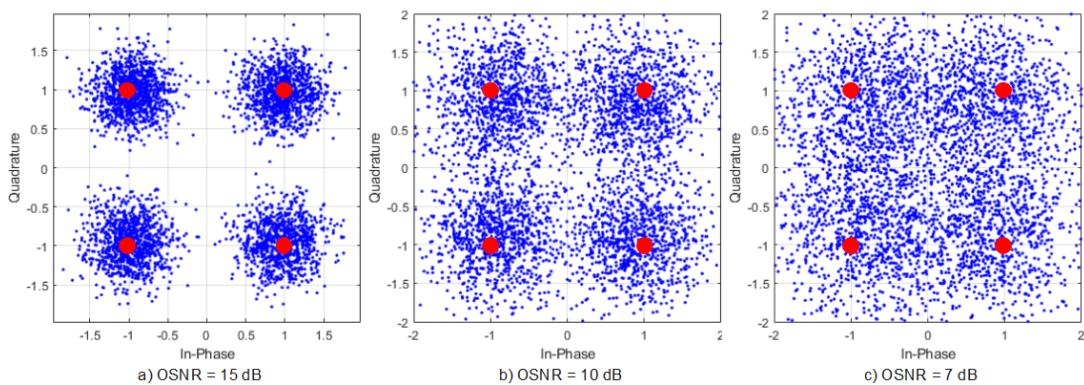
Figure 4.8: Received constellation of the QPSK signal with ASE noise (one sample function) for an OSNR of: a) 15 dB. b) 10 dB. c) 7 dB. The ideal constellation is also represented by the red filled circles.

In Figure 4.8, received constellations with different OSNRs (7, 10 and 15 dB) are shown at the decision circuit input. In each iteration of the MC simulator, the received constellation is

compared with the transmitted constellation to detect symbols with errors. We can see in Figure 4.8, that in constellations with lower OSNR, the received symbols are more spread due to the stronger ASE noise power, leading to a higher number of errors. With higher OSNRs, the received constellation shows that almost all symbols are in the right quadrant, leading to a lower number of symbols with errors. Each time, a symbol with an error is detected, that error is counted to estimate the BER. The BER is obtained by DEC using [26]:

$$BER = \frac{N_{errors}}{N_{MC} N_{symbols} \log_2(N_s)} \tag{4.3}$$

where N_s is the number of symbols used in the modulation, N_{errors} is the total number of symbol errors counted, N_{MC} is the number of MC simulator iterations, and $N_{symbols}$ is the number of transmitted symbols in each iteration of the MC simulator. In equation (4.3), a Gray coding has been assumed. In order to have a reliable result in the BER estimation the simulation is stopped when the number of errors reaches at least 1000 errors.
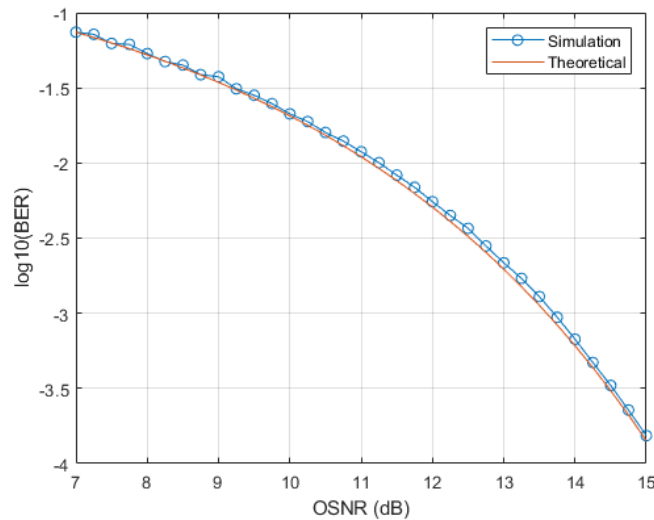
Figure 4.9: OSNR required to reach a target BER in a B2B on the reference bandwidth and configuration considering a 100Gbps QPSK signal.

In Figure 4.9, the OSNR required to achieve a target BER, in the reference bandwidth of 12.5 GHz, is presented considering a 100 Gbps QPSK signal. It is possible to observe that the OSNR obtained by simulation is very similar to the OSNR obtained analytically using equations (3.25) and (3.26). For example, in the simulation, to reach a line BER of 2.7×10^{-2} ($\log_{10}(BER) = -1.56$), an OSNR of 9.6 dB is required, whereas the analytical OSNR is 9.5 dB. So, with Figure 4.9, we show that the BERs obtained by simulation and analytically are in a very good agreement, for all the OSNRs considered, and therefore, it is possible to conclude

that the simulator is validated for a B2B scenario with 100 Gbit/s QPSK signals, meaning that optical transmitter, optical receiver and procedure for estimating the BER with ASE noise are correctly implemented.

4.3 Simulation of the passband narrowing effect in a cascade of ROADMs with spatial-wavelength granularity

In this section, we are going to simulate and analyze the filtering effects of the WSSs presented in the studied ROADM nodes.
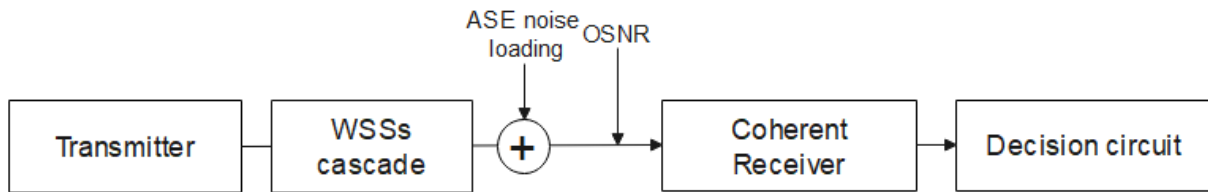
Figure 4.10: Simulation model used to estimate the effect of the WSSs passband narrowing on the OSNR.

In Figure 4.10, the model used to estimate the passband narrowing effect along a cascade of WSSs and the point in the communication system where the OSNR is evaluated is shown. The simulation of the passband narrowing effect for an increasing number of cascaded WSSs is performed iteratively, and for filters with different orders and bandwidths. The simulation starts with no cascaded WSSs, so the OSNR is calculated in a B2B configuration only with ASE noise for a specific target BER. In each iteration of the simulation, the number of WSSs is increased and the OSNR is calculated for the same target BER, now by taking into account the effect of the passband narrowing. The OSNR penalty is obtained by performing the difference between the OSNR calculated with the passband narrowing effect and the OSNR calculated with only ASE noise, for a specific target BER.

Each WSS is modelled using the passband transfer function given by equation (3.22). In Figure 4.11, the transfer functions of the 2nd, 4th and 5th order super-Gaussian passband filters with different orders and -3 dB bandwidths are shown.

64
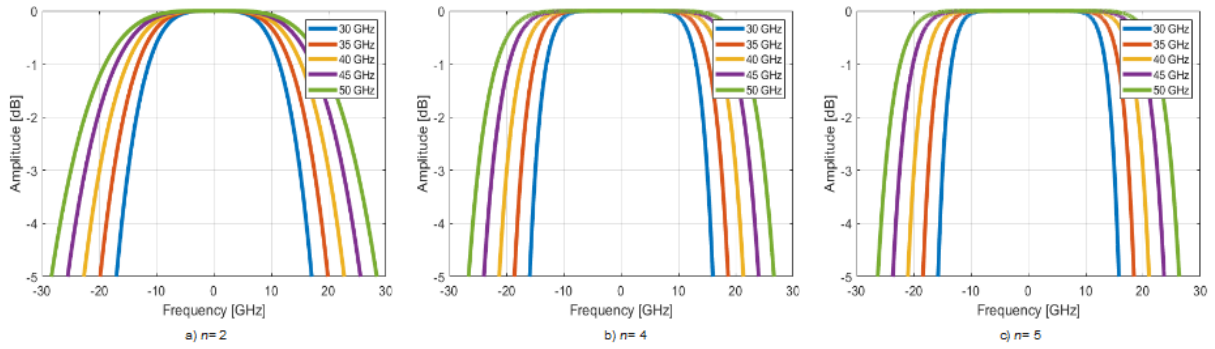
Figure 4.11: Transfer functions of super-Gaussian passband filters with different -3 dB bandwidths for filters with different orders. The different colors represent different -3 dB bandwidths.

As observed in Fig. 4.11, for the -3 dB amplitude, the bandwidth of the filters corresponds to the bandwidth value imposed on the simulation. This fact allow us to conclude that the super-Gaussian filters are correctly implemented. It is also possible to conclude from Figure 4.11, that for the same -3 dB bandwidth, with higher order filters, the filter shape approaches more closely the ideal rectangular shape, being the transition to the cut-off bandwidth much more abrupt and sharp.
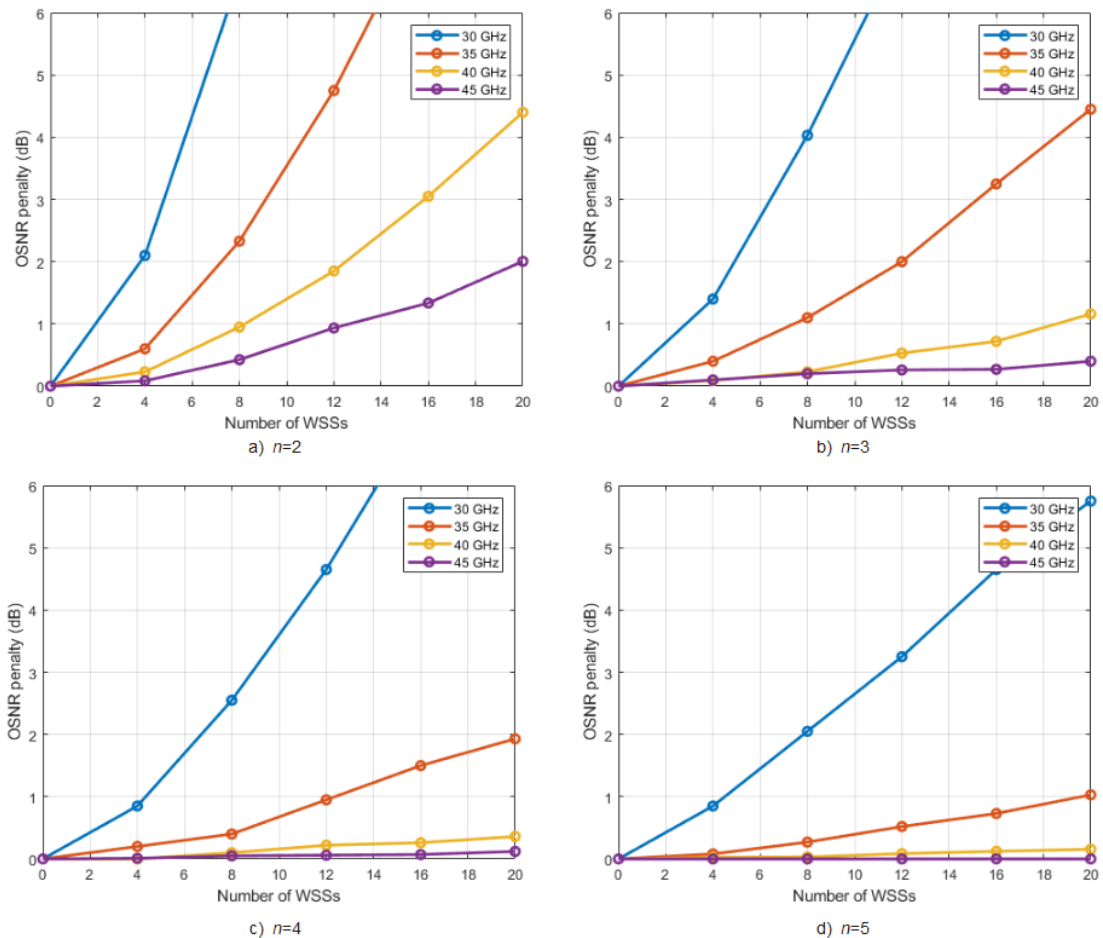
Figure 4.12: OSNR penalty due to passband narrowing for several super-Gaussian filter orders and -3 dB bandwidths. The different colors represent different -3dB bandwidths.

In Figure 4.12, the OSNR penalty due to passband narrowing is presented for super-Gaussian filters with different orders and different -3 dB bandwidths, considering a maximum of 20 cascaded filters. To confirm that the procedure to assess the OSNR penalty is correctly implemented, we have simulated the OSNR penalty with the same parameters that were used in [29] and have concluded that our results are in a very good agreement with the ones presented in Figure 1 d) of [29]. It is also possible to observe that the OSNR penalty behavior in Figure 4.12 is very similar to the one observed in Figure 3 of [37]. For super-Gaussian filters with a -3 dB bandwidth of 40 GHz, the OSNR penalty after 20 cascaded WSSs, is 1.16 and 0.36 dB, respectively, for 3rd and 4th order filters. For the -3 dB bandwidth of 35 GHz, the OSNR penalty is much higher, achieving around 4.45 and 1.93 dB of OSNR penalty, respectively, for 3rd and 4th order filters. For filters with -3 dB bandwidth of 30 GHz, the OSNR penalty is the highest, because the filters bandwidth is very similar to the signal bandwidth, and for 45 GHz, only for n=2, the OSNR penalty becomes relevant after a 20 filters cascade. Bandwidths above 50 GHz (above the WDM channel spacing) are not recommended, since the OSNR penalty due to inter-channel crosstalk would be enhanced [29].

From Figure 4.12, it is possible to observe that with the increase of the filters order and -3 dB bandwidth, the OSNR penalty due to passband narrowing decreases. For our network, in order to minimize, the OSNR penalty due to passband narrowing effect, without introducing much inter-channel crosstalk, 4th order filters with -3 dB bandwidth of 45 GHz are considered.

4.4 Simulation of a cascade of ROADMs based on spatial-wavelength granularity considering the PLIs due to optical amplification, filtering and fiber non-linear effects

In this section, we are going to analyze a cascade of ROADMs with spatial-wavelength granularity considering the ASE noise, optical filtering and NLI effect. In Figure 4.13, the model used to study and simulate this scenario is presented.

In Figure 4.13, $s_{add}(t)$ is the QPSK signal generated by the optical transmitter and $s_{exp,j}(t)$ are the signals at the output of the jth ROADM (with j=1, ..., n_r) along the network, where n_r is the total number of ROADMs in the cascade. In the simulation model depicted in Figure 4.13, the first ROADM is used to add the signal into the network. At the output of this ROADM, the signal went through 3 WSSs and one optical amplifier. The next ROADMs are used as express ROADMs, the signal is expressed from a ROADM input to a ROADM output, and in

this case, the signal goes through 2 WSSs and 2 optical amplifiers. Finally, the signal is dropped from the optical network in the last ROADM, where it goes through 3 WSSs and one amplifier.
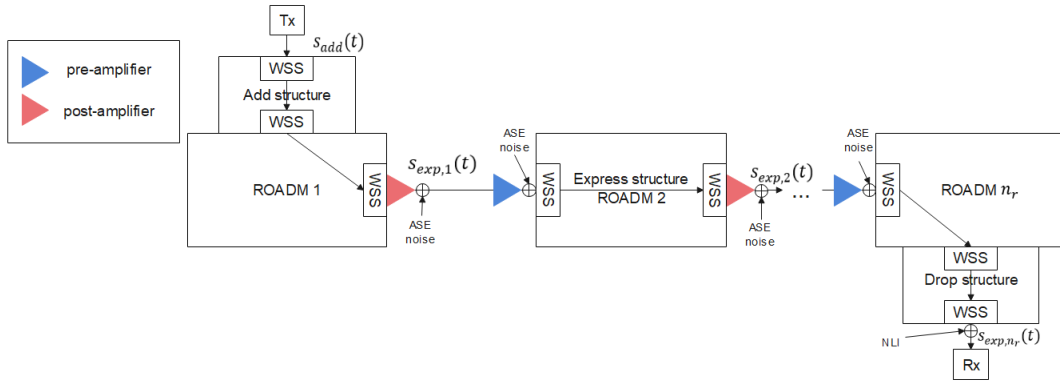
Figure 4.13: Simulation model of a cascade of n_r ROADMs based on spatial-wavelength granularity considering the PLIs due to optical amplification, filtering and NLI effects.

The optical amplifiers considered in the simulation and represented in Figure 4.13 are assumed to perfectly compensate the network losses and add ASE noise to the signal. In the Matlab simulation, the ASE noise power is defined by setting each sample function of noise with a power defined by equation (3.5). Furthermore, the NLI noise of the fiber is computed and added only at the input of the coherent optical receiver, as indicated in Figure 4.13. Notice that the simulation model represented in Figure 4.13 considers only single channel propagation and one single fiber for transmission. However, in this work, WDM signal transmission in one fiber is taken into account by assessing the impact of NLI on the system performance using the Gaussian model described in section 3.4 and by also assessing the in-band crosstalk impact at the node from channels in other directions. SDM transmission in multiple parallel fibers is taken into account by considering the in-band crosstalk impact arising from the SDM ROADM node on the primary signal.

In this work, we assess the system performance by measuring the OSNR at the input of the optical receiver using two different methodologies. The first one calculates the OSNR considering only the noise power and signal power as in equation (3.9), so signal distortion is not accounted in this methodology. This methodology will be referred as Power-based method. In the second one, the OSNR is calculated through the BER estimated by the simulator, which is assessed by the DEC method. This methodology takes into account the signal distortion due to filtering in the ROADMs WSSs (this distortion is almost inexistent due to the filters order and bandwidth used), and also the distortion on the primary signal caused by in-band crosstalk. This methodology will be referred as BER-based method.

Next, we are going to present and discuss the results of the OSNR at the optical receiver input after the signal went through a cascade of ROADMs with spatial-wavelength granularity considering the PLIs due to optical amplification, filtering and fiber non-linear effects as depicted in Figure 4.13. For this scenario, using the two OSNR methodologies previously referred, similar results are obtained. Therefore, it can be concluded that in this scenario, the signal distortion does not affect the results, because, the only PLI that can cause signal distortion is the passband narrowing effect, but due to the filter order and -3 dB bandwidth chosen, respectively, 4th order and 45 GHz, the OSNR penalty due to this PLI is negligible, as can be observed in Figure 4.12 c).

Table 4.2: Network parameters considered in the simulation with accumulation of ASE, optical filtering and NLI.

$B_{-3dB,WSS}$ (GHz)	n (WSS filter order)	D_λ (ps/nm/km)	γ ($W^{-1}km^{-1}$)	P_s (dBm)	v_0 (THz)	Δv_{ch} (GHz)	F_n (dB)	ρ	L_{sec} (km)	α (dB/km)
45	4	18	1.1	0.43	193.8	50	6.9	0.1	80	0.2

The network parameters used in this simulation are presented in Table 4.2, which are the same ones considered in chapter 3. In this simulation scenario (Figure 4.13) the ASE noise generated in each optical amplifier is added to the accumulated ASE noise generated by the previous amplifiers along the network, hence, we are considering that the ASE noise is distributed, which is a different scenario, but more realistic, than the one considered in section 4.3. where the ASE noise is loaded at the receiver input.

Table 4.3: ASE noise power added by each pre-amplifier, ASE noise power added by each post-amplifier, total ASE noise accumulated power and NLI noise power measured at the receiver input and OSNR measured at the receiver input after 10 cascaded ROADMs with and without the NLI noise.

	Pre-amplifier ASE noise power (μW)	Post-amplifier ASE noise power (μW)	Total ASE noise power (μW)	NLI power (μW)	OSNR without NLI (dB)	OSNR with NLI (dB)
Analytical (chapter 3)	1.02	0.37	12.47	6.25	16.16	14.40
Simulation	0.98	0.31	12.63	6.28	16.2	14.44

Table 4.3 shows the ASE noise power generated in each pre-amplifier and post-amplifier, as well as the total ASE noise power, NLI power, OSNR with and without NLI at the receiver input for a cascade of 10 ROADMs obtained by simulation and analytically using the reasoning presented in chapter 3. As can be observed in Table 4.3 the simulated and the analytical values are in a very good agreement, validating the implementation in the simulator of the ASE noise

accumulation and NLI effect along the network. The simulated values have been obtained by averaging the results of 100 simulation runs. The analytical OSNR obtained in section 3.3 is subtracted by the 0.3 dB filtering penalty considered in section 3.7. It is also possible to see that the OSNR difference, obtained by simulation and analytically, without and with NLI is of around 1.76 dB, as it should be.
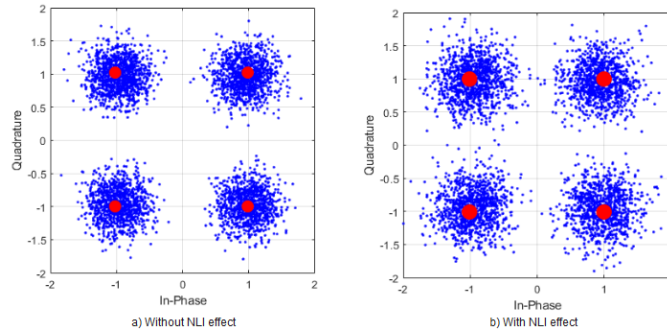
Figure 4.14: Constellations at the decision circuit input after 10 cascaded ROADMs.

In Figure 4.14 a) and b), the constellations at the input of the decision circuit, respectively, with and without NLI after 10 cascaded ROADMs, considering an OSNR = 16.2 dB in Figure 4.14 a) and an OSNR = 14.4 dB in Figure 4.14 b), are shown. In the constellation without NLI, the received QPSK symbols are closer to the symbols in the ideal constellation than the symbols in the constellation with NLI, hence, leading to a received signal with less noise and improved system performance, as expected.
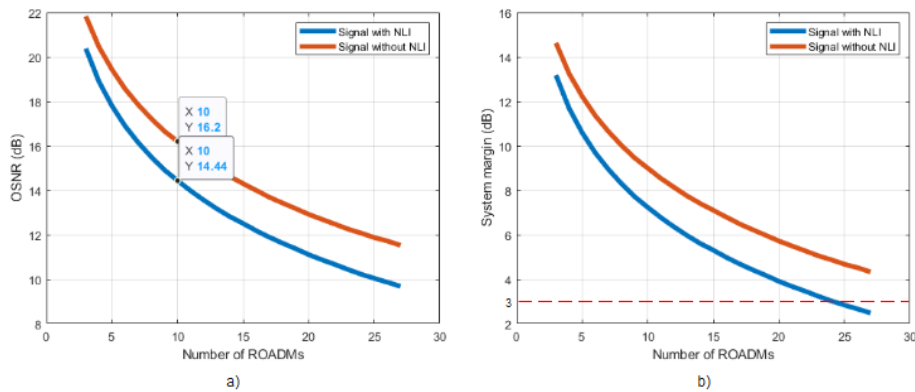
Figure 4.15: OSNR measured at the signal bandwidth and System margin, measured at the input of the coherent optical receiver as a function of the number of ROADMs, without and with NLI.

In Figure 4.15 a) and b), it is shown, respectively, the OSNR in the signal bandwidth and the system margin, obtained by simulation, as a function of the number of ROADMs, with and without NLI. For the computation of the system margin in Figure 4.15 b), a transmission penalty of 1.5 dB is considered, as in equation (3.28).

As can be observed in Figure 4.15 a), the OSNR decreases as the number of cascaded ROADMs grows due to an increase of ASE noise power and also due to a slight filtering penalty as the number of cascaded WSSs increases. From Figure 4.15 a), we can also confirm that for 10 cascaded ROADMs, an OSNR of 16.2 dB is obtained when the NLI noise is not considered, whereas when this noise is considered an OSNR of 14.4 dB is obtained, which is in accordance with the values presented in Table 4.3. Another observation from Figure 4.15 is that, after a cascade of 27 ROADMs, an OSNR of around 11.6 dB and 9.9 dB is obtained, respectively, for a signal without NLI and with NLI. Both OSNRs are superior to the minimum OSNR needed (5.7 dB) to reach the target BER of 2.7×10^{-2} in the signal bandwidth.

From Figure 4.15 b), we can conclude that, for the case without NLI, at the end of the cascade up to maximum number of ROADMs considered (27 ROADMs), the system margin is always above the 3 dB minimum defined in equation (3.28). For the case with NLI, the system margin is above the minimum, for a ROADM cascade of 23 ROADMs.

4.5 Simulation of a network with ROADM based on a spatial-wavelength granularity architecture with ASE noise, optical filtering, NLI and in-band crosstalk

In this section, we are going to simulate and analyze the performance of a network with ROADMs with spatial-wavelength granularity architecture, which is impaired by ASE noise, optical filtering, NLI and in-band crosstalk. Regarding to the previous section, the only difference is the addition of the in-band crosstalk to the system. The number of in-band crosstalk signals generated in each ROADM depends if the signal is added, expressed or dropped from that ROADM, as explained in section 3.5. The model of the referred network is shown in Figure 4.16.

In Figure 4.16, the interfering terms $I_{cr,add,j}(t)$, with $j=1, \ldots, (D \times M) - 1$, in the worst case scenario as concluded in Table 3.5, represent in-band crosstalk terms of 2nd order that are added in the add structure, the 2nd order interfering terms $I_{cr,exp,j}(t)$, with $j=1, \ldots, (D - 1) \times M$, represent the in-band crosstalk arising in each ROADM express structure, and the in-band crosstalk terms arising in the drop structure are of 2nd order and are represented by $I_{cr,drop,j}(t)$, with $j = 1, \ldots, (D \times M) - 1$.
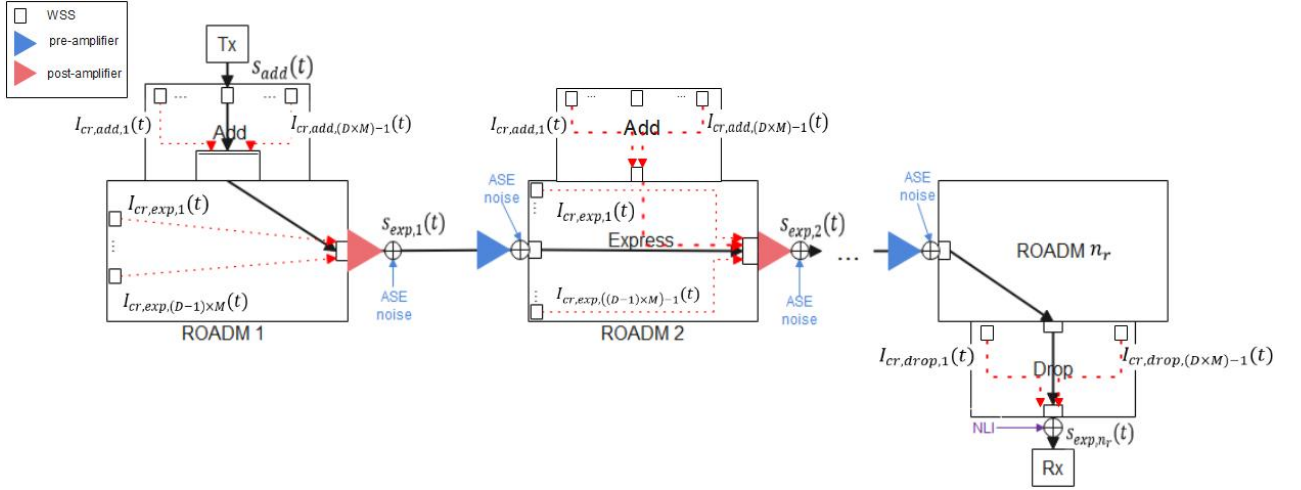
Figure 4.16: Simulation model of a network with ROADMs with spatial-wavelength granularity architecture, impaired by ASE noise, optical filtering, NLI and in-band crosstalk.

In the simulator, we assume the worst-case scenario regarding the in-band crosstalk, and, hence, the number of interfering terms is calculated with the expressions presented in Table 3.5. For $D = 16$ and $M = 19$, in the add scenario, 588 interfering terms are generated, in the express scenario, 587 interfering terms and in the drop scenario, 303 interfering terms, all of 2nd order. Therefore, in a network with 10 ROADMs with D=16 and M=19, there are a total of 5587 interfering terms of 2nd order, whereas with D=16 and M=1 (single spatial channel) there are only 277 2nd order interfering terms.

The simulation model for the in-band crosstalk signals considers that they are generated with the same characteristics of the primary signal (which is a QPSK signal), but for each interfering term, the bits are generated randomly. The interfering signals are generated also with a phase difference and a time misalignment, in relation to the original signal. The time misalignment and phase difference are modelled as a uniformly distributed random variable, respectively, between $[0, T_s]$ and between $[0, 2\pi]$ as in [7]. After generation, each second order interfering term must go through two blocking filters that simulate 2nd order leakage in WSSs. The transfer function of the blocking filters is given by equation (3.24).

In Table 4.4, the crosstalk level, total in-band crosstalk power, OSNR, OSNR penalty due to crosstalk and system margin measured at the input of the coherent optical receiver, are shown after a cascade of 10 ROADMs, considering two isolation values for the WSSs (-30 and -25 dB). It can be observed that the OSNRs obtained analytically are in a very good agreement with the OSNRs obtained by simulation when using the Power-based method, defined in section 4.3. For $A = -30$ dB, there is only a 0.12 dB difference and for $A = -25$ dB, there is a 0.18 dB difference. However, when the OSNR is obtained using the BER-based method, a more

significant difference between the analytical and simulated values is observed. For $A = -30$ dB, the difference is 0.35 dB, whereas for $A = -25$ dB, this difference reaches 2 dB.

Table 4.4: In-band crosstalk power, OSNR and system margin measured at the optical coherent receiver input after 10 cascaded ROADMs with D=16 and M=19.

	Isolation (dB)	Crosstalk Level (dB)	Crosstalk Power (μW)	OSNR (dB)	OSNR Penalty (dB)	System margin (dB)
Analytical	−30	−22.5	3.098	13.74	0.66	6.54
	−25	−12.5	30.98	10.17	4.23	2.97
Simulation (Power-based method)	−30	−21.9	3.5598	13.62	0.82	6.42
	−25	−12.3	32.94	9.99	4.45	2.80
Simulation (BER-based method)	−30	−21.9	3.6062	14.09	0.35	6.89
	−25	−12.34	32.338	12.2	2.24	5

The most rigorous results are the ones obtained with the BER-based method, because, in this method, the waveform distortion caused by the crosstalk signal on the primary signal in the performance degradation along the ROADM cascade is taken into account. The OSNR penalties predicted by the BER-based method are lower than the ones given by the analytical and Power-based method cases. This behavior is attributed to the random walk-off between symbols of the interfering terms and symbols of the primary signal, a behavior that is captured when the waveform distortion is taken into account to obtain the OSNR.

In order to validate our results, we have compared our results with the results presented in Figure 5.13 of [33], that considers a QPSK modulation, and for the same levels of crosstalk (-22 dB and -12.3 dB) OSNR penalties of around 0.25 dB and 2.3 dB can be observed. These penalties are in a very good agreement with the results for the BER-based method shown in Table 4.4.

From Table 4.4, we can also conclude that the system margin obtained by simulation, with the BER-based method, is always above the minimum (3 dB) for both isolation levels. In the system margin analysis and from now on, due to its improved accuracy, only the BER-based method will be used to assess the OSNR penalty due to in-band crosstalk.

In Figure 4.17, the OSNR and crosstalk level (defined in equation 3.18) as a function of the number of ROADMs are shown, for $A = -30$ dB, 16 directions and different numbers of spatial channels. In Figure 4.17 a), it is possible to observe that for $A = -30$ dB, for all the numbers of spatial channels studied, the OSNR with in-band crosstalk is almost the same as the OSNR without in-band crosstalk, being the OSNR penalty due to in-band crosstalk insignificant e.g., the OSNR penalty for $M = 19$ (the worst case scenario) achieves only 0.33 dB.

Figure 4.17: OSNR and crosstalk level as a function of the number of ROADMs for a system with ASE noise, passband narrowing due to filtering, NLI and in-band crosstalk for A= -30 dB, D=16 and different numbers of spatial channels.

In Figure 4.17 b), it can be observed that the crosstalk level after 27 cascaded ROADMs, is below -20 dB, for all of the number of spatial channels considered. These results are in agreement with the results presented in figure 5.13 of [33], where for the QPSK modulation and similar crosstalk levels, the OSNR penalty is negligible. In Figure 4.17 b), it is also possible to observe that the crosstalk level increases with a higher slope in the first cascaded ROADMs, being almost constant after 15 ROADMs. This happens because, in the initial nodes, the total crosstalk power is low and, therefore, the crosstalk terms added at one ROADM will have a higher impact in the total crosstalk power. In the final ROADMs, the total crosstalk power is much higher than the power added by each interfering term and, therefore, the crosstalk level remains almost constant.

Figure 4.18: OSNR and crosstalk level as a function of the number of ROADMs for a system with ASE noise, passband narrowing due to filtering, NLI and in-band crosstalk level for A= -25 dB, D=16 and a different number of spatial channels.

73

In Figure 4.18, the OSNR and crosstalk level as a function of the number of ROADMs, for $A = -25$, 16 directions and different numbers of spatial channels is represented. In Figure 4.18 a), it is possible to observe that the impact of in-band crosstalk on the OSNR is enhanced as the number of spatial channels grows. For $M = 1$, the in-band crosstalk impact is negligible. For $M = 4$, $M = 8$, $M = 16$ and $M = 19$, after 27 cascaded ROADMs, the OSNR penalty due to in-band crosstalk is, respectively, 0.5 dB, 1.2 dB, 1.9 dB and 2 dB. For these cases, in Fig. 4.18 b), the crosstalk levels achieved at the end of the cascade of 27 ROADMs are -17.6 dB, -15.1 dB, -12.7 dB and -12.4 dB, respectively, for $M = 4$, 8, 16 and 19. In [33], for the same crosstalk levels, the OSNR penalty obtained was, respectively, 0.55 dB, 1.2 dB, 1.8 dB and 2 dB, for QPSK signals, which is in a very good agreement with our results. In comparison with the scenario with $A = -30$ dB (Figure 4.17 a)), the worst OSNR penalty after 27 cascaded ROADMs (in the scenario $M = 19$ and $D = 16$) obtained for $A = -25$ dB (Figure 4.18 a)) is 2 dB, 1.7 dB higher, than for $A = -30$ dB.

To keep the system performance, the system margin needs to be higher than 3 dB, which corresponds to a minimum OSNR of 10.2 dB obtained from equation (3.28). Therefore, for $A = -30$ dB (Figure 4.17 a)), $D = 16$ and $M \leq 8$, $M = 16$ and $M = 19$, the signal can cross a maximum of 24, 23 and 22 ROADMs, and still accomplish this margin. For $A = -25$ dB (Figure 4.18 a)), $D = 16$ and $M = 1$, 4, 8, 16 and 19 , to accomplish this margin, the signal can cross, respectively, 24, 21, 19, 16 and 15 ROADMs.

a)   b)

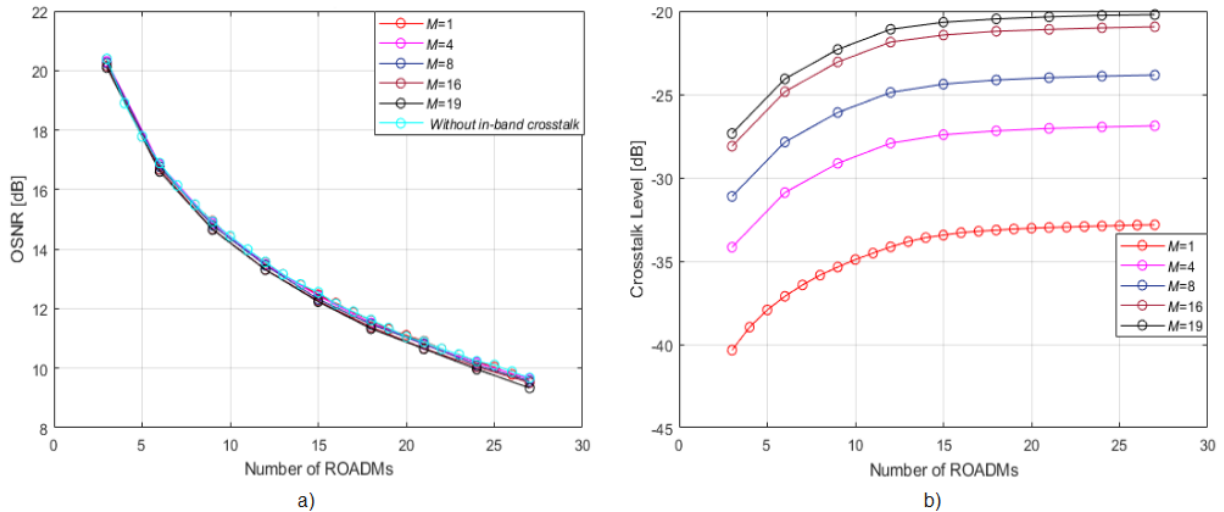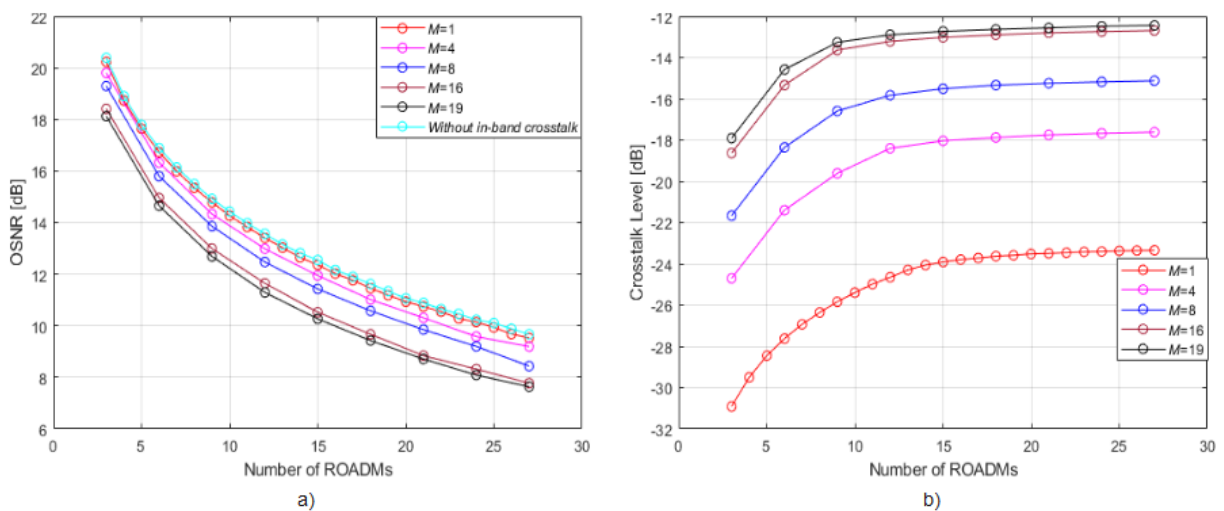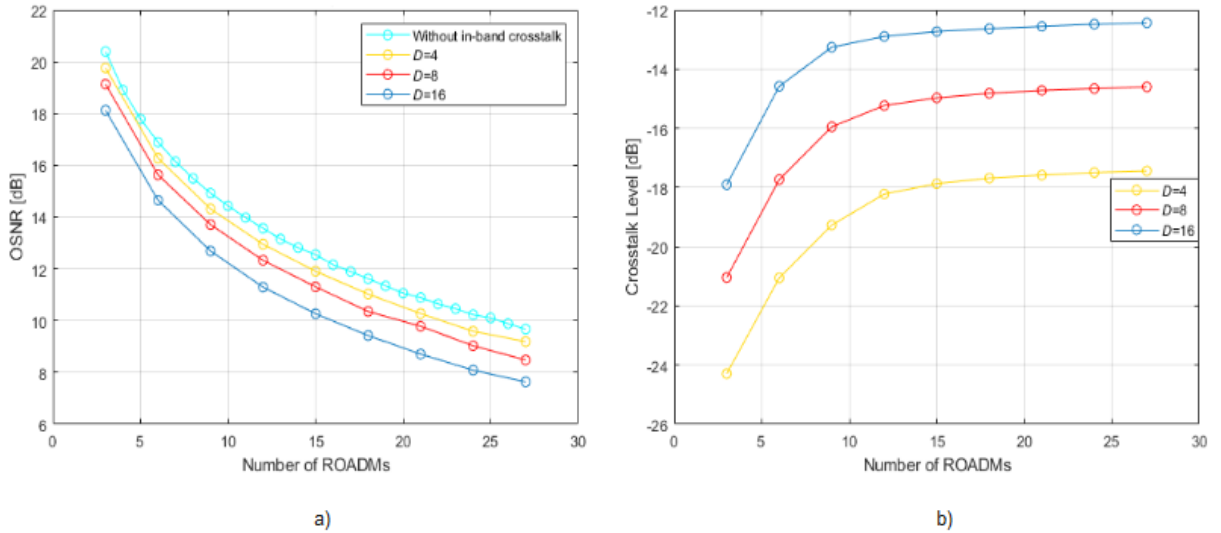*Figure 4.19: OSNR and crosstalk level as a function of the number of ROADMs for a system with ASE noise, passband narrowing due to filtering, NLI and in-band crosstalk level for A= -25 dB, M=19 and different numbers of ROADM directions.*

In Figure 4.19, the OSNR and crosstalk level as a function of the number of ROADMs, for $A = -25$, $M = 19$ and different numbers of ROADM directions is represented. Figure 4.19

shows that by decreasing the number of ROADM directions, the impact of in-band crosstalk is reduced due to lower number of interfering terms. In Figure 4.19 a), after 27 cascaded ROADMs, the OSNR penalties due to in-band crosstalk decrease 1.5 dB and 0.8 dB, respectively, for $D = 4$ and $D = 8$, in relation to the OSNR penalty obtained for $D = 16$. In Figure 4.19 b), the crosstalk level has increased 2.84 dB and 2.2 dB, each time the number of directions has doubled.

To keep the system performance, the system margin needs to be higher than 3 dB, therefore, to accomplish the margin, for $D = 4$, $D = 8$ and $D = 16$, a signal can cross, respectively, 22, 19 and 15 ROADMs.

4.6 Conclusion

In this chapter, the performance of a network based on ROADMs with spatial-wavelength granularity was assessed by MC simulation. This simulation has included the most relevant PLIs, both due to fiber transmission and ROADM node architecture, such as NLI, insertion losses, ASE noise, and in-band crosstalk.

Firstly, a B2B coherent transmission system considering QPSK modulation has been implemented through simulation and the estimation of the OSNR required to achieve a target BER has been validated in presence of ASE noise.

Then, the passband narrowing due to optical filtering cascading effect on the network performance, has been studied for several Super-Gaussian filter orders and different -3 dB bandwidths. It has been verified that the OSNR penalty simulation results obtained are in a very good agreement with results published in other works. From the analysis of the OSNR penalty due to passband narrowing, the 4$^{\text{th}}$ order super-Gaussian filter with -3 dB bandwidth of 45 GHz has been chosen in order to lead to negligible OSNR penalties after 20 cascaded WSSs.

Then, to assess the impact of the PLIs, ASE noise accumulation, NLI and passband narrowing due to optical filtering, in a cascade of ROADMs, two methods have been implemented, the power-based method and BER-based method. With these PLIs, the OSNRs obtained using both methods were very similar, showing that the waveform distortion is not relevant. For 10 cascaded ROADMs, with $D = 16$ and $M = 19$, an OSNR of 14.4 dB and a system margin of 7.2 dB, were obtained. While still accomplishing the minimum system margin, the optical signal can cross a maximum of 24 cascaded ROADMs.

Finally, the in-band crosstalk effect was added to the simulator, in order to model a cascade of ROADMs with spatial-wavelength granularity architecture and assess the in-band crosstalk impact in that cascade of ROADMs. Firstly, the analysis has been performed for 10 cascaded

ROADMs with $D = 16$ and $M = 19$, to conclude about the most suitable method to assess the OSNR penalty due to in-band crosstalk. The OSNRs obtained with the BER-based method, are more rigorous and are almost 2 dB lower than the OSNRs obtained with the Power-based method. Therefore, it was concluded that for a more exhaustive and accurate analysis of the impact of the in-band crosstalk that impairs a cascade of ROADMs with spatial-wavelength granularity, the Power-based method should be avoided. Using the BER-based method, the network performance (by assessing the OSNR and crosstalk level) for different number of cascaded ROADMs, different WSS isolations and different numbers of spatial channels has been assessed. We have assumed that the crosstalk effect on the OSNR becomes significant when the OSNR penalty reaches 1 dB. For $A = -25$ dB, this penalty is achieved when $M = 8$ and the crosstalk level is higher than -15.7 dB, for 27 cascaded ROADMs. For $A = -30$ dB, the OSNR penalty never reaches 1 dB, and the crosstalk effect can be considered insignificant.

We have also studied the OSNR and crosstalk levels for ROADMs with $D = 8$ and $D = 4$, and compared with the results obtained for $D = 16$. With this study, we have concluded that a signal can cross, with $D = 4$ and $D = 8$, respectively, more 7 and 4 cascaded ROADMs than for $D = 16$.

Chapter 5: Conclusions and future work

In this chapter, the main conclusions and suggestions for future work are presented.

5.1 Final conclusions

In this dissertation, four switching strategies for SDM ROADMs architectures (spatial, spatial-wavelength, wavelength and fractional spatial-full wavelength) have been studied for networks that consider parallel fibers as spatial channels, which is known in the literature as the uncoupled SDM scenario.

In Chapter 2, the four switching strategies for SDM ROADMs are explained and one possible architecture implementation for each strategy is presented. The hardware required to build these architectures is also presented and the architectures are analyzed in terms of cost per bit, power consumption and flexibility. The ROADM architectures with wavelength and fractional space-full wavelength granularity have a higher cost per bit, more power consumption and less flexibility than the architecture with spatial-wavelength granularity. Therefore, these former two architectures bring no benefits in being used in uncoupled scenarios. The architecture with spatial granularity has lesser cost, lesser power consumption, but it is also the less flexible in terms of wavelength routing. The architecture with spatial-wavelength granularity has a higher cost and power consumption, but leads to a much superior routing flexibility. The choice between these two architectures will depend strongly on the network specifications and the PLIs that affect the network transmission performance.

In Chapter 3, the assessment of the PLIs effect in the architectures with spatial and spatial-wavelength granularity is performed analytically, for 10 cascaded ROADMs. Firstly, only ASE noise is studied, and we have concluded that the ROADM architecture with spatial granularity leads to a 0.85 dB higher OSNR than the one obtained with the ROADM architecture with spatial-wavelength granularity. With ASE noise, NLI effect, passband narrowing effects and considering optimal signal power in both architectures, the OSNR achieved after 10 cascaded ROADMs is 0.6 dB higher in the architecture with spatial granularity. Finally, with in-band crosstalk added to the system, we have concluded that the architecture with spatial granularity leads to an OSNR that is 1.1 dB higher than the OSNR obtained for the architecture with spatial-wavelength granularity. It was also concluded that, after 10 cascaded ROADMs, both ROADMs architectures are able to reach the system margin estimated for a specific target BER. As both architectures accomplish the system margin after 10 cascaded ROADMs, due to the higher routing flexibility, the MC simulator has been developed to simulate the architecture with spatial-wavelength granularity.

In Chapter 4, a Monte Carlo simulator has been used to analyze the performance of a network composed by a cascade of ROADMs with the spatial-wavelength granularity architecture. This simulator takes into account the impact of ASE noise accumulation, NLI, filtering passband narrowing and in-band crosstalk and has been validated for several scenarios. Without in-band crosstalk, for a network impaired by only ASE noise, passband narrowing and NLI, the OSNR obtained by simulation is practically the same than the one obtained analytically, meaning that the waveform distortion has practically no impact in the network performance, even for long ROADM cascades (above 20). With in-band crosstalk, the waveform distortion impact on the performance is meaningful, and to obtain rigorous results, the OSNR should be obtained from the BER. It has been observed that, for a WSS isolation of -30 dB, the impact of in-band crosstalk is practically insignificant, even after a long cascade of ROADMs. In this case the signal can cross 22 cascaded ROADMs. For $A = -25$ dB, the impact of the in-band crosstalk becomes significant for $M \geq 8$. For $D = 16$ and $M = 19$ (worst case scenario), after 27 cascaded ROADMs, the OSNR penalty reaches 2 dB. In this scenario the signal can cross only 15 ROADMs, without degrading the system performance.

5.2 Future work

For the future investigation, we propose the following topics:

- Study of the PLIs impact for SDM ROADMs architectures with wavelength and fractional space-full wavelength granularities, for uncoupled networks.
- Study of the PLIs impact for SDM ROADMs architectures with wavelength and fractional space-full wavelength granularities for networks with multiple core fibers and multiple mode fibers (coupled networks), where the crosstalk between cores can have a significant impact on the system performance.
- Study of a B&S architecture with spatial-wavelength switching strategy and compare the PLIs (ASE noise, NLI, passband narrowing and in-band crosstalk) with the R&S architecture.

References

[1]   A. Napoli at al., "Towards multiband optical systems," *Advanced Photonics Conference*, Paper NeTu3E.1, California USA, 2018.

[2]   D. M. Marom *et al.*, "Survey of photonic switching architectures and technologies in support of spatially and spectrally flexible optical networking [invited]," *Journal of Optical Communications and Netwworking*, vol. 9, no. 1, pp. 1–26, Jan. 2017.

[3]   D. M. Marom and M. Blau, "Switching solutions for WDM-SDM optical networks," *IEEE Communications Magazine*, vol. 53, no. 2, pp. 60–68, Feb. 2015.

[4]   P. J. Winzer and D. T. Neilson, "From Scaling Disparities to Integrated Parallelism: A Decathlon for a Decade," *Journal of Lightwave Technology*, vol. 35, no. 5, pp. 1099–1115, March 2017.

[5]   J. Pan, C. Pulikkaseril, L. Stewart, and S. Tibuleac, "Comparison of ROADM filter shape models for accurate transmission penalty assessment," 2016 IEEE Photonics Conference (IPC), pp. 550-551, Waikoloa USA, Oct. 2016.

[6]   K. Saitoh and S. Matsuo, "Multicore fiber technology," *Journal of Lightwave Technology*, vol. 34, no. 1, pp. 55–66, Jan. 2016.

[7]   D. Sequeira, L. Cancela, and J. Rebola, "CDC ROADM design tradeoffs due to physical layer impairments in optical networks," *Optical Fiber Technology*, vol. 62, no. 102461, pp. 1-11, Jan. 2021.

[8]   A. Anchal, D. Marom," Practical SDM-ROADM designs for uncoupled spatial channels and their switching capacity," 2019 Optical Fiber Communications Conference and Exhibition (OFC), pp. 1-3, San Diego USA, Mar. 2019.

[9]   Y. Mori, K. Yamashita, and M. Jinno, "Feasibility Demonstration of Integrated Fractioanal Joint Switching WSS Applicable for Few-Mode Multicore Fiber," *2018 Photonics in Switching and Computing Conference (PSC)*, pp. 1–3, Limassol Cyprus, Sep. 2018.

[10]   T. Ye and K. Chen, "Modular WSS-based OXCs for Large-Scale Optical Networks" *ArXiv*, vol. 2005.12751. pp. 1–8, May 2020.

[11]   J. Hernandez *et al.*, "Comprehensive model for technoeconomic studies of next-generation central offices for metro networks," *Journal of Optical Communications Networking*, vol. 12, no. 12, pp. 414–427, Dec. 2020.

[12]   T. Zami, B. Lavigne, and M. Bertolini, "How 64 Gbaud optical carriers maximize the capacity in core elastic WDM networks with fewer transponders per Gb/s," Journal of

Optical Communications Networking, vol. 11, no. 1, pp. A20–A32, Feb. 2019.

[13]   M. Stepanovsky, "A Comparative Review of MEMS-Based Optical Cross-Connects for All-Optical Networks from the Past to the Present Day," *IEEE Communications Surveys and Tutorials*, vol. 21, no. 3, pp. 2928–2946, Jan. 2019.

[14]   R. Soref, "Design of low-energy on-chip electro-optical $1 \times M$ wavelength-selective switches," Photonic Research, vol. 5, no. 4, pp. 340–345, Aug. 2017.

[15]   K. Kikuchi, "Fundamentals of Coherent Optical Fiber Communications," Journal of Lightwave Technology, vol. 34, no. 1, pp. 157-179, Jan. 2016.

[16]   J. Lai, R. Tang, B. Wu, S. Li, X. Zhao, X. Tang, W. Zhao, and H. Zhang, "Research on passband narrowing effect of cascaded WSS in various ROADM links," in Asia Communications and Photonics Conference, Guangdong China, Nov. 2017.

[17]   R. -J. Essiambre, G. Kramer, P. J. Winzer, G. J. Foschini and B. Goebel, "Capacity Limits of Optical Fiber Networks," *Journal of Lightwave Technology*, vol. 28, no. 4, pp. 662-701, Feb. 2010.

[18]   JDSU, "21 . 5 dBm Controlled Erbium Doped Fiber Amplifier (EDFA) for Long Haul and Ultra Long Haul Applications OA 4500 Amplifier Series," Available: http://www.optus.kr/system/21dBEDFA-G3.pdf?PHPSESSID=992332a2ff8f2d395e92daf27006b6f2.

[19]   Corning, "Corning SMF-28 Ultra Optical Fiber," Available: https://www.corning.com/media/worldwide/coc/documents/Fiber/SMF-28%20Ultra.pdf.

[20]   G. Tzimpragos, C. Kachris, I. B. Djordjevic, M. Cvijetic, D. Soudris and I. Tomkos, "A Survey on FEC Codes for 100 G and Beyond Optical Networks," IEEE Communications Surveys & Tutorials, vol. 18, no. 1, pp. 209-221, Oct. 2014.

[21]   K. Chang, Enabling Technologies for High Spectral-efficiency Coherent Optical Communication Networks, John Wiley & Sons, 2016.

[22]   P. Poggiolini and Y. Jiang, "Recent Advances in the Modeling of the Impact of Nonlinear Fiber Propagation Effects on Uncompensated Coherent Transmission Systems," Journal of Lightwave Technology, vol. 35, no. 3, pp. 458-480, Feb. 2017.

[23]   P. Johannisson and E. Agrell, "Modeling of Nonlinear Signal Distortion in Fiber-Optic Networks," Journal of Lightwave Technology, vol. 32, no. 23, pp. 4544-4552, Dec. 2014.

[24]   P. Poggiolini, "The GN Model of Non-Linear Propagation in Uncompensated Coherent Optical Systems," Journal of Lightwave Technology, vol.30, no. 24, pp. 3857-3879, Dec. 2012.

[25] I. Monroy and E. Tangdiongga, Crosstalk in WDM Communication networks, Springer, 2002.

[26] B. Pinheiro, "Impact of In-Band Crosstalk on the Performance of Optical Coherent Detection Communication Systems," Master's dissertation in Telecommunications and Computer Engineering, ISCTE-IUL, 2015

[27] D. G. Sequeira, L. G. Cancela and J. L. Rebola, "Impact of physical layer impairments on multi-degree CDC ROADM-based optical networks," 2018 International Conference on Optical Network Design and Modeling (ONDM), pp. 94-99, Dublin Ireland, May 2018.

[28] E. Iannone, R. Sabella, M. Avattaneo, and G. De Paolis, "Modeling of in-band crosstalk in WDM optical networks," Journal of Lightwave Technology, vol. 17, no. 7, pp. 1135–1141, Jul. 1999.

[29] A. Morea, J. Renaudier, T. Zami, A. Ghazisaeidi and O. Bertran-Pardo, "Throughput comparison between transparent networks," IEEE/OSA Journal of Optical Communications and Networking, vol. 7, no. 2, pp. A293–A300, Feb. 2015.

[30] Santec, "Flexible-grid Wavelength Selective Switch WSS-100," Available: http://ainnotech.com/ainnotech/pdf/05/2_6/2ST-WSS-100-edm_Flexible grid%20Wavelength%20Selective%20Switch.pdf.

[31] H. Kawahara et al., "First investigation and reduction of inter-WSS crosstalk in multiple-arrayed WSSs for large-scale optical node," 2017 Opto-Electronics and Communications Conference (OECC) and Photonics Global Conference (PGC), pp. 1-2, Singapore, Aug. 2017.

[32] L. Cancela, J. Rebola, J. Pires," Implications of in-band crosstalk on DQPSK signals in ROADM-based metropolitan optical networks," Optical Switching and Networking, vol. 19, pp. 135-144, Jul. 2016.

[33] D. Sequeira, " Impact of In-Band Crosstalk in an Optical Network based on Multi-Degree CDC ROADMs," Master's dissertation presented in Telecommunications and Computer Engineering, ISCTE-IUL, 2017.

[34] K. Ho, "Effects of Homodyne Crosstalk on Dual-Polarization QPSK Signals," Journal of Lightwave Technology, vol. 29, no. 1, pp. 124-131, Jan. 2011.

[35] C. Pulikkaseril, L. Stewart, M. Roelens, G. Baxter, S. Poole, and S. Frisken, "Spectral modeling of channel band shapes in wavelength selective switches," Optical Express, vol. 19, no. 9, pp. 8458-8470, Apr. 2011.

[36] E. Agrell and M. Secondini, "Information-Theoretic Tools for Optical Communications

Engineers," 2018 IEEE Photonics Conference (IPC), pp. 1-5, Reston USA, Oct. 2018.

[37]   João Pedro, "Designing Transparent Flexible-Grid Optical Networks for Maximum Spectral Efficiency [Invited]," Journal of Optical Communications and Netwworking, vol.9, no.4, pp. C35-C44, Apr. 2017.

[38]   V.López and L. Velasco, Elastic Optical Networks, Springer, 2016.

[39]   C. Yao and C. Chien, "Design of a square-root-raised-cosine FIR filter by a recursive method," 2005 IEEE International Symposium on Circuits and Systems, pp. 512-515, Kobe Japan, May 2005.

[40]   J. Proakis and M. Salehi, Communication systems engineering, Prentice Hall, 2002.

[41]   M. Seimetz and C.Weinert, "Options, Feasibility, and Availability of 2×4 90º Hybrids for Coherent Optical Systems," Journal of Lightwave Technology, vol. 24, no. 3, pp. 1317–1322, Mar. 2006.

82

Appendix A: Cost per bit as a function of the number of groups

In Figure A.1, a cost comparison between the architecture with fractional space-full wavelength granularity with 2 groups and 4 groups, is shown. The increase of the number of groups causes an increase of flexibility but, as shown in Figure A.1, also causes a small increase of the cost per bit. The architecture with fractional space-full wavelength granularity with 4 groups, in a scenario with M=4, has the same flexibility than the architecture with space-wavelength granularity, but has higher cost. The architecture with fractional space-full wavelength granularity have a cost per bit of 3.12 and the architecture with space-wavelength granularity have a cost per bit of 1.63.
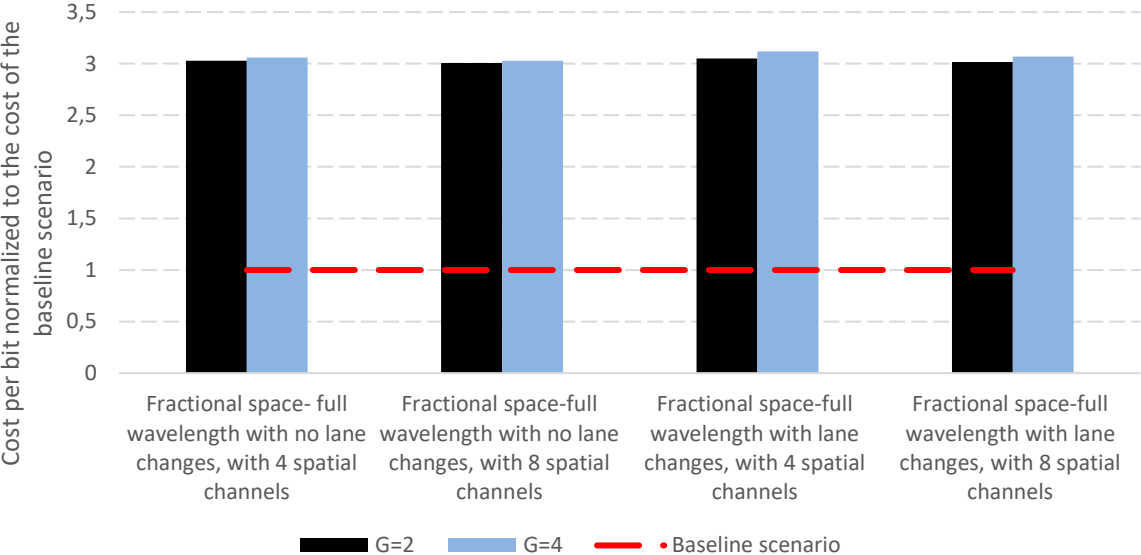
Figure A.1: Cost per bit, normalized to the baseline scenario, of the fractional space-full wavelength architecture when the number of groups is 2 and 4.

Space division multiplexing nodes architectures: cost per bit, power consumption, flexibility and performance

Marco Q. Silva[1], Luís G. Cancela[1,2], and João L. Rabola[1,2]

[1] Optical Communications and Photonics Group, Instituto de Telecomunicações, Lisbon, Portugal
[2] Department of Information Science and Technology, Instituto Universitário de Lisboa (ISCTE-IUL), Portugal
Emails: mqsas@iscte-iul.pt; luis.cancela@iscte-iul.pt; joao.rebola@iscte-iul.pt

Abstract— **Current optical networks are reaching their maximum transport capacity. Between other solutions, space division multiplexing (SDM) can be used to overcome this capacity limit. To use SDM, the reconfigurable optical add/drop multiplexers (ROADMs) need to be adapted to support this multiplexing. In this work, four switching strategies used in SDM ROADMs and the respective SDM ROADM architectures to implement these strategies are explained and analyzed, for uncoupled scenarios, in terms of cost per bit, power consumption. The impact of the physical layer impairments (PLIs), namely, amplified spontaneous emission noise, non-linear interference, passband narrowing due to optical filtering and in-band crosstalk are assessed, for cascades of ROADMs with the two most promising architectures: spatial and spatial-wavelength granularities. In terms of PLI the higher difference between optical networks with one spatial channel and with multiple spatial channels is the in-band crosstalk. The in-band crosstalk in networks with only one spatial channel or in a SDM network with the ROADM architecture with spatial granularity has an insignificant impact but in a SDM network with spatial wavelength granularity can cause an OSNR penalty of around 2 dB.**

Keywords— *Amplified spontaneous emission noise, in-band crosstalk, non-linear interference, passband narrowing filtering, reconfigurable optical add/drop multiplexers, spatial division multiplexing.*

I. INTRODUCTION

Optical transport networks are approaching its capacity limits, mainly due to new applications and services that require a huge amount of resources (i.e., bandwidth), like video services and cloud services. To increase the network capacity transmission, as well as switching efficiency, advanced modulation formats, that allow to transport more bits in a symbol and reconfigurable optical add/drop multiplexer (ROADM) with added features, like colorless, directionless and contentionless that bring more dynamism to the network, have been implemented. However, the referred solutions are nowadays almost fully exploited. Another solution to surpass the possible capacity crunch consists in using additional fiber bands (than the common C-band), the so-called multiband solution [1]. This is usually considered a short to medium term solution. A long-term solution is to use spatial-division multiplexing (SDM) in the optical domain, which leads to the concept of SDM-based optical networks [2,3]. Multicore fibers (MCF), multimode fibers (MMF) or multiple fibers (MF) in parallel are examples of SDM solutions for optical networks [2,3]. In this work it is considered uncoupled scenarios (MF solution is an exemple of an uncoupled scenario). In an uncoupled scenario the crosstalk between spatial channels do not exist.

In this work, several SDM ROADM switching strategies and the corresponding ROADM architectures are presented and explained. The SDM ROADM architectures are compared in relation to the reference architecture, the

ROADM architecture with only one spatial channel currently in use, in terms of cost per bit and power consumption. In the ROADM architectures with spatial and spatial-wavelength granularities, which are the most promising candidates for uncoupled scenarios, the impact of the physical layer impairments (PLIs), namely, amplified emission spontaneous (ASE) noise, non-linear interference (NLI), passband narrowing effects and in-band crosstalk, is also studied.

In [1],[2] and [3], four SDM switching strategies and the corresponding ROADM express structures are presented and a simple cost per bit comparison is performed. In this work, we propose express and A/D structures for SDM ROADM architectures, the cost per bit comparison is more complete and considers more hardware. Furthermore, a power consumption and the impact of PLIs in SDM networks are assessed.

This paper is organized as follows. Section II describes the SDM switching strategies and the ROADM architectures used to implement these switching strategies. In section III, the cost per bit and power consumption in SDM ROADM architectures are studied in comparison with the reference ROADM architecture with a single spatial channel. In section IV, the PLIs impact in SDM ROADM architectures with spatial-wavelength and spatial granularities is assessed and discussed. In section V the main conclusions of this work are presented.

II. SDM ARCHITECTURES

The switching in ROADMs for SDM networks can be performed in two dimensions (space and wavelength). In this section, we are going to present and explain the four possible switching strategies in SDM ROADMs: space granularity, space-wavelength granularity, wavelength granularity and fractional space-full wavelength granularity [2,3]. Furthermore, for each one of the switching strategies, we are going to present and explain a possible SDM ROADM architecture implementation.
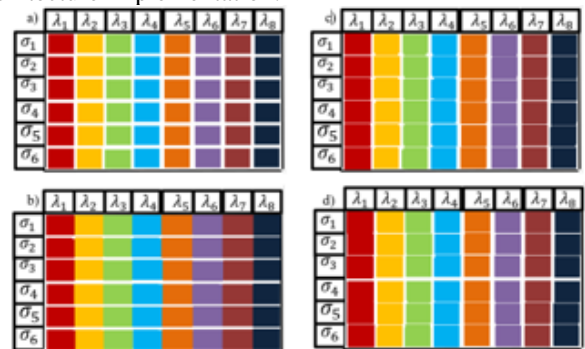

Figure 1. SDM switching strategies taken from [3]. The thick "white" lines define the switching granularity of the different strategies

In the space granularity strategy, represented in Figure 1 b), the switching is performed between spatial channels, by

switching the entire spectrum corresponding to a WDM signal [2,3]. The space granularity switching also demands uncoupled SDM fibers.

For the ROADM architecture with spatial granularity switching strategy, we have proposed a route and select (R&S) architecture with colorless and directionless as add and drop (A/D) functionalities. The express structure of this architecture has a single OXC to perform the switching of the spatial channels between all directions, all spatial channels, and also to receive and send the spatial channels to the A/D structures. The drop structure has one WSS for all the spatial channels with the same index. These WSSs are linked to multiple receivers and have also one link towards the add structure to return the wavelength channels that are not dropped. To have an A/D structure with contentionless functionality, one WSS for each spatial channel in each direction is required. In figure 2, a SDM ROADM architecture, with spatial granularity, considering 2 directions (D=2), 4 spatial channels (M=4), 80 wavelength channels (N=80) for each spatial channel, and an A/D ratio of 20% is presented.
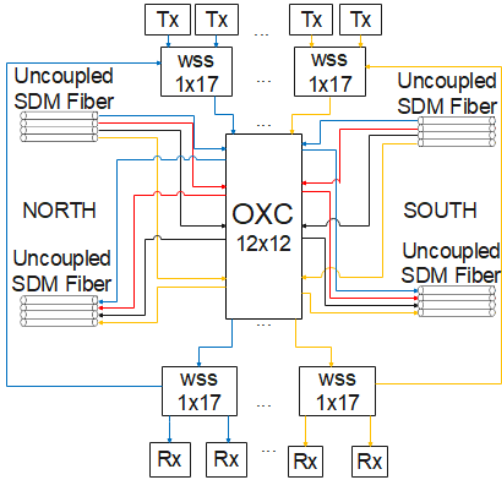

Figure 2. SDM ROADM architecture with spatial granularity

In the space-wavelength granularity strategy represented in Figure 1 a), the switching is performed between wavelength channels in any spatial channel. This strategy must use independent spatial and wavelength channels, hence, requiring uncoupled SDM fibers, such as the multiple fibers in parallel solution or the weakly-coupled MCF solution. This strategy is the one that leads to a most flexible switching architecture, since the switching is performed at the wavelength level granularity, but at the cost of more complexity [2,3].

For the ROADM architecture with spatial-wavelength granularity switching strategy, we have proposed a R&S architecture with colorless, directionless and contentionless (CDC) as A/D functionalities. In each direction of the express structure, there exists one input and output WSS for each spatial channel. Each WSS is responsible for routing/receiving wavelength channels to/from any spatial channel of any direction. Each WSSs has also M links towards the A/D structures. There are M A/D structures in order to reduce the dimensions of the WSSs that would be needed if only one A/D structure is used and also to avoid a single point of failure. Each add and drop structure corresponds to a WSS with multiple inputs and multiple outputs that has links to the input/output WSSs of all directions. The architecture R&S with CDC A/D functionalities presented in the current WDM

networks is a specific case of the spatial-wavelength granularity with one spatial channel, i. e., M=1 and it is our baseline scenario. In figure 3, a SDM ROADM architecture, with spatial-wavelength granularity, considering D=2 and M=2 is presented, and in figure 4, it is represented the A/D structure used in this architecture considering N=80 for each spatial channel, and an A/D ratio of 20%.
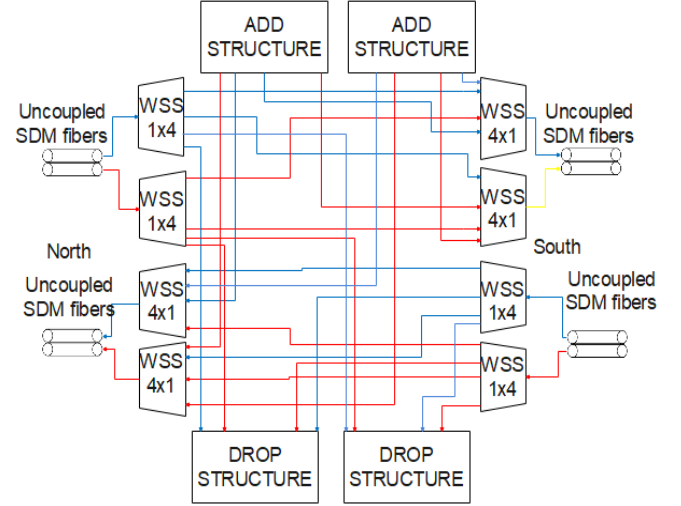
Figure 3. SDM ROADM architecture with spatial-wavelength granularity
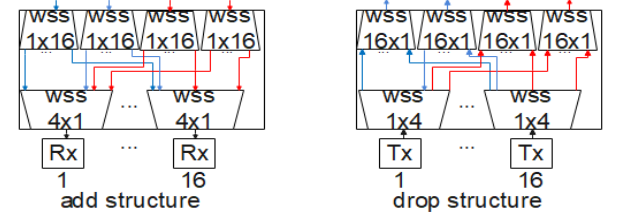
Figure 4. A/D structure for the SDM ROADM architecture with spatial-wavelength granularity

In the wavelength granularity strategy, represented in Figure 1 c), the switching is performed between groups of channels with the same wavelength, which form a spatial superchannel, i.e., all wavelength channels λ_1, forming a spatial superchannel in one direction, are switched together to another direction. A joint switch WSS must be used to perform this operation [2,3].

For the ROADM architecture with wavelength granularity switching strategy, we have proposed a R&S architecture with CDC as A/D functionalities. In each direction of the express structure, there exists one input and output joint switch WSS. Each joint switch WSS is responsible for routing/receiving spatial superchannel to/from joint switch WSSs of other directions. Each joint switch WSS has also a link towards the A/D structure. There is one A/D for each direction responsible for extract/add a spatial superchannel, which must also use joint switch WSS.

In the fractional space-full wavelength strategy, represented in Figure 1 d), the switching is done between subgroups of channels with the same wavelength index (subgroup 1 composed by the wavelength channels in the spatial channels $\sigma_1, \sigma_2, \sigma_3$ and subgroup 2 composed by $\sigma_4, \sigma_5, \sigma_6$). This solution is very similar to solution c), still supported by spatial superchannels, but with this solution, the degree of spatial granularity is increased.

For the ROADM architecture with fractional space-full wavelength granularity switching strategy, we have proposed a R&S architecture with CDC as A/D functionalities. In each direction of the express structure there exists G (corresponding to the number of superchannels groups) input and output joint switch WSSs. Each input joint switch WSS is responsible for routing the spatial superchannel from its group to the output joint switch WSSs or to the drop structure. The output joint switch WSSs are responsible for receiving the superchannels from the input WSSs and from the add structure. There is one A/D structure for each direction. This A/D structure has one joint switch WSS for group. Each joint switch WSS is responsible for extract/add the spatial superchannels from their respective groups.

III. COST PER BIT AND POWER CONSUMPTION ANALYSIS

In this section, we are going to analyze the SDM ROADM architectures proposed in the previous chapter in terms of cost per bit and power consumption.

To perform this analysis, first we need to count the hardware used in the express structure (structure responsible for routing the signal to the respective direction or to the A/D structure) and in the A/D structure (structure responsible for adding or dropping wavelength channels). In table 1 and 2 it is presented the expressions used to determine the number of hardware in each structure.

Table 1. number of components and their size in the express structure for each of the SDM architectures

Granularity	Number of components	inputs	outputs
Spatial	$N_{OXC} = 1$	$M \times (D+1)$	$M \times (D+1)$
Spatial-Wavelength	$N_{WSS} = 2 \times M \times D$	1	$D \times M$
Wavelength	$N_{jointWSS} = 2 \times D$	M	$D \times M$
Fractional space-full wavelength	$N_{jointWSS} = 2 \times D \times G$	$\frac{M}{G}$	$\frac{M}{G} \times [(D-1) \times G + 1]$

In table 1 and 2 it is possible to observe that the architecture with spatial granularity is the architecture that uses less hardware in the express structure (only one OXC with high dimension), and in the A/D structure, and it is also the less flexible architecture.

The architecture with spatial-wavelength is the architecture that needs more hardware in both, express and A/D structure. It is also the architecture with the higher switching flexibility.

The architectures with wavelength and fractional space-full wavelength granularity use more hardware and are more flexible than the architecture with spatial granularity. These architectures use less hardware than the architecture with spatial-wavelength granularity and are also less flexible, but in these two architectures, the number of needed transponders is much higher.

The OXC in the architecture with spatial granularity can be done with MEMs (Micro Electro Mechanical Systems) or WSSs. The WSSs approach is more expensive and has functionalities that we don't need, but we have not found any cost relation between the MEMs and the other hardware components, therefore we are considering that the WSS and MEMs approach have the same cost.

Table 2. number of components and their size in the A/D structure for each of the SDM architectures.

Granularity		Spatial	Spatial-wavelength	Wavelength	Fractional space-full wavelength
Number of A/D structures per architecture ($N_{A/D}$)		2	$2 \times M$	$2 \times D$	$2 \times D$
Number of WSSs or joint switches WSSs per A/D structure	Input WSS drop/ output WSS add	M	$D \times M$	1	G
	Output WSS drop/ input WSS add		$A/D_{ratio} \times N$		
Number of inputs of the A/D structure	Input WSS	1	1	M	$\frac{M}{G}$
	Output WSS		$D \times M$		
Number of outputs of the A/D structure	Input WSS	$A/D_{ratio} \times N + 1$	$A/D_{ratio} \times N$	$M \times A/D_{ratio} \times N$	$A/D_{ratio} \times N \times \frac{M}{G}$
	Output WSS		1		
Number of transponders		$N_{A/D} \times A/D_{ratio} \times N$	$M \times A/D_{ratio} \times N \times N_{A/D}$	$M \times A/D_{ratio} \times N$	$A/D_{ratio} \times N \times \frac{M}{G} \times N_{A/D} \times G$

Table 3. Hardware cost

Twin WSS	Cost	Power (W)
1 × 2	0.25	50
1 × 4	0.5	100
1 × 10	1	150
1 × 20	1.5	200
1 × 40	2.25	240
Joint switch WSS		
20 ports	1	100
40 ports	1.5	120
80 ports	2.25	140
160 ports	3.375	160
320 ports	5.0625	180
100 Gbit/s transponder	1.14	120

The next step to conclude this analysis is to determine the hardware cost by analyzing the literature. The costs for the WSSs and joint switches WSSs presented in Table 3 were obtained following the method explained in [2](in this method it is stated that a WSS with two times the complexity is 50% more expensive e.g., A WSS 1×20 has 2 times the complexity of a WSS 1×10, hence this WSS will cost 50% more than the WSS 1×10) and normalized to the cost of the 1×10 twin WSS (A twin WSS works as an entry WSS and exit WSS at the same time [2]). The transponder is a hardware component that is not considered in [2], for the cost calculation, and therefore, the transponder cost has been

taken from [4], where it was shown that this hardware has a cost 4.54 times higher than a 1×4 WSS. Using this information, it is possible to normalize the transponder cost to the cost of the 1×10 twin WSS, e.g., if the transponder is 4.54 times more expensive than a 1×4 WSS, is 2.27 times more expensive than a twin 1×4 WSS. Hence, if a twin 1×4 WSS has a normalized cost of 0.5, the transponder will have a normalized cost of 1.14.
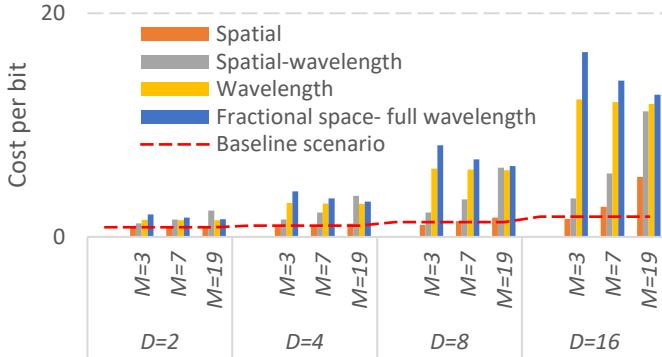

Figure 5. Cost per bit of the SDM ROADM-based architectures normalized to the cost per bit of the baseline scenario with 4 directions, as a function of the number of ROADM directions, D, and number of spatial channels, M.

In Figure 5, the cost per bit, as a function of the number of ROADM directions and number of spatial channels, for all SDM ROADM-based architectures and for the baseline scenario is shown. This cost is normalized to the cost of the baseline scenario with D=4. For all directions, it can be concluded that an increase in the number of spatial channels causes: 1) an increase of the cost per bit of the architectures with spatial and spatial-wavelength granularity, 2) a decrease of the cost per bit of the architecture with fractional space-full wavelength granularity and 3) practically does not affect the cost per bit of the wavelength granularity architecture.

When the number of directions is increased, a substantial increase in the cost per bit of all architectures is observed, except for the architecture with space granularity, where the cost increase is not so pronounced.

in these conditions are less expensive than the architecture with space-wavelength granularity, because with the increase of the number of spatial channels the number of WSSs for the architecture with spatial-wavelength increase (causing a high increase in the cost), but for the architectures with wavelength and fractional space-full wavelength granularity this increase in the number of WSSs does not exist, for this architectures the number of WSSs increase when the number of directions increase. Therefore, when the number of spatial channels is high, and the number of directions is low the architectures with wavelength and fractional space- full wavelength are less expensive than the architecture with space-wavelength granularity and have some cost advantages in being use.

Figure 6. Power consumption of the SDM ROADM-based architectures normalized to the cost per bit of the baseline scenario with 4 directions, as a function of the number of ROADM directions, D, and number of spatial channels, M.

In Figure 6, the power consumption in [KW], as a function of D and M, for all SDM ROADM-based architectures, is shown. The power consumption for the baseline scenario is not shown in Figure 6, because it is too low. The power consumption for the baseline scenario varies from 9.9 kW (scenario with 2 directions), to 21.1 kW (scenario with 16 directions). For all architectures, a higher number of directions or number of spatial channels causes a higher power consumption. The increase of spatial channels leads to a more significant power consumption growth, for
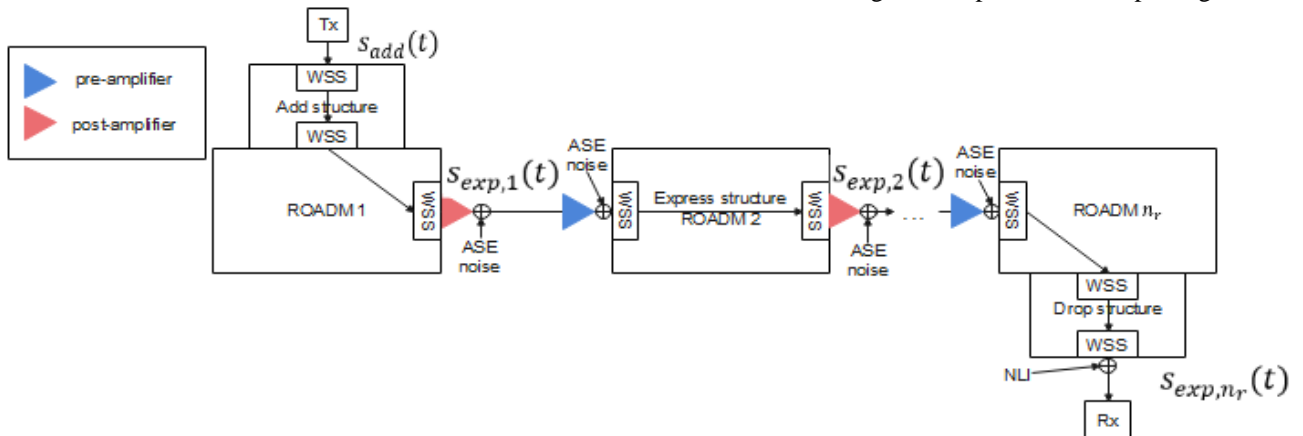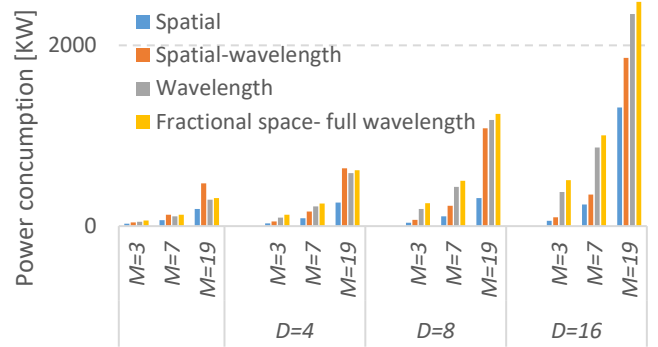

Figure 7. Simulation model of a cascade of n_r ROADMs based on spatial-wavelength granularity considering the PLIs due to optical amplification, filtering and NLI effects.

From Figure 5, it can be also concluded that the architectures with wavelength and fractional space-full wavelength granularity can lead to some cost advantages, in uncoupled scenarios, when $D < 8$ and $M = 19$ because, in these conditions, they are less expensive than the architecture with space-wavelength granularity. The architectures with wavelength and fractional space-full wavelength granularity

the architecture with spatial-wavelength granularity. For example, with D=8 the increase of spatial channels from 7 to 19 leads to a power consumption, 2.91, 4.78, 2.69 and 2.47 times higher, respectively, for the architectures with space, spatial-wavelength, wavelength and fractional space-full wavelength granularities. The increase of the number of directions causes a higher power consumption for the

architectures with wavelength, spatial-wavelength and fractional space-full wavelength granularity. This appends because for the architecture with space granularity the increase of the number of directions does not increase, the number of WSSs or number of A/D structures, as much as in the others architectures.

From Figure 6, it can be concluded that the architectures with wavelength and fractional space-full wavelength granularity can lead to some advantages regarding the power consumption when $D<8$ and $M=19$, in comparison with the architecture with space-wavelength granularity. The reason for this has explained when Figure 5 has analyzed.

IV. PHYSICAL LAYER IMPAIRMENTS ANALYSIS IN THE ARCHITECTURES WITH SPATIAL AND SPATIAL-WAVELENGTH GRANULARITY

In this section, we perform an analysis of the impact of the PLIs (physical layer impairments) amplified spontaneous emission (ASE) noise, non-linear interference (NLI), passband narrowing effects and in-band crosstalk. This analysis was performed both analytically for the architectures with spatial and spatial-wavelength granularities, and with a a Monte Carlo simulator for the architectures with spatial-wavelength granularity. In this analysis, the architectures with wavelength and fractional space-full wavelength granularities weren't studied, because in the previous section we have concluded that these architectures do not have cost and power consumption advantages in being used in uncoupled scenarios.

A. ROADM cascade without in-band crosstalk.

In this sub-section, the PLIs ASE noise, NLI effect, and passband narrowing are assessed analytically for the architecture with spatial and spatial-wavelength granularity and by simulation for the architecture with spatial-wavelength granularity. For the analytical assessment, the ASE noise is calculated with the expressions present in [5],[6],[7] and [8], the passband narrowing effect is obtained from [9] and [10] and the NLI effect it is calculated with the expressions presented in [11],[12] and [13].

The OSNR was obtained for a network with the following parameters: p_s=optimum signal power, R_b (binary rate) of 100 Gbit/s, $R_{b,l}$ (line binary rate) of 120 Gbit/s, modulation 4-QAM, B_o (optical bandwidth) of 30 GHz, F_n (amplifier figure noise) of 6.9 dB, v_o (frequency of the central channel) of 193.8 THz, L_{sec} (fiber section length) of 80 km, α (attenuation coefficient)of 0.2 dB/km, $G_{pre_{amp}}$ (pre-amplifier gain)of 16 dB, $G_{post_{amp}}$ (post amplifier gain) of 19.2 dB for the architecture with spatial granularity or 20.4 dB, symbol rate (R_s) of 30 GBaud, 80 wavelength channels, fiber dispersion coefficient (D_s) of 18 ps/nm/km, nonlinear fiber coefficient (γ) of 1.1 $W^{-1}km^{-1}$, channel spacing of 50 GHz, passband and stopband filters of 4th order with -3 dB bandwidth of 45 GHz.

The OSNR in the architecture with spatial granularity after 10 cascaded ROADMs is 15 dB and in the architecture with spatial-wavelength granularity is 14,40 dB. The architecture with spatial granularity has a higher OSNR (0.6 dB higher) but is less flexible.

For the architecture with spatial-wavelength granularity, it is performed a more precise analysis with the support of a simulator. In Figure 7, the model used to study and simulate this scenario is presented. In this simulation the passband narrowing was studied and compared with the results of [9]

and [10], concluding that the OSNR penalty caused by this PLI is insignificant (in a cascade of 10 ROADMs the OSNR penalty due to passband narrowing is 0.2 dB).
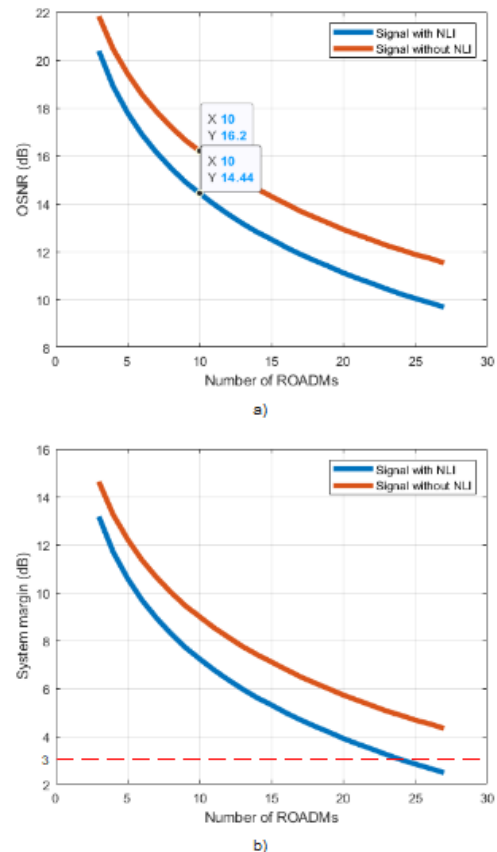

Figure 8. OSNR measured at the signal bandwidth and System margin, measured at the input of the coherent optical receiver as a function of the number of ROADMs, without and with NLI.

In Figure 7, $s_{add}(t)$ is the QPSK signal generated by the optical transmitter and $s_{exp,j}(t)$ are the signals at the output of the jth ROADM (with j=1, ..., n_r) along the network, where n_r is the total number of ROADMs in the cascade. In the simulation model depicted in Figure 7, the first ROADM is used to add the signal into the network. At the output of this ROADM, the signal went through 3 WSSs and one optical amplifier. The next ROADMs are used as express ROADMs, the signal is expressed from a ROADM input to a ROADM output, and in this case, the signal goes through 2 WSSs and 2 optical amplifiers. Finally, the signal is dropped from the optical network in the last ROADM, where it goes through 3 WSSs and one amplifier. The optical amplifiers considered in the simulation and represented in Figure 7 are assumed to perfectly compensate the network losses and add ASE noise to the signal. In the Matlab simulation, the ASE noise power is defined by setting each sample function of noise with the respective power. Furthermore, the NLI noise of the fiber is computed and added only at the input of the coherent optical receiver, as indicated in Figure 7.

In Figure 8 a) and b), it is shown, respectively, the OSNR at the signal bandwidth and the system margin, obtained by simulation, as a function of the number of ROADMs, with and without NLI. For the computation of the system margin in Figure 8 b), a transmission penalty of 1.5 dB is considered.

As can be observed in Figure 8 a), the OSNR decreases as the number of cascaded ROADMs grows due to an increase of ASE noise power, NLI effects and also due to a

slight filtering penalty as the number of cascaded WSSs increases. From Figure 8 a), we can also confirm that for 10 cascaded ROADMs, an OSNR of 14.4 dB is obtained, which is in accordance with the values obtain analytically.

From Figure 8 b), we can conclude that, for the case without NLI, at the end of the cascade up to maximum number of ROADMs considered (27 ROADMs), the system margin is always above the 3 dB minimum considered by us. For the case with NLI, the system margin is above the minimum, for a ROADM cascade of maximum 23 ROADMs.

B. ROADM cascade with in-band crosstalk.

The crosstalk is a physical layer impairment, that is caused mainly by the finite isolation of optical components [14], [15]. The imperfect isolation of these components causes power leakages that lead to signal degradation at the receiver. These power leakages are the interfering terms that will impair the selected signal. There are two types of crosstalk, in this work, we only consider the in-band crosstalk, that occurs when the interfering signals have the same nominal wavelength of the selected signal [16],[14], [15]. The first step to study the in-band crosstalk is to determinate expressions to allow us to obtain the number of interfering terms in the SDM architectures.

Table 4. Number of in-band interfering terms at the ROADM output and at the input of the optical receivers of the drop structure in the baseline, spatial-wavelength granularity and spatial granularity architectures

Architectures	Baseline architecture or SDM architecture with spatial wavelength granularity	SDM architecture with spatial granularity
2nd order interfering terms at the receivers input of the drop structure	$(D \times M) - 1$	-
2nd order interfering terms at the ROADM output	$((D-1) \times M) + ((D \times M) - 1)$	-
1st order interfering terms at the ROADM output	-	1

In Table 4, the expressions that allow the calculation of the number of 1st order and 2nd order in-band interfering terms at one ROADM output for the worst-case scenario in the baseline, spatial-wavelength and spatial granularities architectures, are presented. The architecture with less in-band interfering terms is the architecture with space granularity. This architecture has always one in-band interfering term, because the switching in this architecture is performed by the OXC, which has a very high isolation. The architecture with more in-band interfering terms is the architecture with spatial-wavelength granularity. This architecture has more interfering terms because, as shown in Table 4, the number of interfering terms increases with the number of spatial channels. The baseline architecture is a special case of the spatial-wavelength granularity architecture, by considering M=1. The derived expressions of the baseline scenario have been validated and are in agreement with the expressions presented in Table 4.1 of [16].

To assess the OSNR penalty due to in-band crosstalk we are going to consider that the in-band crosstalk can be modeled as an additive noise with a Gaussian distribution [18] and we have used the expressions presented in [16] and [18] to assesses the OSNR penalty caused by in-band crosstalk. The OSNR penalty due to in-band crosstalk, for 10 cascaded ROADMs, in the architecture with spatial-

wavelength granularity with A = -30 dB and A =-25 dB is, respectively, 0.66 dB and 4.23 dB. For the architecture with spatial granularity with A =-30 dB and A=-25, the OSNR penalty obtained is, respectively, only 0.14 dB and 0.44 dB.

Considering the OSNR penalties due to in-band crosstalk, for a WSSs with isolation of -30 dB, the OSNR at the optical receiver input after 10 cascaded ROADMs with D=16, M=19 and spatial-wavelength granularity architecture, is 14.05 dB. For the same scenario but using the architecture with spatial granularity, the OSNR is 15.15 dB. So, by considering the in-band crosstalk penalty, our analytical results show that the architecture with spatial granularity leads to an OSNR improvement of about 1.1 dB in relation to the spatial-wavelength architecture.

The simulator model is similar to the one presented in figure 7, but in this simulation, we add to the signal the interfering terms. The number of interfering terms is obtained with the expressions in table 4 and the interfering terms are added to the main signal at the ROADM output or at the receivers input. Each in-band crosstalk signal is generated with the same characteristics of the primary signal (which is a QPSK signal), but for each interfering term, the bits are generated randomly. The interfering signals are generated also with a phase difference and a time misalignment, in relation to the original signal. The time misalignment and phase difference are modelled as a uniformly distributed random variable, respectively, between $[0, T_s]$ and between $[0, 2\pi]$ as in [17]. After generation, each second order interfering term must go through two blocking filters that simulate 2nd order leakage in WSSs.
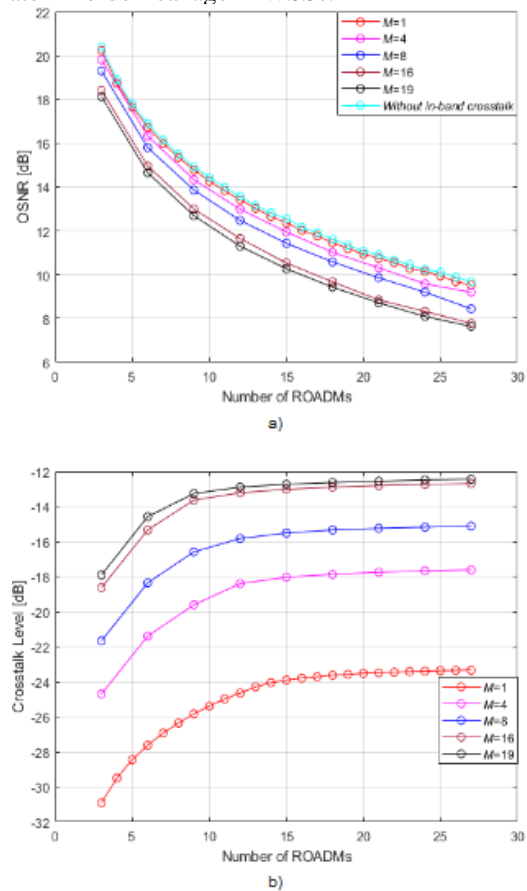

Figure 9. OSNR and crosstalk level as a function of the number of ROADMs for a system with ASE noise, passband narrowing due to filtering, NLI and in-band crosstalk level for A= -25 dB, D=16 and a different number of spatial channels.

The OSNR penalties predicted by simulation are lower than the ones predicted by the analytical analysis. This behavior is attributed to the random walk-off between symbols of the interfering terms and symbols of the primary signal, a behavior that is captured when the waveform distortion is taken into account to obtain the OSNR.

In Figure 9, the OSNR and crosstalk level as a function of the number of ROADMs, for A=-25, 16 directions and different numbers of spatial channels is represented. In Figure 9 a), it is possible to observe that the impact of in-band crosstalk on the OSNR is enhanced as the number of spatial channels grows. For M=1 and M=4, the in-band crosstalk impact is negligible. For M=8, M=16 and M=19, after 27 cascaded ROADMs, the OSNR penalty due to in-band crosstalk is, respectively, 1.2 dB, 1.9 dB and 2 dB. For these cases, in figure 9 b), the crosstalk levels achieved at the end of the cascade of 27 ROADMs are -15.1 dB, -12.7 dB and -12.4 dB, respectively, for M=4, 8, 16 and 19. In [19], for the same crosstalk levels, the OSNR penalty obtained was, respectively, 1.2 dB, 1.8 dB and 2 dB, for QPSK signals, which is in a very good agreement with our results.

To keep the system performance, the system margin needs to be higher than 3 dB, which corresponds to a minimum OSNR of 10.2 dB. Therefore, for A=-25 dB (Figure 9 a)), D=16 and M=1, 4, 8, 16 and 19, to accomplish this margin, the signal can cross, respectively, 24, 21, 19, 16 and 15 ROADMs.

V. CONCLUSION

In this work the architectures used to implement the SDM switching strategies were analyzed in terms of cost per bit and power consumption. First it is shown the hardware needed to build the express and A/D structures of each SDM RAODM architecture and the cost and power consumption of each hardware is presented. With the cost and power consumption analysis we have concluded that the architectures with wavelength and fractional space-full wavelength granularities do not have benefits in being used in uncoupled scenarios, because have a cost per bit and power consumption higher than the architecture with spatial-wavelength granularity but are less flexible. Next, an assessment of the physical layer impairments on the architecture with spatial and spatial-wavelength granularity was performed. With this assessment was concluded that the architecture with spatial granularity has a OSNR 1.1 dB higher than the architecture with spatial-wavelength granularity but is less flexible. We have also observed that in SDM ROADMs with spatial-wavelength granularity the in-crosstalk is much higher than in single spatial channels RAODMs, and that the OSNR penalty due to in-band crosstalk can reach 2 dB and the signal in this case is able to cross 9 less ROADMs.

ACKNOWLEDGMENT

REFERENCES

[1] A. Napoli at al., "Towards multiband optical systems," *Advanced Photonics Conference*, Paper NeTu3E.1, California USA, 2018.

[2] D. M. Marom *et al.*, "Survey of photonic switching architectures and technologies in support of spatially and spectrally flexible optical networking [invited]," *Journal of Optical Communications and Netwworking*, vol. 9, no. 1, pp. 1–26, Jan. 2017.

[3] D. M. Marom and M. Blau, "Switching solutions for WDM-SDM optical networks," *IEEE Communications Magazine*, vol. 53, no. 2, pp. 60–68, Feb. 2015.

[4] J. Hernandez et al., "Comprehensive model for technoeconomic studies of next-generation central offices for metro networks," Journal of Optical Communications Networking, vol. 12, no. 12, pp. 414–427, Dec. 2020.

[5] K. Kikuchi, "Fundamentals of Coherent Optical Fiber Communications," Journal of Lightwave Technology, vol. 34, no. 1, pp. 157-179, Jan. 2016.

[6] J. Lai, R. Tang, B. Wu, S. Li, X. Zhao, X. Tang, W. Zhao, and H. Zhang, "Research on passband narrowing effect of cascaded WSS in various ROADM links," in Asia Communications and Photonics Conference, Guangdong China, Nov. 2017.

[7] R. -J. Essiambre, G. Kramer, P. J. Winzer, G. J. Foschini and B. Goebel, "Capacity Limits of Optical Fiber Networks," *Journal of Lightwave Technology*, vol. 28, no. 4, pp. 662-701, Feb. 2010.

[8] K. Chang, Enabling Technologies for High Spectral-efficiency Coherent Optical Communication Networks, John Wiley & Sons, 2016.

[9] A. Morea, J. Renaudier, T. Zami, A. Ghazisaeidi and O. Bertran-Pardo, "Throughput comparison between transparent networks," IEEE/OSA Journal of Optical Communications and Networking, vol. 7, no. 2, pp. A293–A300, Feb. 2015.

[10] João Pedro, "Designing Transparent Flexible-Grid Optical Networks for Maximum Spectral Efficiency [Invited]," Journal of Optical Communications and Netwworking, vol.9, no.4, pp. C35-C44, Apr. 2017.

[11] P. Poggiolini and Y. Jiang, "Recent Advances in the Modeling of the Impact of Nonlinear Fiber Propagation Effects on Uncompensated Coherent Transmission Systems," Journal of Lightwave Technology, vol. 35, no. 3, pp. 458-480, Feb. 2017.

[12] P. Johannisson and E. Agrell, "Modeling of Nonlinear Signal Distortion in Fiber-Optic Networks," Journal of Lightwave Technology, vol. 32, no. 23, pp. 4544-4552, Dec. 2014.

[13] P. Poggiolini, "The GN Model of Non-Linear Propagation in Uncompensated Coherent Optical Systems," Journal of Lightwave Technology, vol.30, no. 24, pp. 3857-3879, Dec. 2012.

[14] I. Monroy and E. Tangdiongga, Crosstalk in WDM Communication networks, Springer, 2002.

[15] B. Pinheiro, "Impact of In-Band Crosstalk on the Performance of Optical Coherent Detection Communication Systems," Master's dissertation in Telecommunications and Computer Engineering, ISCTE-IUL, 2015

[16] D. G. Sequeira, L. G. Cancela and J. L. Rebola, "Impact of physical layer impairments on multi-degree CDC ROADM-based optical networks," 2018 International Conference on Optical Network Design and Modeling (ONDM), pp. 94-99, Dublin Ireland, May 2018.

[17] D. Sequeira, L. Cancela, and J. Rebola, "CDC ROADM design tradeoffs due to physical layer impairments in optical networks," *Optical Fiber Technology*, vol. 62, no. 102461, pp. 1-11, Jan. 2021.

[18] K. Ho, "Effects of Homodyne Crosstalk on Dual-Polarization QPSK Signals," Journal of Lightwave Technology, vol. 29, no. 1,

[19] D. Sequeira, " Impact of In-Band Crosstalk in an Optical Network based on Multi-Degree CDC ROADMs," Master's dissertation presented in Telecommunications and Computer Engineering, ISCTE-IUL, 2017.